

AN ABSTRACT OF THE THESIS OF

Fedor A. Zhuravlev for the degree of Doctor of Philosophy in Chemistry presented on November 2, 2001. Title: Mechanistic Studies on Re(V) Mediated C-O Bond Transformations.

Redacted for privacy

Abstract Approved: _____
Kevin Gable

In situ reduction of Cp*ReO₃ by PPh₃ to form (Cp*ReO)₂(μ-O)₂ allows catalytic deoxygenation of epoxides, however, comproportionation between Re^V and Re^{VI} species to form clusters of {(Cp*Re)₃(μ-O)₆}²⁺(ReO₄⁻)₂ and new compound {(Cp*Re)₃(μ²-O)₃(μ³-O)³ReO₃}⁺(ReO₄⁻) leads to removal of rhenium from the catalytic cycle and loss of activity. The epoxide deoxygenation mediated by (Cp*ReO)₂(μ-O)₂ at least partially occurs through the intermediacy of the corresponding Re(V) diolates, which are unstable under conditions at which they form (72-112°C); the following cycloreversion leads to a formation of Cp*ReO₃ and alkene.

Primary ¹³C and secondary ²H kinetic isotope effects (KIE) show that cycloreversion of 4-methoxystyrene from Tp'Re(O)(OCH(Ph-4-OMe)CH₂O) proceeds via a significantly asynchronous but concerted transition state. The primary KIEs are k_{12C}/k_{13C} = 1.041 ± 0.005 at the alpha position, and 1.013 ± 0.006 at the beta position. The secondary KIEs were k_H/k_D = 1.076 ± 0.005 at the alpha position, and 1.017 ± 0.005 at the beta position at 103°C.

Both ^{13}C and D KIEs were obtained from analysis of ^1H NMR spectra using a newly developed procedure. For the first time, D KIEs were alternatively obtained using Bayesian NMR methodology, independently confirming D KIEs derived from ^1H NMR. ^{13}C and D KIEs were found to be consistent with each other in pointing to significantly more bond breaking at the alpha carbon than at the beta carbon. A Hammett study on cycloreversions of substituted styrenes from a series of $\text{Tp}^*\text{Re}(\text{O})(\text{diolato})$ showed dichotomous behavior for electron donors and electron acceptors as substituents: $\rho = -0.65$ for electron donors, but $\rho = +1.13$ for electron-withdrawing groups. Quantitative analysis of the KIEs coupled with the observed impact of aryl substitution on the rate of cycloreversion excludes the possibility of competing single bond-cleaving (stepwise) processes being responsible for the observed KIE values. DFT calculations locate a transition state structure for styrene extrusion that agrees with this picture.

The Hammett behavior opens the possibility that, depending on a substituent, two different mechanisms might be in competition due to very well balanced stereo-electronics of the system where charge perturbation changes the mechanism.

Mechanistic Studies on Re(V) Mediated C-O Bond Transformations

by
Fedor Zhuravlev

A THESIS

submitted to

Oregon State University

in partial fulfillment of the requirements for
the degree of

Doctor of Philosophy

Presented November 2, 2001
Commencement June 2002

Doctor of Philosophy thesis of Fedor A. Zhuravlev presented on November 2, 2001

APPROVED:

Redacted for privacy

Major Professor, representing Chemistry

Redacted for privacy

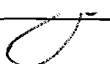
Chair of Department of Chemistry

Redacted for privacy

Dean of Graduate School

I understand that my thesis will become part of the permanent collection of Oregon State University libraries. My signature below authorizes release of my thesis to any reader upon request

Redacted for privacy

 Fedor A. Zhuravlev, Author

ACKNOWLEDGMENTS

I am grateful for the help of many people who made this work possible. First and foremost, I would like to thank my research advisor, Prof. Kevin P. Gable for his encouragements and guidance. I would also like to thank the faculty members: Prof. James D. White and Prof. Max Deinzer for their support. I am indebted to Rodger Kohnert for his help with the NMR and to Alex Yokochi for the X-ray work. I owe many thanks to my fellow graduate student: Sundaram Shanmugham, Eric Brown and Scott Allen. Lastly, I would like to thank my wife, Irina for her understanding and support.

TABLE OF CONTENTS

	<u>Page</u>
Chapter 1. General Introduction	1
Chapter 2. Catalytic Deoxygenation of Epoxides with (Cp*ReO) ₂ (μ-O) ₂	4
Introduction	4
Catalytic deoxygenation of epoxides with (Cp*ReO) ₂ (μ-O) ₂ and clustering phenomenon	11
Intermediacy of Re(V) diolate in rhenium mediated epoxide deoxygenation	19
Chapter 3. Synthetic Studies towards Stable Rhenaoxetanes	25
Introduction	25
Metallaoxetanes in the literature	27
Studies pointing to the stepwise cycloreversion in Re(V) diolates	46
Synthetic approach	48
Starting materials. Improved practical synthesis of Cp*ReO ₃	51
Reaction of Cp*Re(O)Cl ₂ with ortho - Li, Mg and Zn nucleophiles	52
Synthesis of some new Tp, Tp', and Tk rhenium(Oxo)dihalides and reaction with organozinc phenolates	54
The synthesis of TpRe(O)I(OPh) and its photochemistry	59
Reaction of the Cp* dimer with cyclooctyne	61
Concluding remarks	62
Chapter 4. Kinetic Isotope Effects in Cycloreversion of Rhenium (V) Diolates	65
The concept of concertedness	65
Experimental techniques for exclusion of a concerted mechanism	69
Stereochemical integrity	69
Isotopic label scrambling	70

TABLE OF CONTENTS (Continued)

	<u>Page</u>
Independent synthesis of a reactive intermediate and its kinetic consistency with the reaction in question	70
Isoinversion kinetic relationship	71
Experimental techniques for exclusion of a stepwise mechanism and other general techniques.	72
Kinetic isotope effects.	73
Double isotope fractionation	74
Computational approach.	75
Organometallic systems under investigations: Asymmetric Dihydroxylation	76
Rate studies.	78
Study of electronic effects.	79
Studies on the origin of enantioselectivity in the AD reaction.	80
Nonlinear plot of stereoselectivities vs. $1/T$	82
Computational work.	83
Kinetic isotope effects.	83
Selected organometallic systems under investigations:	
Re(V) diolate cycloreversion	85
Conformational studies.	86
Strain/Kinetic isotope effect studies.	87
Computational studies	88
Predicted kinetic isotope effects in cycloreversion of Re(V) diolates	88
Experimental design.	89
General methodology.	89
Synthesis of labeled diolates.	92
Estimation of conversion.	99
Estimation of R/R_0 from ^{13}C NMR and D NMR using integration.	101
Theoretical and practical consideration of data acquisition and analysis	101
Integration of ^{13}C and D NMR spectra.	105

TABLE OF CONTENTS (Continued)

	<u>Page</u>
Alternative methods of NMR data analysis. Bayesian analysis of time domain data	107
Deficiencies of frequency domain data analysis	107
Background to the Bayesian approach	108
Benchmarking BAYES against simulated data	109
Bayesian analysis of real data	111
Concluding remarks	113
KIE estimation from the ¹ H NMR.	114
Hammett studies	117
Computational work	118
Methodology	119
Optimization of the ground state structures and location of the transition state.	120
Discussion	124
Stepwise migrations: Coordinated epoxide and rhenaoxetane	124
Concerted cycloreversion.	125
Chapter 5. Conclusion	128
Chapter 6. Experimental	132
General procedures	132
NMR Measurements	133
Catalytic deoxygenation of epoxides.	134
Synthetic Procedures	134
Cp*Re(CO) ₃	134
Cp*ReO ₃	135
<i>bis</i> -TMS peroxide.	135
Oxidation of Cp*Re(CO) ₃ with BTMSP/Re ₂ O ₇	136
Reaction of Cp*ReO ₃ and (Cp*ReO) ₂ (μ-O) ₂	136

TABLE OF CONTENTS (Continued)

	Page
Oxidation of $\{(\text{Cp}^*\text{Re})_3(\mu^2\text{-O})_3(\mu^3\text{-O})_3\text{ReO}_3\}^+(\text{ReO}_4^-)$	137
$\text{Cp}^*\text{Re}(\text{O})\text{Cl}_2$	137
<i>ortho</i> -lithiophenolate.	138
Reaction of <i>ortho</i> -Li phenolate with $\text{Cp}^*\text{Re}(\text{O})\text{Cl}_2$	138
Mg/Li exchange in <i>ortho</i> -Li phenolate	139
Hydrido-tris-(3,5-dimethylpyrazolyl)boratorhenium (V) (oxo)dichloride.	139
Hydrido-tris-pyrazolylboratorhenium (V) (oxo)dibromide.	140
Hydrido-tris-pyrazolylboratorhenium (V) (oxo)diiodide	141
Tetrakis-pyrazolylboratorhenium(V) (oxo)dibromide	141
Tetrakis-pyrazolylboratorhenium(V) (oxo)diiodide.	142
Photolysis of $\text{TpRe}(\text{O})\text{IOPh}$	142
Tris-pyrazolylboratorhenium(V) (oxo)phenoxiodide.	143
Cyclooctyne.	144
Pentamethylcyclopentadienyl	
1-rhena(oxo)-4-oxacyclohexa-2,5-cyclooctadiene	144
Synthesis of unlabeled hydrido-tris-(3,5-	
dimethylpyrazolyl)boratooxorhenium (V)	
(4-methoxy-phenyl)-ethane-1,2-diolate	145
(4-Methoxy-phenyl)-[1- ^2H]ethane-1,2-diol	146
(4-Methoxy-phenyl)-[2- ^2H]ethane-1,2-diol	147
(4-[$^2\text{H}_3$]methoxy-phenyl)-ethane-1,2-diol	148
(4-Methoxy-phenyl)-[1- ^{13}C]ethane-1,2-diol	148
(4-Methoxy-phenyl)-[2- ^{13}C]ethane-1,2-diol	150
Synthesis of 1-(4-[^{13}C]methoxy-phenyl)-ethane-1,2-diol.	150
Cycloreversion of ^{13}C and D labeled	
hydrido-tris-(3,5-dimethylpyrazolyl) boratooxorhenium (V)	
(4-methoxy-phenyl)-ethane-1,2-diolates	151
General procedure.	151
Isotopic molar ratios	151
Experimental details for the structural characterization of	
$[(\text{Cp}^*\text{Re})_3(\mu^2\text{-O})_3(\mu^3\text{-O})_3\text{ReO}_3][\text{ReO}_4] \cdot \text{NCMe}$	153
Bibliography	155
Appendix	165

LIST OF FIGURES

<u>Figure</u>	<u>Page</u>
1. The X-ray structure of $[(\text{Cp}^*\text{Re})_3(\mu^2\text{-O})_3(\mu^3\text{-O})_3\text{ReO}_3^+][\text{ReO}_4^-]$	17
2. Kinetics of alkene production from Cp* dimer + 1,2-decanepoxide	23
3. More O'Ferral-Jencks diagram	66
4. The structure of the major, anti diastereomer as determined by the NOE	98
5. The structure of the minor, <i>syn</i> diastereomer as determined by the NOE	99
6. Eyring plot of Re(V) diolate extrusion	100
7. Construction of noise-containing FID	111
8. Bayesian analysis of Re(V) diolate isotopomeric mixture	112
9. Hammett plot for cycloreversion of substituted phenylethanediolates	118
10. Optimized structure of TpReO_3 at the B3LYP/LACVP*+ level	121
11. Optimized structure of $\text{TpRe}(\text{O})(\text{OCH}_2\text{CHPhO})$ at the B3LYP/LACVP*+ level	122
12. Optimized structure of the transition state at the B3LYP/LACVP*+ level	123

LIST OF TABLES

<u>Table</u>	<u>Page</u>
1. Reaction of epoxides with catalytic Cp*ReO ₃ + excess PPh ₃	14
2. Yields of rhenium oxohalides LRe(O)X ₂ from various methods	57
3. Bayesian analysis of simulated data vs. numerical integration.	110
4. Relative integral ratios from different methodologies.	112
5. Primary ¹² C/ ¹³ C KIE on extrusion of 4-methoxystyrene.	116
6. Secondary D KIE on extrusion of 4-methoxystyrene.	117
7. Energies for optimized structures at the B3LYP/LACVP*+ level	121
8. Isotopic molar ratio (¹² C/ ¹³ C) at each position as measured by ¹ H NMR .	152
9. Isotopic molar ratio (H/D) at each position as measured by ¹ H NMR. . . .	152

LIST OF APPENDIX TABLES

<u>Table</u>	<u>Page</u>
A1. Crystal data and structure refinement for the cluster.	166
A2. Atomic coordinates ($\times 10^4$) and equivalent isotropic displacement parameters for the cluster.	167
A3. Selected bond lengths [\AA] and angles [$^\circ$] for the cluster.	168
A4. Bond lengths [\AA] and angles [$^\circ$] for the cluster.	171

This thesis is dedicated to my parents, Anatoly and Nina Zhuravlev.

CHAPTER 1. GENERAL INTRODUCTION

Oxidation of organic and inorganic matter by oxygen is a widespread chemical process occurring on Earth. This includes autooxidation, combustion and a large number of enzyme catalyzed oxidations^{1a}.

It has been long recognized that oxidation by O₂ is notoriously difficult to control. The triplet ground state of molecular oxygen results in its kinetic inertness^{1b}. Dioxygen activation can be easily achieved by increasing the reaction temperatures at the expense of a substantial loss of selectivity.

Since living organisms are carbon-based, it is not surprising that carbon-oxygen bond transformations are ubiquitous in biological systems. A closer look reveals that living organisms are capable of making C-O bonds and breaking them not only with great chemoselectivities but also with amazingly high rates and stereoselectivities at ambient temperatures. The majority of those processes use catalysis by transition metal enzymes^{1a}.

Naturally occurring processes provide a great inspiration for chemists who design efficient, selective, catalytic reactions. As ecological issues become more and more important the need for the atom- and energy economical processes in the synthesis of fine and commodity chemicals gradually increases.

Over the last two decades transition metal oxo compounds emerged as key elements in the carbon-oxygen forming reactions. A large variety of transition metals are able to form multiple bonds to oxygen. The metal-oxo moiety can often be transferred to organic substrates. The strength of the M-O bond is a function of the nature of the metal, its oxidation state and the ligand environment. Those can be relatively easily manipulated, thus presenting enormous possibilities for rational design and the control of reactivity. The recent success of asymmetric synthesis and its importance for pharmaceutical industry highlights practical significance of new, highly efficient transition metal oxo catalysts.

Needless to say, a rational reagent design is impossible without good understanding of the reaction mechanism. Unfortunately, organometallic reactions are often complex and poorly understood. A flat potential energy surface in many metal mediated reactions can open up multiple reaction pathways, the outcome of which could be difficult to predict^{1c}. Some reactions feature one or several reactive intermediates, that could be hard to detect experimentally but could be modeled. Thus, practical advantages of understanding the mechanistic details provide great incentive for a rapid development of mechanistic organometallic chemistry.

This work applies physical organic methodology to the mechanistic problem of Re-mediated carbon-oxygen bond transformations. It explores two very significant areas of transition metal catalyzed oxygen transfer: the relationship between different modes of O-atom transfer reactions, such as bishydroxylation

and epoxidation and the nature of the transition state in the Re diolate formation/
cycloreversion.

CHAPTER 2. CATALYTIC DEOXYGENATION OF EPOXIDES WITH $(\text{CP}^*\text{ReO})_2(\mu\text{-O})_2$

INTRODUCTION

Oxidation of organic substrates with oxometal reagents has long been the subject of intense research in inorganic and organometallic chemistry². Reagents such as CrO_3 , OsO_4 , RuO_4 , MnO_2 , and permanganates traditionally played an important role in organic synthesis due to their ability to effect oxidation of organic substrates selectively under mild conditions.

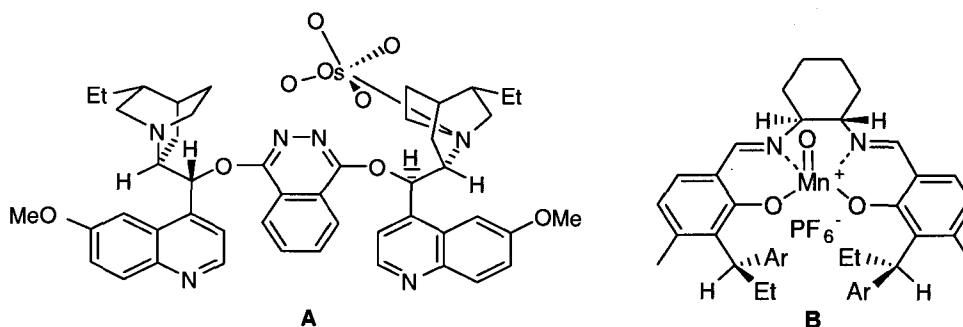
Interest in asymmetric synthesis in the 1970s provided a driving force for intensive research program in the field of the nonenzymatic asymmetric oxidation. The discovery of Sharpless asymmetric dihydroxylation³ (AD) and Jacobsen-Katsuki asymmetric epoxidation are notable achievements in this field⁴.

In the AD reaction, otherwise T_d symmetric osmium (VIII) oxide is rendered asymmetric by complexation with a chiral tertiary amine (Scheme 1A). The complexation also has a beneficial impact on the rate of the reaction. In the Jacobsen-Katsuki asymmetric epoxidation (salen)Mn (V) oxo species is believed to be an O-atom donor (Scheme 1B). Both reactions sparked hot debates over the possible mechanisms, particularly over the viability of an oxametallacyclic intermediates⁵

On an industrial scale, polyoxometalates, particularly bismuth molybdate $\text{Bi}_2\text{Mo}_2\text{O}_9$ enjoyed great popularity as primary heterogeneous gas-phase cata-

lysts in the production of commodity chemicals, such as acrolein and acrylonitrile⁶.

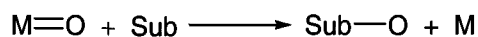
Scheme 1.



O-atom transfer reactions (*vide infra*) have recently received renewed attention because of their possible importance in biological systems such as cytochrome P-450 and the molybdoenzyme sulfite oxidase⁷. An attempt to model reactivity of these systems led to the design of a new class of metalloporphyrins as oxygenating catalysts⁸.

The key mechanistic feature common to reactions mentioned above is the participation of one or more M=O groups in the O-atom transfer processes. (Scheme 2).

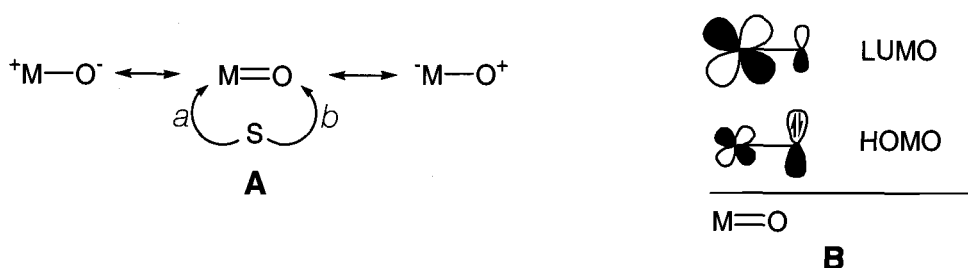
Scheme 2.



A better understanding of the chemistry of M=O fragment can be achieved by looking at the resonance structures (Scheme 3A) and at the corresponding MO diagrams (Scheme 3B). Oxometal group can be represented as the reso-

nance hybrid of the covalent and the dipolar forms. In many metal oxides the LUMO is metal based and the oxo ligand is typically nucleophilic⁹. As the metal oxo π^* orbital drops in energy and acquires more oxygen character an oxo complex becomes more electrophilic at the oxygen¹⁰.

Scheme 3.



Under this scenario O-atom transfer to electron rich substrates such as triphenylphosphine involves direct attack of the substrate at the electrophilic oxo ligand¹¹.

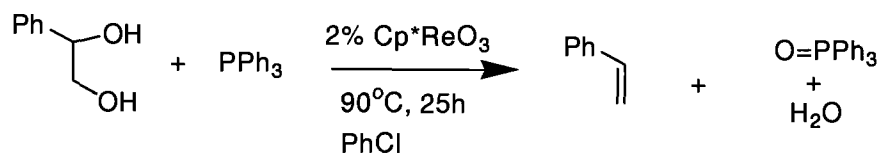
It was recently recognized that the cleavage of C-O bonds with concomitant formation of one or more new M=O bonds can also be of practical importance. An example of this is the exploration of nonoxidative routes to oxygenated organic compounds starting from renewable biomass carbohydrates¹². This project came as an effort to find a more environmentally friendly alternative to conventional hydrocarbon oxidation processes. Since carbohydrates are too oxygen-rich relative to many important target compounds, efficient removal of carbohydrate hydroxyl group is a key step to a successful reductive process. The idea is to design a catalyst that mediates O-atom transfer from diols and polyols to a suitable stoichiometric O-atom acceptor.

Designing such a catalytic process presents several challenges. From a thermodynamic point of view, cleavage of a relatively strong C-O bond(s) requires a large negative enthalpy of a $M^n/M^{n+2}=O$ couple. Few oxo acceptors have been reported to effect such a transformation. Among them are complexes of the type $WCl_2(PR_3)_3$. High oxophilicity ($W^{2+}/W^{4+}=O$ $\Delta H < -74$ kcal/mol) allows for deoxygenation of sterically unencumbered phosphine oxides¹³. For the purpose of designing a catalytic cycle, however, additional factors must be taken into account. Oxophilic properties of the organometallic system must be finely balanced so that the high rate of the initial O-atom transfer from substrate to the complex is followed by an easy oxygen abstraction by a stoichiometric reductant. An oxide with very strong metal oxygen bonds, such as WO_3 (BDE = 150 kcal/mol)¹⁴ and $WOCl_4$ (BDE = 195 kcal/mol)¹⁵ would appear to be a thermodynamic sink and could not be turned over. Therefore, the choice of the metal is of paramount importance.

Recent interest in rhenium oxo chemistry highlights the structural diversity of $LReO_n$ systems and the practical possibility to adjust overall thermodynamics through structural modifications of organorhenium compound.

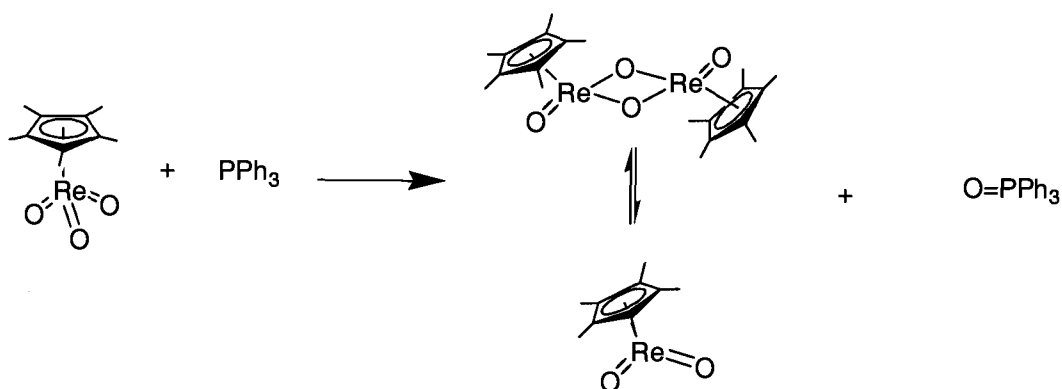
One particular process that was reported by Andrews^{12c} features a reaction that converts vicinal diols or polyols to alkenes (Scheme 4).

Scheme 4.



This catalytic process is based on the earlier observation that pentamethylcyclopentadiene rhenium (V) diolates extrude alkene at elevated temperature. Catalysis takes advantage of favorable thermodynamics of Re(V) dioxo – Re(V) oxo – Re(VI) trioxo chemistry. The reduction of Cp*ReO₃ to Re(V) with triphenylphosphine easily occurs at room temperature. (Scheme 5). This reaction is enthalpically favorable. The strengths of Re=O was estimated to be 110-116 kcal/mol¹⁶ while the strength of the P=O bond in triphenylphosphine is about 130 kcal/mol¹⁷.

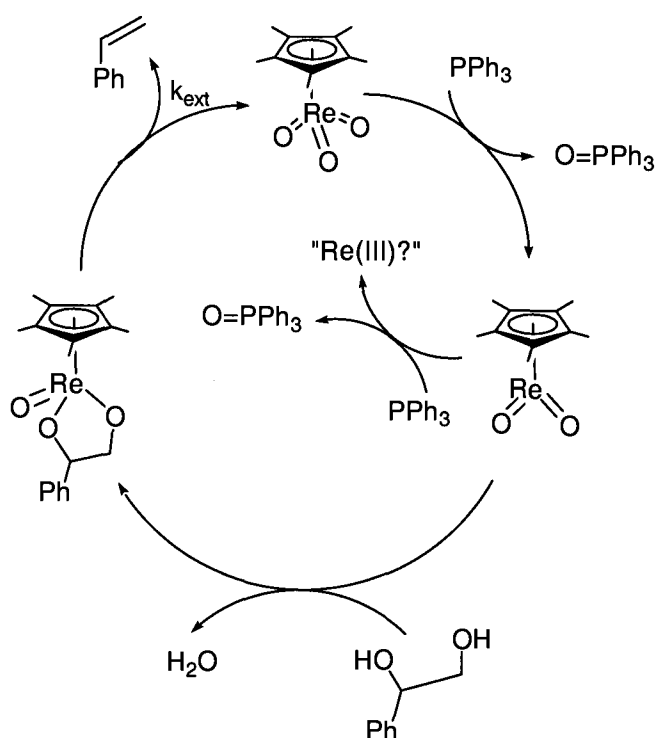
Scheme 5.



The resulting Cp*ReO₂ is a 16 e⁻ complex. In solution, it was shown to be in equilibrium with its 18 e⁻ μ-oxo-bridged dimer, either of which may participate in the condensation with diol forming Re(V) diolate and releasing one equivalent of

water. When the rhenium diolate cycloreverts the resulting Cp^*ReO_3 is reduced and is returned to the catalytic cycle as Re(V) which again reacts with the diol (Scheme 6). However, the overall catalytic reaction was found to be inefficient. Turnovers ranged from 1 to 60. The low turnover numbers were attributed to the formation of a catalytically inactive Re(III) compound which was not characterized.

Scheme 6.



To get better insight into the thermodynamics of Re mediated O-atom transfer it is important to investigate the structure-properties relationships of LReO_n compounds.

Unexpected, and perhaps, the most intriguing structural feature of Cp^*ReO_3 is the coexistence of the metal in its highest oxidation state with elec-

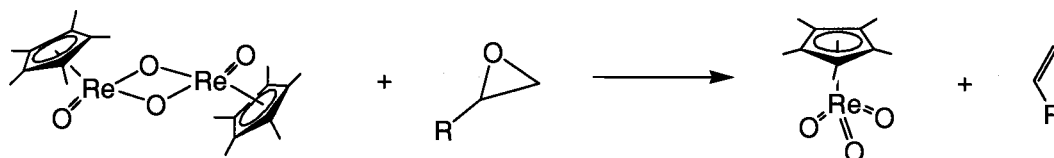
tron rich spectator ligand¹⁸. One of the consequences of this is a broad spectrum of reactivity of LReO_3 with respect to the O-atom transfer. As has been previously noted, the reaction of Cp^*ReO_3 with regular olefins is essentially thermoneutral. The cycloaddition becomes unfavorable because of the negative change in the entropic term of the associative process. In accord with these observations it was found that Cp^*ReO_3 will reversibly add across a strained C=C bond^{16b}. The necessary gain in enthalpy in this process comes from the strain relieved. The basic thermodynamic implication is that the Re=O bond is too strong for efficient cycloaddition but just right for cycloreversion. In a number of experimental and computational studies it was shown that the bond dissociation energy is the function of the ligand L. Sigma electron donors with no π -donation (alkyl, σ -aryl) increase the BDE compared to that of the σ/π -donors such as Cp and Cp^* . As a practical consequence, methyl rhenium trioxide (MTO) is much weaker as an oxidant (BDE = 153 kcal/mol). Although being a stronger Lewis acid, MTO is reduced by phosphines incompletely¹⁸, while Cp^*ReO_3 easily oxidizes triphenylphosphine¹⁹. The overall bonding situation was recently analyzed on the basis of high level DFT calculations²⁰. It was shown that two main factors contribute to the Re=O bond strength: (1) σ/π -orbital interaction of the ligand and ReO_3^+ fragment, (2) the electron affinity of ReO_3 and ReO_2 fragments. The accepting orbitals of ReO_3 moiety have π -antibonding Re-O character. As a consequence, the stronger orbital interaction leads to a weaker Re=O bond. Charge

destabilization comes into play in the product, LReO_2 . This works in the opposite direction. Being more electronically rich than the trioxide, LReO_2 is destabilized by the charge donation from the ligand to a much larger degree than LReO_3 complex. The latter effect often dominates the overall thermochemistry. The interplay of the two counteracting phenomena explains the prediction why, in fact, CpReO_3 is a better O-atom donor than the Cp^*ReO_3 (BDE = 109 vs. 113 kcal/mol respectively). While the π -donation abilities of Cp^* and Cp are roughly equivalent, Cp^*ReO_3 is much more polar than CpReO_3 (6.5D vs. 5.5D). This indicates that the charge destabilization effect in Cp^*ReO_2 overrides the orbital effect. Recent experimental findings of charge effects on oxygen transfer in $[(\text{HCpz}_3)\text{ReOCl}_2]^+$ provide additional support for this hypothesis²¹.

CATALYTIC DEOXYGENATION OF EPOXIDES WITH $(\text{Cp}^*\text{ReO})_2(\mu\text{-O})_2$ AND CLUSTERING PHENOMENON

In 1995 Gable and co-workers showed that epoxides react with $(\text{Cp}^*\text{ReO})_2(\mu\text{-O})_2$ producing alkene and Cp^*ReO_3 ²² (Scheme 7)

Scheme 7.



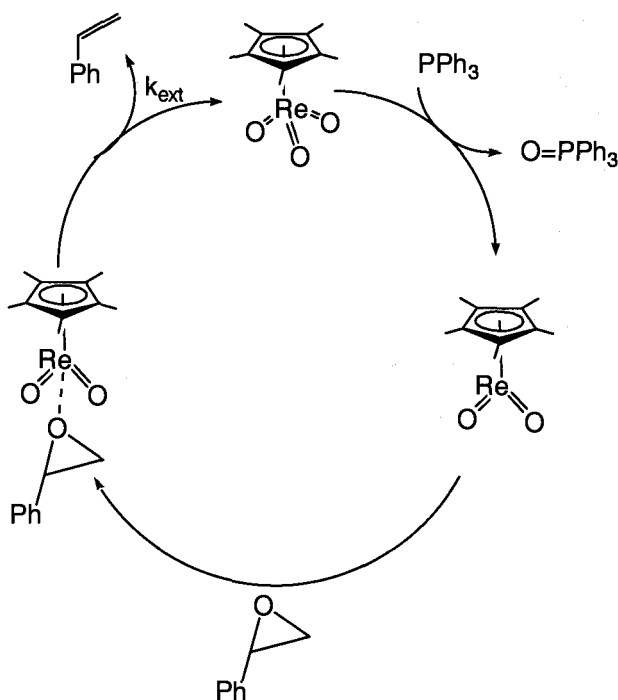
A number of epoxides have been tested, including styrene oxide, 1,1-dimethyloxirane, (*E*)- and (*Z*)-1,2-dimethyloxirane, with styrene oxide being more reactive than the aliphatic epoxides. As originally reported in this study the stoichiometric reaction proceeded without the formation of any byproducts in 50 – 105°C range. The formation of Cp*ReO₃ was quantitative. No intermediates have been reported in this reaction, either. The reaction was found to be highly stereospecific, giving retention of configuration as evidenced by NMR.

Following this report we decided to investigate some possible practical applications of this reaction. Initial studies indicated that electron withdrawing substituents substantially accelerate O-atom abstraction. Since in epoxidation reactions an overepoxidation can sometimes be a problem and given the sufficient difference in rates one can hope the electron deficient double bond can be selectively and stereospecifically deoxygenated.

O atom transfer from epoxides to form an olefin has been preceded in the literature. Triphenylphosphine is known to bring about epoxide deoxygenation. The reaction proceeds with inversion of configuration and requires some 200°C²³. The use of organometallic complexes containing oxophilic metals such as V²⁴ and W²⁵ allows one to effect deoxygenation under relatively mild conditions. As was noted in the previous section, the disadvantage of V and W systems, in particular is a difficulty in devising an efficient and inexpensive stoichiometric reductant for a catalytic version of the deoxygenation reaction.

The authors²² also evaluated the rate law for deoxygenation of styrene oxide with $(\text{Cp}^*\text{ReO})_2(\mu\text{-O})_2$ which led to the first order dependence on the epoxide concentration and the half order dependence on the concentration of $(\text{Cp}^*\text{ReO})_2(\mu\text{-O})_2$. This identifies the Re(V) active species as Cp^*ReO_2 and suggests that the dissociation of $(\text{Cp}^*\text{ReO})_2(\mu\text{-O})_2$ must occur prior to the interaction with an epoxide molecule. Noting that the product, Cp^*ReO_3 can be converted to the Cp^*ReO_2 with the PPh_3 the conceptual catalytic cycle would involve $(\text{Cp}^*\text{ReO})_2(\mu\text{-O})_2$ (or its monomer) as a resting state of a catalyst (Scheme 8).

Scheme 8.



Practical implementation of the conceptual catalytic cycle however, posed some unexpected difficulties. An initial study of deoxygenation of 1,2-epoxydode-

cane using 5 mol% of Cp^*ReO_3 gave traces of alkene after extensive reaction times. The increase in the proportion of rhenium led to improved conversion but the turnover numbers remained low.

Epoxydes with electron-withdrawing substituents reacted faster; moderate turnover numbers (12.9) can be achieved with 3-fluoropropylene oxide (Table 1).

Table 1. Reaction of epoxydes with catalytic Cp^*ReO_3 + excess PPh_3

	Epoxyde	c/M	$[\text{Cp}^*\text{ReO}_3]/\text{M}$	t/h	$T/^\circ\text{C}$	Conversion	Turnover
1	1,2-Epoxy-decane	0.16	0.007	20	116	5	1.1
2	1,2-Epoxy-dodecane	0.14	0.007	18	112	<5	—
3	1,2-Epoxy-dodecane	0.14	0.029	13	112	20	0.9
4	1,2-Epoxy-dodecane	0.14	0.059	13	112	70	1.6
5	1,2-Epoxy-dodecane	0.14	0.14	13	112	>90	0.9
6	1,2-Epoxy-dodecane	0.14	0.007 ^a	13	112	50	10
7	2,3-Epoxy-nor-bomane	0.23	0.009	6	116	<5	—
8	p-Bro-mostyrene Oxide	0.12	0.007	16	90	20	3.4
9	3-Fluoro-propylene Oxide	0.28	0.005	3	116	23	12.9

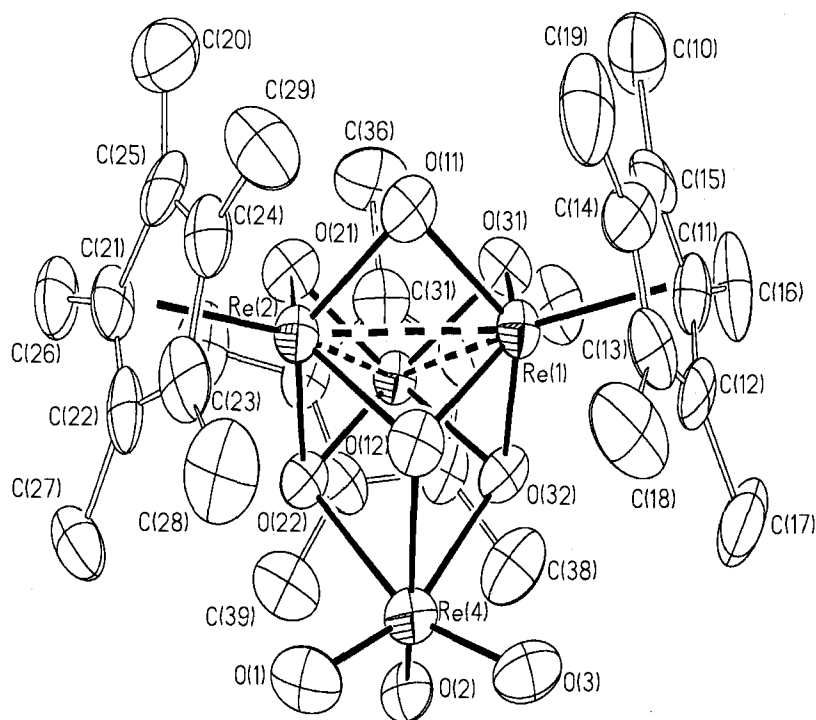
a. $[\text{PPh}_3] = 0.17\text{M}$ except entry 6, $[\text{PPh}_3] = 0.35\text{M}$.

We suspected that the reason for such a low turnover was that the catalyst was involved in an irreversible side reaction that effectively removed Re from the catalytic cycle. Careful examination of the runs where particularly poor turnover was observed revealed formation of a green precipitate. This green solid was isolated by filtration and washing with benzene, and was spectroscopically identified as trinuclear cluster $\{(\text{Cp}^*\text{Re})_3(\mu\text{-O})_6\}^{2+}(\text{ReO}_4^-)_2$ first characterized by Herrmann et al²⁶. The central core of the cluster is C_3 symmetrical cation $(\text{Cp}^*\text{Re})_3(\mu\text{-O})_6^{2+}$ (Scheme 9). Three Cp^*ReO_2 groups are equivalent and the metal atoms have a formal oxidation state of $+5/3$. We found that perrhenate anions can be easily exchanged with NaI in water; this is accompanied by the disappearance of the $\text{Re}=\text{O}$ (908 cm^{-1}) stretch in IR. As expected, the cluster was unreactive toward epoxides at elevated temperature. However, the cluster can be reoxidized to Cp^*ReO_3 with Jones' reagent in 37% yield.

Cluster formation under strictly anaerobic conditions of our experiment was puzzling. The trinuclear cluster $\{(\text{Cp}^*\text{Re})_3(\mu\text{-O})_6\}^{2+}(\text{ReO}_4^-)_2$ is normally formed by an air oxidation of $(\text{Cp}^*\text{ReO})_2(\mu\text{-O})_2$ or by an oxidation with one electron oxidant such as AgBF_4 . Since our experiments were performed in deoxygenated solvents in sealed glass tubes (3-4 pump-thaw cycles) the only candidate for the external oxidant was the starting material, Cp^*ReO_3 . Control experiment confirmed that Cp^*ReO_3 and $(\text{Cp}^*\text{ReO})_2(\mu\text{-O})_2$ do not react with each other at room temperature but when heated at 110°C for 14 hrs did produce the trinuclear clus-

ter along with an air stable purple solid. While the trinuclear cluster is insoluble in chloroform, the purple compound showed good solubility and could be separated by re-precipitation from the CHCl_3 or CH_2Cl_2 solution upon addition of benzene. Aside from the dramatically different visible spectrum the only difference from the trinuclear cluster was a new IR peak at 736 cm^{-1} and weak shoulder on a very strong perrhenate Re–O stretch at 908 cm^{-1} . A single sharp peak appeared in the ^1H NMR (δ 2.23 in CD_2Cl_2). This purple compound was also found in several of our catalytic runs along with the green trinuclear cluster. Furthermore, this second compound became predominant at relatively high Re concentrations (Table 1 entries 4,5). Since little information could be obtained from NMR and IR we resorted to X ray crystallography. Layering (Et_2O)/MeCN) produced crystals of good quality.

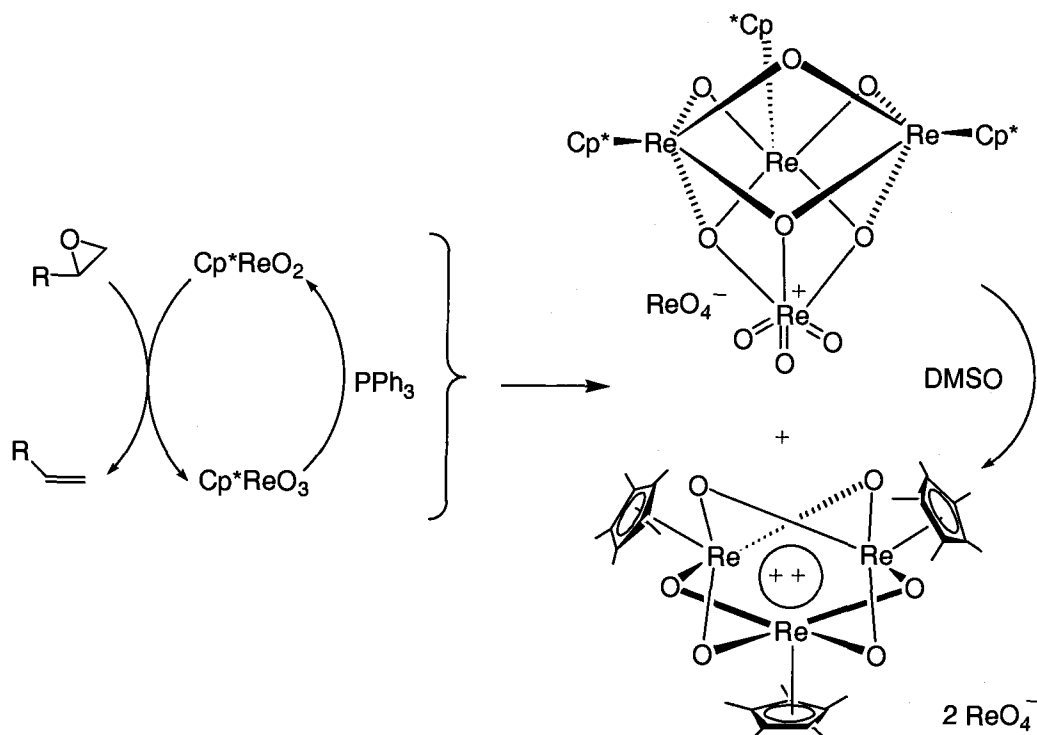
Figure 1. The X-ray structure of $[(\text{Cp}^*\text{Re})_3(\mu^2\text{-O})_3(\mu^3\text{-O})_3\text{ReO}_3^+][\text{ReO}_4^-]$



As evidenced by X-ray diffraction analysis the new compound is a cluster structurally somewhat similar to $\{(\text{Cp}^*\text{Re})_3(\mu\text{-O})_6\}^{2+}(\text{ReO}_4^-)_2$. It can be viewed as the neutral $(\text{Cp}^*\text{Re})_3(\mu\text{-O})_6$ core coordinated to ReO_3^+ . The ReO_3 unit is a slightly distorted octahedral rhenium in a typical LReO_3 environment: the terminal oxo bond lengths are normal (1.668(10), 1.685(13), 1.707(12) Å) as are the O-Re-O angles ($103.2(6)^\circ$, $105.9(6)^\circ$, $104.1(6)^\circ$). The $\text{Re}_3(\mu\text{-O})_6$ core is similar to the trinuclear dication. With the Re-Re distances of 2.750(1) and 2.759(1) Å a bonding interaction between metal atoms seems to be unlikely (compare with 2.75 Å Re-

Re in metal). The most striking difference from trinuclear cluster is the strong distortion of the two sets of bridging oxo ligands which is most likely caused by the coordination of oxygen atoms to ReO_3 fragment. The bond lengths average to 1.94 Å and 2.02 Å. The O-(ReO_3) distances are long at an average of 2.18 Å. The average oxidation state of Re in the tetranuclear cluster is 5 and, therefore, this compound is more electron-rich than the trinuclear cluster. Oxidation with DMSO (100°C, 2hrs) results in quantitative conversion of $[(\text{Cp}^*\text{Re})_3(\mu^2\text{-O})_3(\mu^3\text{-O})_3\text{ReO}_3^+][\text{ReO}_4^-]$ to $\{(\text{Cp}^*\text{Re})_3(\mu\text{-O}_6)\}^{2+}(\text{ReO}_4^-)_2$ (Scheme 9). Although we did not test the reactivity of Cp^*ReO_3 towards the tetranuclear cluster it is very likely that it is a precursor to the trinuclear cluster. A control experiment showed that the trinuclear cluster is unreactive towards epoxides.

Scheme 9.



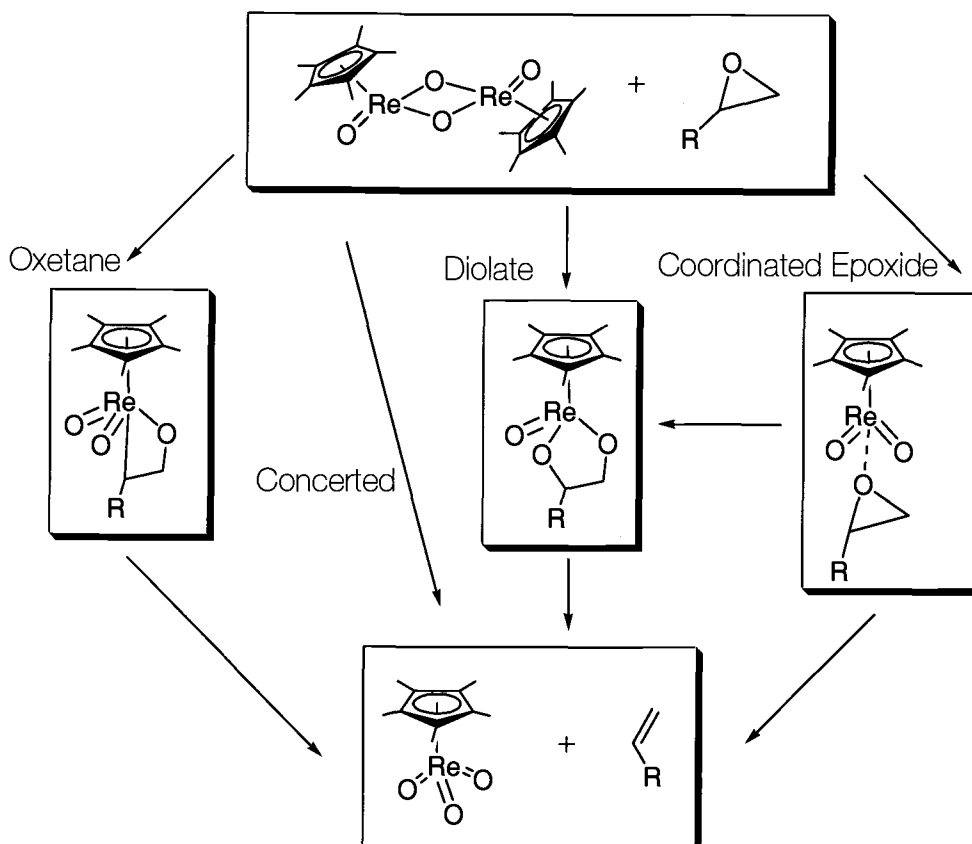
It is clear that the inherent reactivity of the Cp^*ReO_3 towards other rhenium species at elevated temperature is the main obstacle to the implementation of an efficient catalytic cycle. The obvious solution to this problem would be a total removal of Cp^*ReO_3 . This, however can not be achieved because Cp^*ReO_3 is regenerated every time the deoxygenation of epoxide occurs. Since all relevant reactions take place under kinetic control the turnover is determined by the relative rate of the reduction vs. that of conproportionation/oxidation. Faster reduction of Cp^*ReO_3 ought to lead to a decrease in a concentration of Re (VII) in solution, and consequently, to a lesser chance to undergo clusterization reaction. This hypothesis was tested by increasing the concentration of the PPh_3 ; a 2.4 fold excess led to an increase in conversion from <5% to 50%. (Table, entry 6). Although this required almost a saturated solution of PPh_3 and renders the overall reaction impractical it shows that the key to an improved system is to suppress the clustering phenomena.

INTERMEDIACY OF Re(V) DIOLATE IN RHENIUM MEDIATED EPOXIDE DEOXYGENATION

Mechanistically, deoxygenation of epoxides provides even greater number of possibilities than Re(V) diolate cycloreversion does. In addition to concerted cycloreversion and formation of a rhenaoxetane, Re(V) might coordinate epoxide; resulting complex then decomposes at rate limiting step. The final possibility is the

ring expansion either directly from epoxide/Re(V) or from the coordinated epoxide (Scheme 10).

Scheme 10.

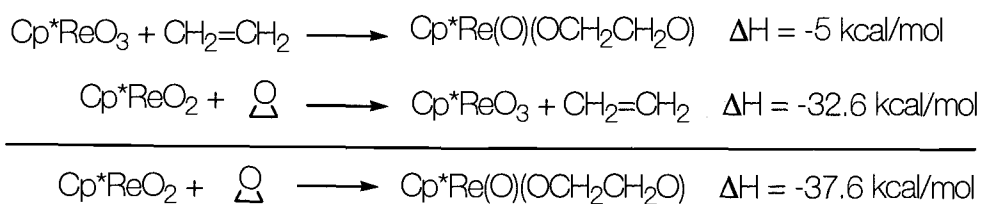


Although ring expansion by oxidative addition of Re(V) oxo compounds to epoxides have not been yet documented, CH₃ReO₃ does undergo facile conversion to Re(VII) oxo diolate when reacted with epoxides²⁷. In the presence of triphenylphosphine Re(VII) oxo diolate cycloreverts producing MTO and alkene.

To get a better insight into the mechanism of O-atom abstraction and the viability of the diolate formation we estimated the thermodynamics of the ring expansion. Using the reaction enthalpy of olefin epoxidation by Cp*ReO₃ from

recent DFT calculations done by Ziegler²⁸ and the enthalpy of dihydroxylation^{16a} we can compute the enthalpy of the epoxide insertion to be -37.6 kcal/mol (Scheme 11).

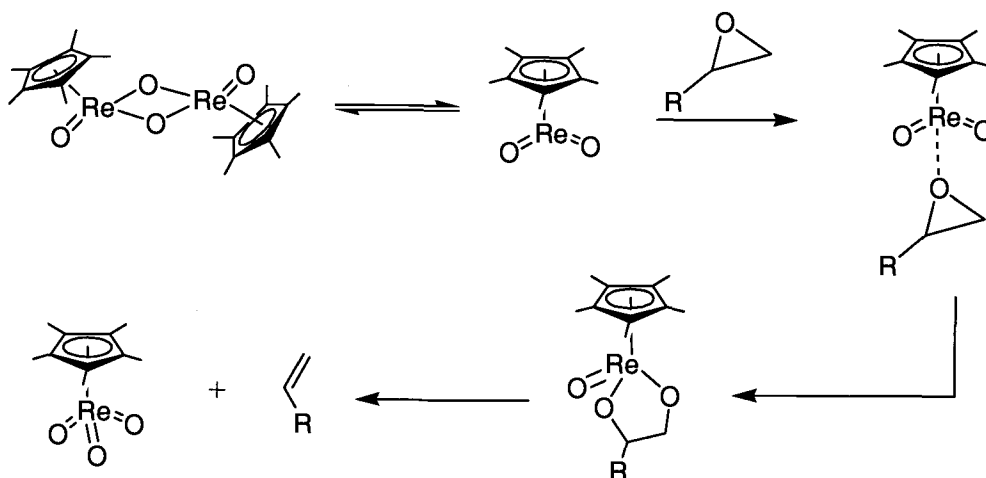
Scheme 11.



Such favorable thermodynamics and the absence of a apparent symmetry restrictions for ring expansion process suggests, according to the Hammond Postulate²⁹ that the diolate ought to be accessible kinetically.

One also must to keep in mind that under typical conditions of epoxide deoxygenation Re(V) diolates are unstable with respect to the alkene and LReO_3 . In general, higher temperatures are expected to favor a dissociative process (cycloreversion) more than an associative process (diolate formation). Therefore, a low temperature regime is expected to lead to a higher concentration of a Re(V) diolate. The choice of epoxide is also of great importance. Although it is tempting to test a strained epoxide that would easily ring expand but would have unfavorable thermodynamics with respect to a cycloreversion, we thought that an unbiased system would allow us to make more general observations (Scheme 12).

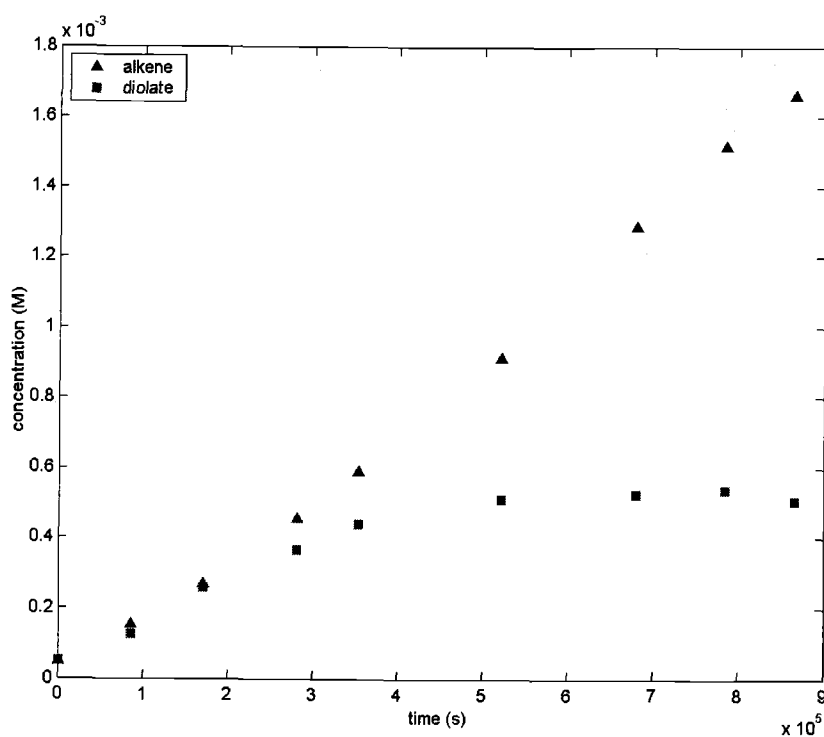
Scheme 12.



With these considerations in mind, $(\text{Cp}^*\text{ReO})_2(\mu\text{-O})_2$ obtained by reduction of Cp^*ReO_3 with polymer-supported triphenylphosphine was reacted with 1,2-epoxydecane at 72°C . As expected, at early stages of the reaction the formation of alkene was not detected. On the other hand, a group of signals around 4 ppm appeared and continued to grow as the reaction proceeded. At higher conversions olefin signals became clearly visible and also continued to grow. To confirm the signals at ~ 4 ppm indeed belonged to the diolate the latter was independently synthesized by reacting the Cp^*ReO_3 with triphenylphosphine and the diol^{30a}. The diolate produced that way was isolated as an inseparable mixture of *syn* and *anti* ($\sim 1:1$) diastereomers. In fact, the reaction of the Cp^* dimer with the epoxide also gives both, in approximately the same ratio. The concentration of the Re(V) decane-diolate reaches maximum at $\sim 30\%$ conversion of epoxide. After that point both rate of alkene production and the alkene concentration decreases. This behavior is indicative of Re(V) decane-diolate being responsible for alkene

production. We confirmed that by measuring Re(V) decanediolate cycloreversion kinetics at 72°C . It was first order with rate constant typical for aliphatic Re(V) diolates extrusion.

Figure 2. Kinetics of alkene production from Cp^* dimer + 1,2-decanepoxide.



Following decene production by NMR we were unable to see Cp^*ReO_3 signal, normally a sharp strong singlet at 1.6 ppm in benzene. This was not surprising in view of the efficient clustering process we discovered earlier. Indeed, NMR intensities estimation showed that 30% epoxide conversion corresponds roughly to 70% consumption of the dimer. A substantial amount of trinuclear cluster was isolated from the run.

At 100°C the system's behavior is qualitatively the same. The cycloreversion of the Re(V) decane diolate appears to be rate-determining; the only difference was much higher rates of the overall reaction. A related substrate, 1,2-dodecane epoxide shows very similar reactivity. The reaction was run at 112°C and the presence of a Re(V) dodecane diolate was clearly seen by NMR. Surprisingly, no reaction was observed with Cp*ReO₃, PPh₃ and norbornene oxide as evidenced by proton NMR.

The intermediacy of Re(V) diolate in rhenium mediated epoxide deoxygenation is also seen for pyrazolyl borate ligands. This time the reaction was done on a preparative scale. A suspension of (TkReO)₂(μ-O)₂ (Tk = *tetrakis*(pyrazolyl)borate), obtained by the reduction of TkReO₃ with PPh₃ in THF was reacted with 1,2-epoxidecane at 80°C. The diolate was isolated as a mixture of *syn* and *anti* isomers in 20% yield. We saw no evidences of clustering this time. The identity of the Tk Re(V) diolates were confirmed by an independent synthesis of the *syn*- and *anti*- diastereomers by reductive cyclization of TkReO₃ with diol and PPh₃^{30b}.

CHAPTER 3. SYNTHETIC STUDIES TOWARDS STABLE RHENAOXETANES

INTRODUCTION

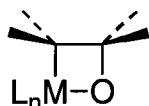
The intermediacy of metallaoxetanes in oxygen transfer reactions is one of the most significant recent controversies in mechanistic chemistry. A number of groups have actively participated in the discussion and made critical contributions to the topic^{4,31,32}.

A metallaoxetane is a four member metallocycle structurally similar to an oxetane but containing a metal fragment in place of one carbon moiety. A plethora of reactive pathways leading from a metallaoxetane and interconnecting a variety of major structural types or organic and organometallic compounds can be constructed. The most important pathways are (*vide infra*): (a) [2+2] cycloreversion to metal-oxo and alkene or a metal carbene and a carbonyl compound; (b) reductive elimination to an epoxide and, (c) if a metallaoxetane has an additional metal-oxo bond, ring expansion to a diolate. By applying the principle of microscopic irreversibility one may conclude that a metallaoxetane potentially intersects three fundamental types of chemical transformations: the methathesis, epoxidation and dihydroxylation.

What type of structural changes one would expect to see when going from oxetane to a hypothetical metallaoxetane (Scheme 13). First, both M-C and M-O of metallaoxetane are considerably longer than C-C and C-O bonds ($>2\text{\AA}$

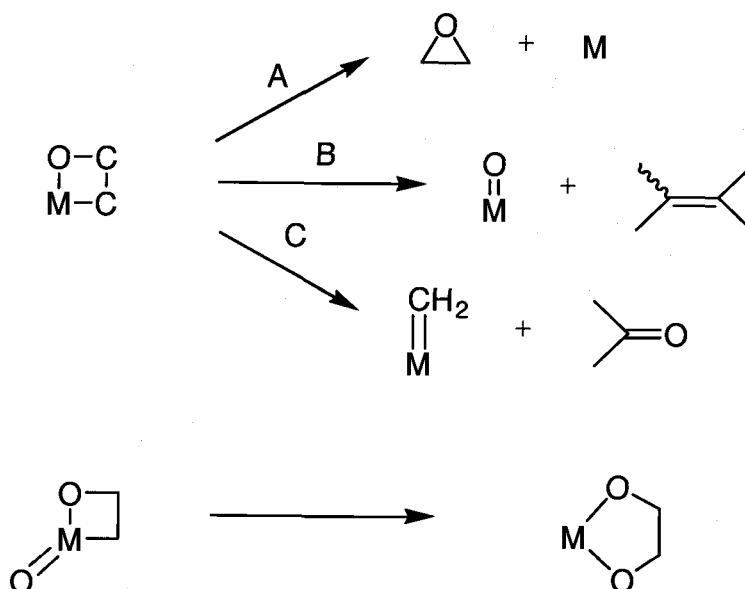
vs. 1.54 and 1.42Å, as evidenced by X ray of several stable metallaoxetanes). This is expected to lead to a reduced torsional strain in the metallocycle. Second, coordination flexibility of the metal center provides better means to accommodate angle strain, which is a second important source of strain in small carbocycles.

Scheme 13.



The question of relative stability of the metallaoxetane moiety must also be considered with respect to the possible pathway of its decomposition. Three general pathways can be identified: (A) reductive elimination with the formation of epoxide, (B) extrusion of alkene with concomitant formation of metal-oxo moiety, (C) extrusion of a carbonyl compound with the formation of metal carbene. Additionally, a metal center that possesses an oxo functionality might undergo a ring expansion to the five-membered diolate. Each of the net reactions might, in turn, proceed concertedly or through the formation of intermediates. (Scheme 14).

Scheme 14.

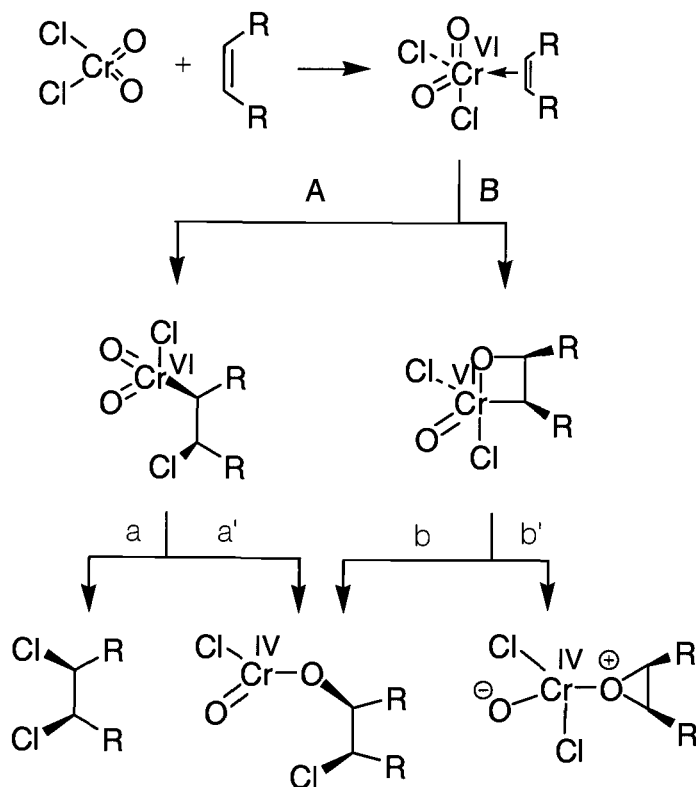


METALLAOXETANES IN THE LITERATURE

The first reference to oxometallic intermediate dates back to 1973 when De Pasquale³³ invoked the intermediacy of nickelaoxetane to explain the formation of ethylene carbonate from Ni-catalyzed reaction of ethylene and CO_2 . His hypothesis, however remained unappreciated until 1977 when Sharpless suggested the involvement of chromaoxetane to account for the formation of epoxides, chlorohydrins and dichlorides in chromyl chloride oxidation of alkenes⁹. In fact, two processes were proposed to compete. The reaction presumably starts with a pre-coordination of the olefin to form a Cr(VI) - alkene π complex. In path A the insertion of olefin into chromium-chlorine bond generates the alkyl chromium intermediate (Scheme 15). Reductive elimination would lead to dichlo-

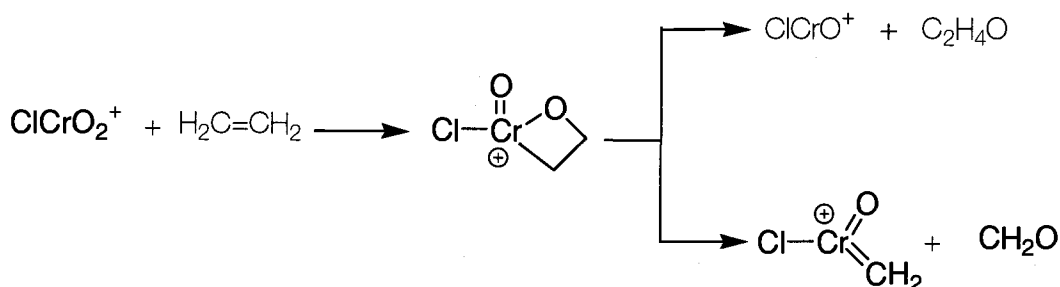
ride. An organometallic analog of Stevens or Wittig type rearrangement earlier documented for several phenyl oxovanadium species³⁴ and recently, for oxorhenium complexes by Mayer¹⁰ would furnish a chlorohydrin after a work up. Both of these processes would have to occur with retention of configuration at the carbon center in order to account for overall *syn* addition observed experimentally. Reductive eliminations to form carbon-halogen bonds are well known to proceed with retention at carbon. In carbanion-type [1,2]-shifts the observed stereochemistry ranges from complete retention of configuration to complete racemization^{35,36}.

Scheme 15.



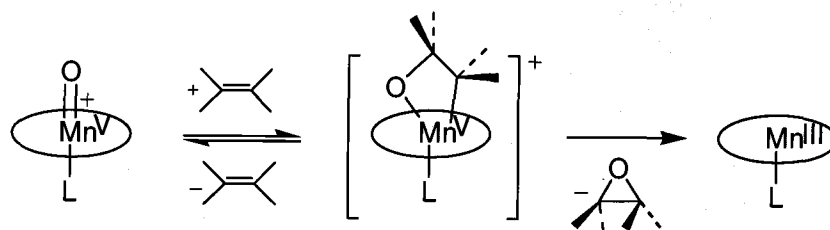
In path B a chromaoxetane (VI) is formed via [2+2] cycloaddition. Reductive elimination produces a coordinated epoxide or the chlorohydrin precursor. Both processes would occur with the retention of configuration. No direct experimental evidence of a chromaoxetane intermediate was established. However, computational work by Rappe and Goddard provided strong support for Sharpless hypothesis³⁷. GVB/CI theory predicted chromaoxetane (VI) formation is 14 kcal/mol downhill compared to the starting materials. Formation of ethylene oxide leads to further stabilization by 21 kcal/mol. The driving force for this reaction is the formation of chromium-oxo triple bond. Singlet and triplet chromium (IV) diolates were uphill by 56 and 10 kcal/mol correspondingly. A further support for chromaoxetane comes from the reaction of ClCrO_2^+ and ethylene in the gas phase³⁸. Here, the intermediacy of chromaoxetane provides a straightforward explanation to the formation of all the products in the reaction, particularly chromium carbene. The ethylene oxide is formed by a reductive elimination and the other products by a retro [2+2] cycloaddition (Scheme 16).

Scheme 16.



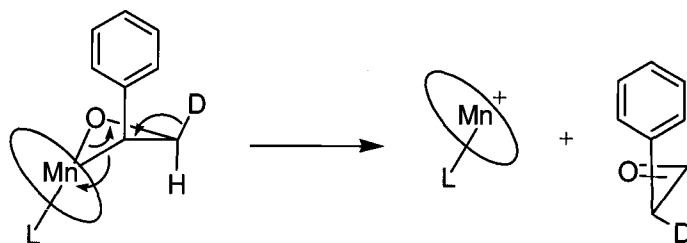
The metallaoxetane hypothesis was soon adopted to explain the details of the alkene oxidation with oxometallo porphyrins (Scheme 17). Kinetic studies by Collman on the oxomanganese porphyrins revealed Michaelis-Menten kinetics³⁹. Lineweaver-Burk analyses established that electron-rich alkenes bind more efficiently than the electron poor ones. Partial loss of stereochemical integrity as often seen in metallaoxo porphyrins or salen metallaoxo catalysts was attributed to the side reactions.

Scheme 17.



From the competitive oxidation of norbornene and *cis*-cyclooctene several important kinetic observations were made: (i) the reaction rate is independent of both the initial concentration of the alkene and the oxidant; (ii) the appearance of the epoxide is a zero-order process; (iii) one alkene inhibits the epoxidation of the other; (iv) rates are different for different alkenes. When styrenes were used as substrates, phenylacetaldehyde was found in the reaction mixture, along with the expected styrene oxide. Isotopic labeling showed that deuterium at the beta position of the styrene ends up at the benzylic carbon in the aldehyde (Scheme 18).

Scheme 18.



The data was rationalized on the basis of the reversible manganaoxetane formation. Once formed, the metallaoxetane then could undergo concerted collapse to form an epoxide or rearrange to aldehyde in the rate-determining step. Lewis acid catalyzed rearrangement of the epoxide was not rigorously ruled out. However, the generation of radicaloids or carbonium ion species is unlikely given the small difference in rates for different substituents.

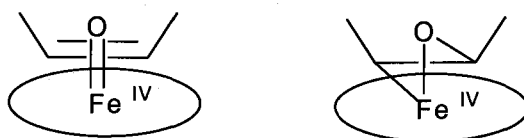
A reinvestigation of the system provided strong arguments against metallaoxetane hypothesis⁴⁰. By kinetic computer simulation of the mechanistic scheme proposed by Collman, Bruice *et al.* established that a steady-state concentration of the metallaoxetane should be expected to be between 75% and 100% of the total concentration of the metalloporphyrin which consequently should lead to its detection. In accordance with Groves⁴¹ the intermediacy of a radical cation was proposed⁴².

The metallaoxetane hypothesis was disputed on steric grounds as well. In the oxidation of adamantylideneadamantane where the formation of the metallaoxetane moiety is sterically impossible, the epoxidation with iron, chromium and

manganese porphyrins proceeds smoothly. It was concluded that the carbocation mechanism was a better description of the process⁴³.

The main limitation of the previously mentioned studies advocating the intermediacy of a metallaoxetane was the absence of any spectroscopic characterization. Direct observation of an intermediate in the olefin epoxidation by oxo-iron(IV) porphyrin was reported by Groves and Watanabe⁴⁴ (Scheme 19). The oxidation of either Fe(TMP)Cl or Fe(TMP)OH (TMP = 5,10, 15, 20-tetramesitylporphyrin) with mCPBA followed by addition of cyclooctene produced a distinct color change and a bathochromically shifted visible spectrum of an intermediate species. This intermediate decayed in a first order fashion with $k = 2.8 \cdot 10^{-4} \text{ s}^{-1}$. The observed rate constant correlated with σ^+ with a large negative ρ^+ (-1.9). The formation of an intermediate was found to be reversible. In the absence of the methanol or imidazole the release of the epoxide was very sluggish. When the reaction mixture was quenched with methanol-styrene a very fast release of cyclooctene oxide was observed. No styrene oxide is formed under those conditions. It was concluded that in the presence of methanol the formation of an intermediate must be rate limiting as well as product determining.

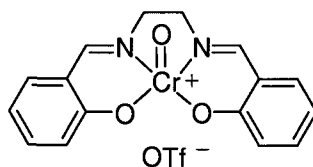
Scheme 19.



Initial electron transfer process as proposed by Ortiz de Montellano⁴⁵ for cytochrome P-450 is consistent with a large negative ρ^+ and two likely possibilities for the structure of an intermediate are an olefin π complex and a metallaoxetane. Unfortunately, no conclusive evidence for the existence of either one was presented later.

The discovery of asymmetric epoxidation mediated by (salen)Mn complexes led to revived interest in metallaoxetanes. The first transition metal salen oxo complex, the Cu-salen was prepared by Combes⁴⁶ in 1889. Later, Kochi isolated and characterized an oxo Cr-salen complex (Scheme 20) by X-ray crystallography⁴⁷. They also demonstrated that oxo Cr-salen complexes transfer one oxygen atom to olefins giving epoxides.

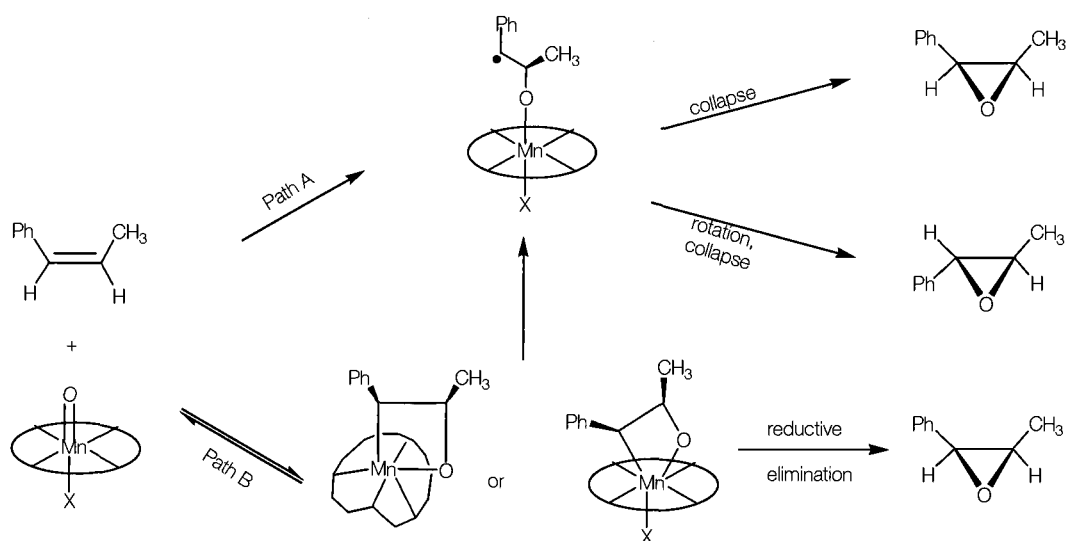
Scheme 20.



Related Mn-salen complexes proved to be especially useful for asymmetric epoxidation⁴. Despite the fact that an oxo Mn-salen complex has never been isolated it is widely considered to be an active O-atom transfer species in olefin epoxidation. When the substrate contains an aryl, alkenyl, or alkynyl group, *cis/trans* isomerization is generally observed, suggesting the formation of radical intermediates. Katsuki et al. reported that in Mn-salen catalyzed asymmetric epoxida-

tion of certain olefins, a non-linear relationship between reaction temperature and enantioselectivity was observed^{32b}. It was found that the enantioselectivity is susceptible to the electronic nature of the aryl substituents in the salen ligands but ee does not necessarily correlate with the Hammett σ values. The experimental data implicate the reversible formation of an intermediate which was proposed to be a manganaoxetane. Jacobsen *et al.* criticized the study pointing out the small variations in enantiomeric excess (<10%), the absence of critical experimental details in Katsuki's publication, such as conversion, yield and the solubility of the stoichiometric oxidant⁴⁸. In their own study on similar substrates, the Eyring plot correlated linearly with asymmetric induction over a range of 100 degrees.

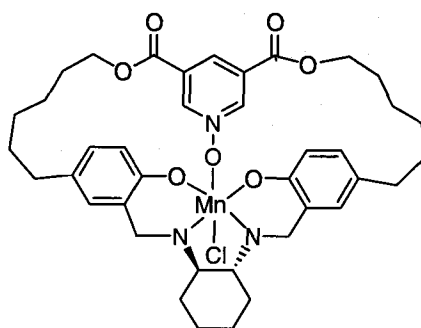
Scheme 21.



Jacobsen argued that the formation of metallaoxetane would require either highly distorted salen ligand in 6-coordinated Mn environment, which is unprecedented, or 7-coordinate Mn (Scheme 21). The latter question was addressed by analyzing

the effect of amine N-oxide additives. Earlier it was established that the addition of amines N-oxides have a highly beneficial impact on rates, yield and enantioselectivities of epoxidation. Assuming the oxidation to the $O=Mn^V(\text{salen})$ is rate limiting, Jacobsen proposed that the observed rate acceleration can be attributed to the complexation of the amine N-oxide to the metal center during generation of reactive oxo intermediate. By synthesizing a catalyst strapped with a pyridine N-oxide derivative (Scheme 22) and showing that: (i) the epoxidation rate with strapped catalyst is not influenced by adding 4-phenylpyridine N-oxide (4-PPNO); (ii) similar rates for strapped catalyst and (unstrapped catalyst + 4-PPNO); it was concluded that the axial ligation to the metal influences every step of the catalytic cycle. The 7-coordinate intermediate was excluded from the consideration on steric grounds. The direct formation of the radical was concluded to be a better explanation of the experimental observations.

Scheme 22.



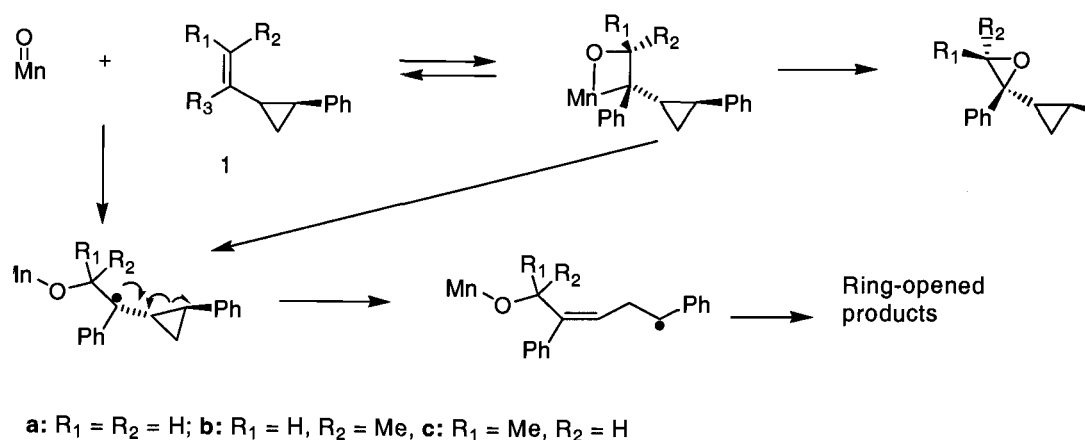
Several features complicate the straightforward interpretation of the data for epoxidation with a strapped catalyst. First, careful examination of the kinetic data reveals quite different behavior of the strapped and unstrapped system. At

the beginning of the reaction, the disappearance of styrene in unstrapped system is much faster; when rates of the two become equal the unstrapped system practically reaches a plateau while the conversion in the strapped system continues to grow at roughly steady rate. Second, other data relevant to the product determining step such as enantioselectivity, yield, *cis/trans* ratio was not reported. A more conservative approach to the interpretation of the strapped catalyst kinetics leads to a more limiting conclusion that an amine N-oxide is participating in the rate-limiting step, whatever it might be. If the rate limiting step and the product limiting step are different which is likely to be the case⁴⁹ then the participation of amine N-oxide in the product limiting step cannot be inferred from the conversion of the starting material vs. time data alone. Consequently, metallaoxetane formation assisted by the dissociation of an amine N-oxide can not be rigorously ruled out.

The main challenge to a radical mechanism is the question of how an essentially flat salene ligand can impose such an exceptional enantioselectivity with a wide range of substrates. An alternative explanation, put forth by Norrby⁵⁰ and based on the reversible formation of a metallaoxetane rationalizes high ee from epoxidation as a direct consequence of the formation of the four-member metallocycle. It leads to a puckering of the salen ligand and creation of a chiral pocket. Calculations of the energies of the diastereomeric metallaoxetanes using MacroModel/MM3 also allowed Norrby to rationalize observed isotope effects. Further support for this hypothesis was seen from phenyl cyclopropane radical probe experiments. In this experiment (Scheme 23), a number of substituted styrenes as well as cyclopropane-modified alkenes were epoxidized with racemic

Jacobsen (salen)Mn catalyst. Control experiment showed similar rates for styrenes and cyclopropane-modified styrenes. Styrenes with alkyl and aryl substituents (stilbenes) yielded a mixture of *E* and *Z* epoxides. However, none of the

Scheme 23.

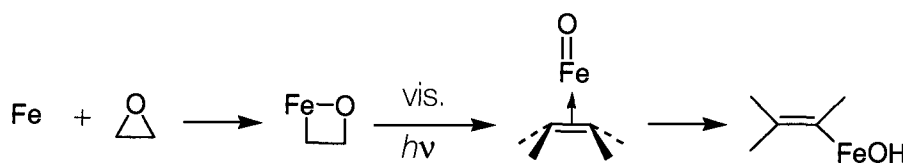


styrenes equipped with a radical probe formed epimeric products! Both 1a and 1b were stereospecifically and quantitatively converted to the epoxides while 1c gave cyclopropane ring opening product. This indicates that radical formation pathway operates for *Z* alkenes and either argues against radical formation in the case of *E* alkenes, or suggests the generation of radical intermediates with unusually short lifetimes. On the other hand, the dichotomic behavior of conjugated alkenes is readily rationalized by the metallaoxetane pathway. Here, the reversible manganoxetane formation is followed by either reductive elimination to stereospecifically yield epoxide or by a homolytic bond cleavage that results in the formation of a radical which subsequently rearranges. When the phenylcyclopropane radical trap is absent the resulting radical lives long enough to undergo a bond rotation giving observed for styrenes and stilbenes *E/Z* isomerization.

A very similar mechanism was proposed by Schwartz⁵¹ to explain the stereochemistry trends and a partial loss of stereospecificity in epoxide deoxygenation by reduced metallocenes. When certain metallocenes $M(\text{Cp})_2\text{X}_2$ ($M = \text{Mo}, \text{W}, \text{Ti}, \text{Zr}, \text{X}_2 = \text{Cl}_2$) are reduced with sodium amalgam the resulting "MCP₂" was proposed to effect an oxidative epoxide ring opening. The resulting biradical either cyclizes to the metallaoxetane or first undergoes a bond rotation, inversion and then cyclizes. The reductive elimination furnishes alkene and a $L_2\text{M}=\text{O}$ species. This mechanism, where the sequence of steps is reversed compared to the previous example allows one to rationalize a decrease in stereospecificity with an increase in the size of the ligand. The less crowded environment at the metal center facilitates ring closure while small substituents expedite the C-C bond rotation.

Spectroscopic evidences for the formation of a ferraoxetane were obtained by Kafafi and co-workers⁵².

Scheme 24.

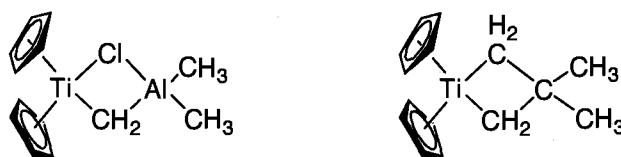


Reaction of atomic iron with ethylene oxide in an Ar matrix leads to the formation of an intermediate that was assigned a ferraoxetane structure on the basis of FT-IR. Irradiation of this intermediate results in the expected photochemical [2+2] cycloreversion, giving iron oxide (II) and ethylene π complex (Scheme 24).

The structural assignment of the proposed intermediates was verified by isotopic substitution (C_2D_4) and *ab initio* calculations.

Another important class of reagents where metallaoxetane hypothesis received strong support is Tebbe's type reagents, " $L_nM=CR_2$ ". Tebbe's reagent is a nucleophilic carbene complex, akin to the Schrock carbenes⁵³. It is prepared by reaction of titanocene dichloride with Me_3Al (Scheme 25). In the presence of

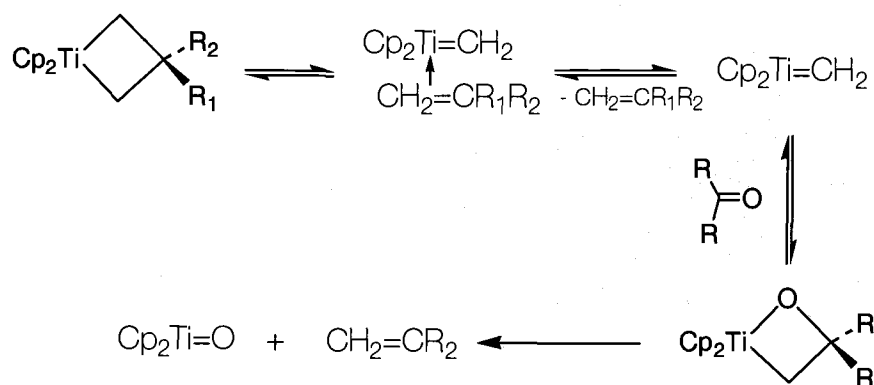
Scheme 25.



pyridine it is converted to what is believed to be $Cp_2Ti=CH_2$. An all-carbon metallocycle is even more stable than its aluminum analog and has been characterized by X-ray crystallography. The reaction of titanocyclobutane with carbonyl compounds is believed to involve the reversible formation of $Cp_2Ti=CH_2$. Alkene dissociation and possible pre-coordination of the carbonyl compound is followed by titanaoxetane formation. Retro [2+2] cycloaddition produces titanocene oxide and an olefin (Scheme 26).

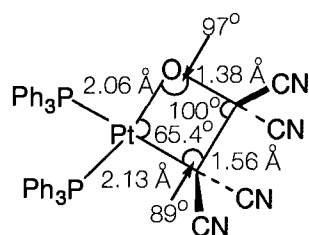
The formation of a strong titanium-oxo bond is the ultimate driving force of the Tebbe olefination. An *ab initio* study by Upton and Rappe showed that [2+2] cycloreversion/cycloaddition has a small activation energy⁵⁴. Furthermore, olefin-methylidene complex is hardly a minimum on the potential energy surface.

Scheme 26.



A number of stable metallaoxetanes have been made and exhaustively characterized. When tetracyanoethylene oxide is reacted with PtL_4 ($\text{L} = \text{PPh}_3, \text{AsPh}_3$) the corresponding platinaoxetane results⁵⁵ (Scheme 27). The four membered cycle is significantly distorted, as evidenced by X-ray crystallography. The atoms in the Pt coordination sphere (P, P, C, O) are essentially coplanar. The main feature is the small Pt-O-C internal angle (65.4°) which, perhaps is due to the bond compression caused by Van-der Waals repulsion between triphenylphosphine groups.

Scheme 27.



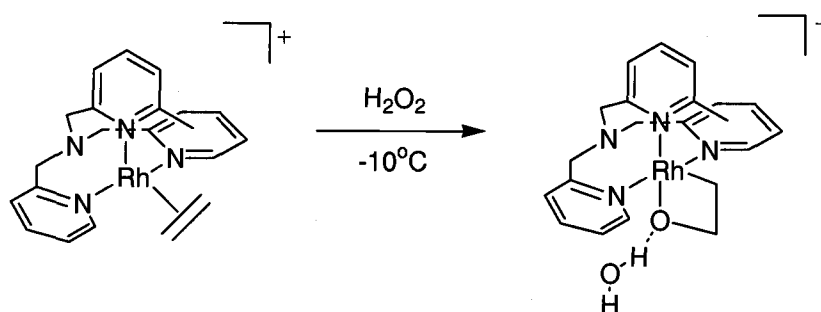
Two mechanisms were proposed for this reaction^{55,56}. First, a nucleophilic attack of PtL_2 on the epoxide gives a zwitterion which then closes to the platinaoxetane. An alternative mechanism includes the pre-coordination of PtL_3 to the epoxide. This results in swapping of the frontier orbitals. The HOMO of the complex becomes Pt-based and the LUMO becomes epoxide-based. The bonding interaction between Pt and the carbon of the epoxide leads to the simultaneous dissociation of the ligand and to the formation of the platinaoxetane moiety.

Several iridium metallaoxetanes have been reported. Bergman⁵⁷ reported that photochemically stimulated C-H insertion of $\text{Cp}^*(\text{PMe}_3)\text{IrH}_2$ into *t*-BuOH with subsequent treatment with CHCl_3 and a hindered base led to an iridaoxetane. The metallocycle is very nucleophilic and readily reacts with electrophiles. Carbon dioxide, for example, rapidly inserts into Ir-O bond giving metallacarbonate.

Recent examples of metallaoxetane formation directly from catalytically oxidizing conditions include Rh(III) and Ir oxetanes (Scheme 28). In the elegant study by Gal and co-workers^{58a} the oxidation of $[\text{N}_4\text{Rh}(\text{C}_2\text{H}_4)]^+$ [N_4 = N,N,N,N-tetrakis(2-pyridylmethyl)amine] with H_2O_2 gave a rhodaoxetane which was characterized by NMR and X-ray crystallography. ^1H NMR spectrum shows a triplet at 4.97 ppm ($^3J_{\text{H,H}} = 7.5$ Hz) and a triplet with 7.5 Hz and rhodium coupling (2.5 Hz) at 2.35 ppm. Further characterization indicated that two molecules of metallaoxetane are linked through the molecule of water via hydrogen bonding. The

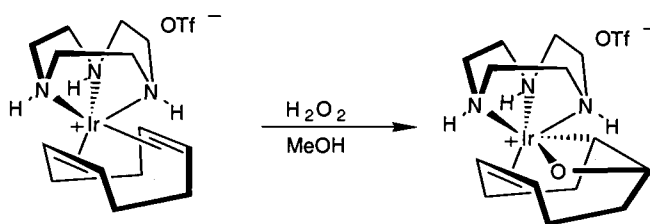
observed hydrogen bonding of water to the 2-rhodaioxetane through the oxetane oxygen parallels the frequently observed hydrogen bonding between alcohols and late transition metal alkoxides. This is the first and the only example of unsubstituted metallaioxetane.

Scheme 28.



Flood^{58b} reported preparation of an iridaioxetane from a somewhat similar iridium-olefin complex (Scheme 29). Authors, however were not able to obtain X-ray quality crystals for synthesized iridaioxetane.

Scheme 29.

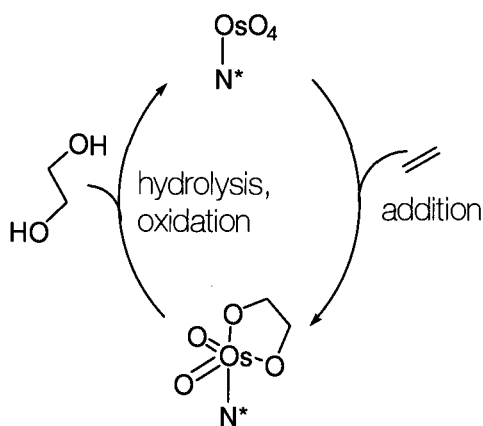


The metallaioxetane hypothesis in osmium-catalyzed dihydroxylation occupies a special place in mechanistic organometallic chemistry. The detailed account of the mechanistic studies will be given in the next chapter. Here we will

present the general description of the problem and the relevance of Os chemistry to rhenium work.

The osmium-catalyzed asymmetric dihydroxylation of olefins represents one of the most outstanding achievements of transition metal catalysis. As a stoichiometric reagent, OsO_4 reacts with practically all olefins and tolerates a great variety of functional groups⁵⁹. The reaction typically proceeds with high yields. In view of high toxicity and the high cost of OsO_4 the catalytic version of the reaction was developed as early as in 1912⁶⁰. The catalytic cycle is based on the hydrolysis of osmium(VI) diolates followed by the reoxidation of Os(VI) to Os(VIII) with the stoichiometric oxidant (Scheme 30).

Scheme 30.

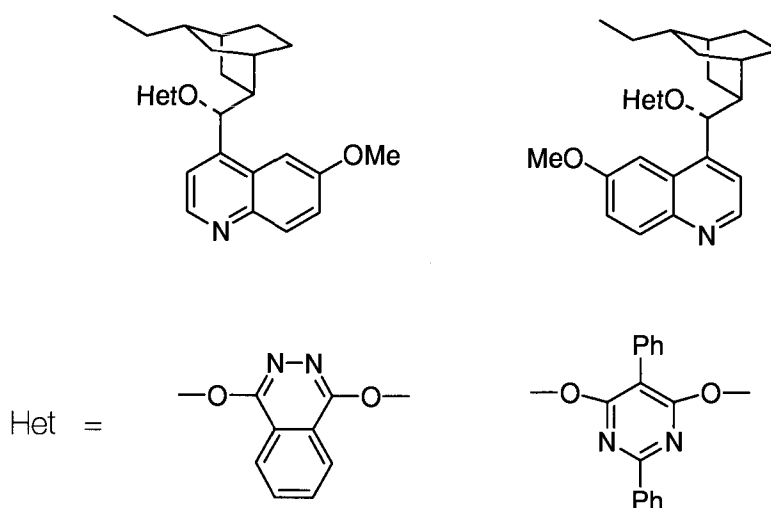


A number of stoichiometric oxidants have been successfully used such as KClO_3 ⁶⁰, H_2O_2 ⁶¹, $t\text{BuOOH}$ ⁶², NMO ⁶³, Me_3NO ⁶⁴, $\text{K}_3\text{Fe}(\text{CN})_6$ ⁶⁵.

The second important feature is the rate acceleration in the presence of a nitrogen-containing ligand⁶⁶. The nitrogen-containing ligand is clearly present in the transition state as evidenced by its inclusion in the rate law of amine assisted

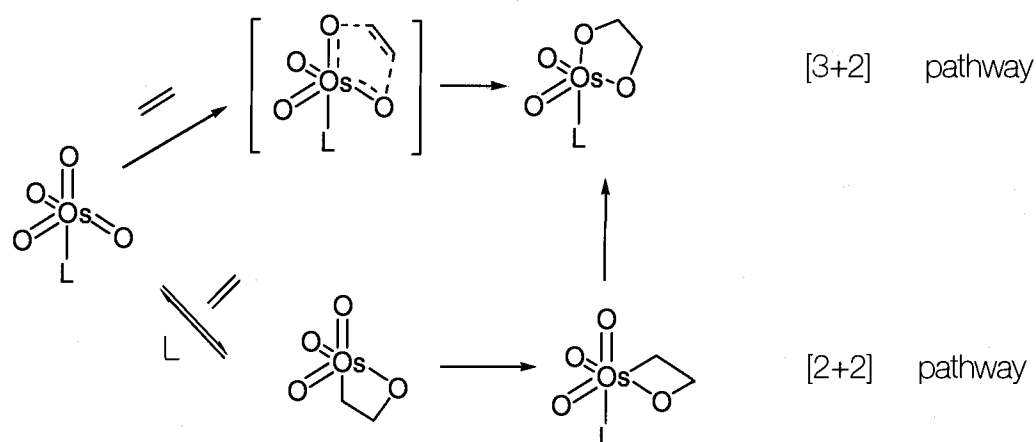
dihydroxylation⁶⁷. Consequently, in the presence of chiral amines the reaction becomes enantioselective. Several generations of chiral amines have been developed. High enantioselectivities can be reliably obtained with cinchona alkaloids linked to phthalazine or pyrazine heterocycles^{31a} (Scheme 31).

Scheme 31.



Two distinct reaction mechanisms of the dihydroxylation reaction were advanced. The concerted [3+2] mechanism shares the main features with 1,3 dipolar cycloaddition. Although 1,3 dipolar cycloadditions are well precedented in organic chemistry⁶⁸ the question whether transition metal-catalyzed pericyclic reactions are truly pericyclic is still unclear⁶⁹. The alternative proposal put forth by Sharpless is formally a [2+2] cycloaddition superficially analogous to the Paterno-Buchi reaction. Here, the Os=O reacts with an olefinic double bond forming osmaoxetane.

Scheme 32.



The presence of d-orbitals on a transition metal center partially lifts the symmetry restrictions for $2\pi + 2\pi$ process and opens up the thermal pathway. Alternatively, the pre-coordination of the double bond to the metal allows for a stepwise pathway to the metallocycle (Scheme 32). *Ab initio* calculations show that, for example, the formation of a titanocyclobutane from $\text{Cl}_2\text{Ti}=\text{CH}_2$ and $\text{CH}_2=\text{CH}_2$ proceeds virtually with no activation barrier^{54,70}. Also, it was found that electron rich alkenes generally react faster than electron poor alkenes. This was initially attributed to the complexation of the olefin to the somewhat Lewis acidic osmium and boosted [2+2] hypothesis.

It is important to point out that both proposed pathways are able to explain several important features of the reaction, such as *syn* addition and the kinetic behavior. A useful mnemonic system has been developed to reliably predict the stereochemical outcome of the reaction⁷¹.

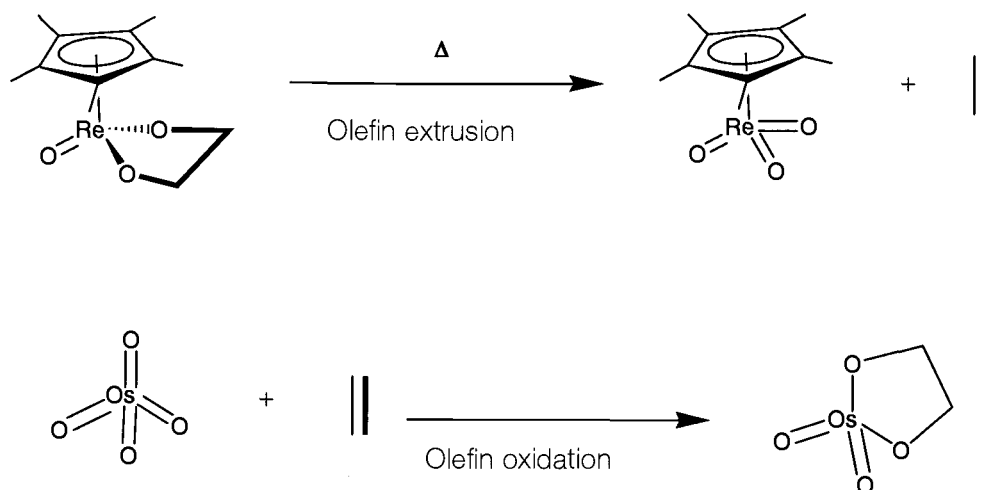
At the same time, neither mechanism provides a complete explanation of the electronic effects, most notably, the curved Hammett plots^{31c}. Asymmetric

dihydroxylation which is usually run under biphasic conditions also demonstrates overall complexity of the system. Apart from the Os diolate formation assisted by the nitrogen base there are at least four additional steps: "in and out" phase migrations, reoxidation and hydrolysis.

STUDIES POINTING TO THE STEPWISE CYCLOREVERSION IN RE(V) DIOLATES

One of the approaches to this complex mechanistic problem is to find a model system which shares the same essential mechanistic features, yet is substantially easier to analyze. LReO_3 is isoelectronic to OsO_4 ($5d^0$) and displays mechanistically significant similarity to OsO_4 chemistry (Scheme 33).

Scheme 33.



While OsO_4 easily adds to alkenes forming diolates, LReO_3 ($\text{L} = \text{Cp}^*$, Tp^+) is at its thermodynamic balance point with respect to the diolate formation. The incorporation of strain in the olefinic double bond shifts equilibrium towards rhenium

diolate formation^{16b}. The rhenium diolates of unstrained olefins, upon heating, undergo entropy driven cycloreversion. Both cycloaddition of strained alkenes and the cycloreversion are completely stereospecific, extending mechanistic relevance of LReO_3 system to osmylation with OsO_4 . Mechanistically, the cycloreversion is the microscopic reverse of cycloaddition, and consequently, all the conclusions drawn for cycloreversion are applicable to the cycloaddition.

Given the mechanistic similarity to osmylation the intermediacy of metal-laooxetane was also implicated in rhenium diolate cycloreversion. An extensive experimental work by Gable argued against concerted cycloreversion and provided circumstantial evidences in favor of a stepwise process.

The first line of evidence comes from conformational studies of Cp^*Re diolates⁷². A series of mono- and di- substituted alkyl diolates were examined by ^1H NMR. The dihedral angles formed by the carbons on the diolate ring and their substituents were obtained from the H-H coupling constants and the Karplus relationship. As expected, rhenium diolates adopt a staggered conformation and the ring is very flexible. It was found that the entropy of activation correlated with the dihedral angle. The flatter the ring, the higher and more negative the entropy of activation becomes. This is inconsistent with the concerted cycloreversion which would favor the eclipsed conformation to maximize orbital overlap.

The second argument is based on the combination of kinetic isotope and strain studies⁷³. Systematic kinetic studies revealed that the strain in alkenes had a significant effect on the enthalpy of activation. However, the extrusion of strained alkenes was virtually insensitive to strain. This, coupled with observed secondary

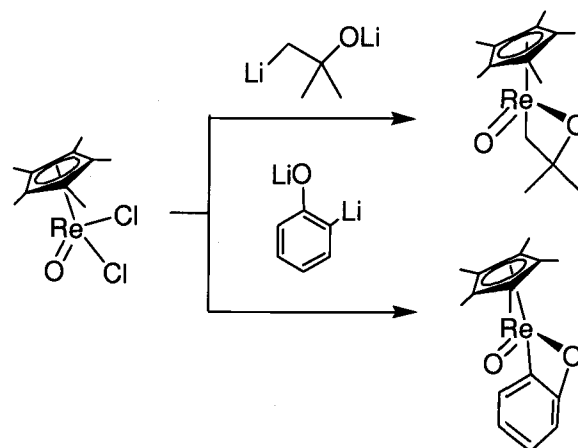
deuterium isotope effect for ethylene extrusion ($k_H/k_{D4} = 1.25$ at 100°C) suggests advanced C–O bond breaking at the transition state without developing much of a sp^2 character. This combination is inconsistent with a concerted process but can be rationalized by the rate-limiting formation of a rhenaoxetane.

SYNTHETIC APPROACH

The following work was intended to directly probe the involvement of the rhenaoxetane in rhenium diolate cycloreversion. A rigorous test for the existence of the rhenaoxetane (VII) would be to independently synthesize this intermediate and to examine whether its kinetic behavior is consistent with that of the rhenium diolate cycloreversion.

Initially, we planned to synthesize a rhenium (VII) rhenaoxetane in two steps: the synthesis of rhenium (V) rhenaoxetane followed by the oxidation of Re(V) to Re(VII) . We envisioned that for the Re(V) complex the synthesis can be carried out through the substitution of the halides in the $\text{Cp}^*\text{Re(O)Cl}_2$ using either dilithioethanol or other organometallic derivatives with the same structural motif (Scheme 34). The resulting rhenaoxetane (V) would then be oxidized at low temperature to Re(VII) using standard O-atom transfer reagents such as DMSO or NMO as had been demonstrated by Mayer et al⁷⁴.

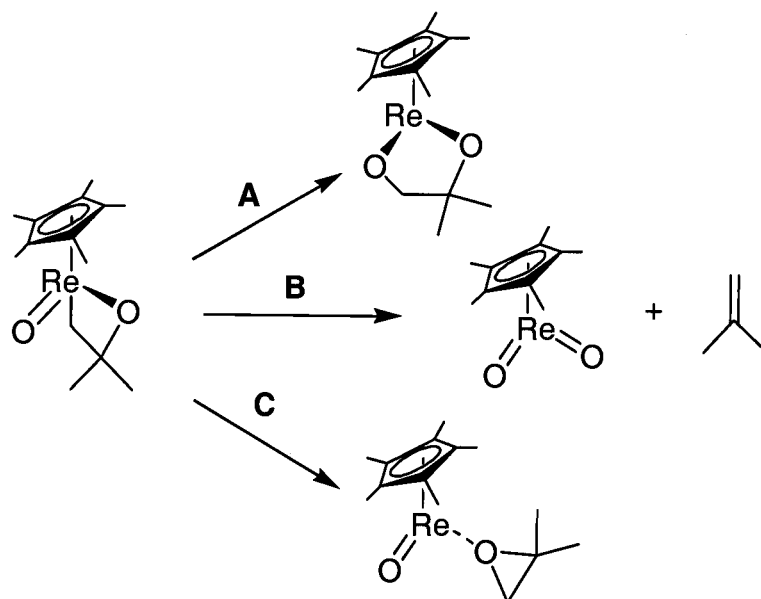
Scheme 34.



From the start we anticipated two possible complications. First, the problems arising from the alkylations of Cp*Re(O)Cl₂ or Cp*ReCl₄ with organolithium reagents⁷⁵ and the reduction of TpRe(O)Cl₂ during the alkylation with alkyl and aryllithiums reported by Mayer^{76,10} hinted at possible complications from electron transfer processes. Based on literature precedent we hoped that this could be avoided by using less basic organometallic reagents. Indeed, both Herrmann and Mayer reported successful alkylations of Re(V) halides with ZnR₂, SnR₄ (partial alkylation) and Grignard reagents. The most notable example is the formation of the rhenia(V)-cyclobutane from Re(V) oxo chloride and a di-Grignard⁷⁷.

Second, if formed, the rhenia(V)-oxetane might undergo a number of subsequent reactions. In the absence of the computational data three processes seemed mechanistically feasible (Scheme 35): (A) ring expansion to the rhenium(III) diolate, (B) [2+2] cycloreversion, or (C) the reductive elimination to the coordinated epoxide (Scheme 35).

Scheme 35.



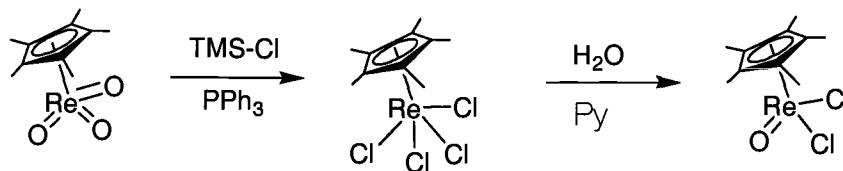
The formation of Cp*Re(III) diolate and Cp*Re(O) as alkyne educts is well established⁷⁸ in the literature. The existence of Cp*ReO₂ was proven kinetically²² though it prefers to dimerize. The mechanistic implication of the pathways A and C, as the potential ways of metallaoxetane decomposition will be discussed later. However, [2+2] cycloreversion (the pathway B) can be effectively precluded by benzannulation. The fragmentation of this species with the extrusion of the benzyne should require a high activation barrier and, therefore give us a better chance to isolate this compound. We, therefore, envisioned the benzorhenaoxetane to be our prime synthetic target. The main benefit of having synthesized the benzorhenaoxetane is the possibility to spectroscopically characterize this species. With the spectroscopic information available we could further pursue the synthesis and characterization of our ultimate target – the alkyl rhenaoxetane.

Starting materials. Improved practical synthesis of Cp*ReO₃

To bring about the desired transformation we had to prepare *ortho*-dilithiophenolate. This was accomplished by *ortho* lithiation of phenol as described by Posner and Canella⁷⁹. Because of the incomplete reaction (~30% yield, as evidenced by quenching the reaction mixture with CO₂ and the isolation of the salicylic acid) we sought a better alternative. The halogen-lithium exchange of *o*-bromophenol with BuLi and subsequent quenching with D₂O furnished *ortho*-deuterated phenol in 85% yield.

We also needed a sufficient quantities of Cp*Re(O)Cl₂ which can be conveniently made from Cp*ReO₃ by reduction and treatment with TMSCl¹⁹ (Scheme 36)

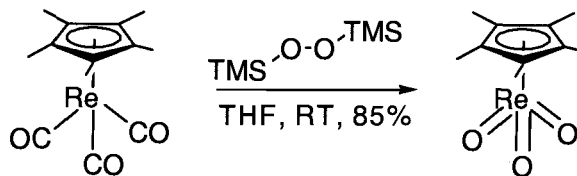
Scheme 36.



The synthesis of Cp*ReO₃, which serves as a starting material for Cp*Re(O)Cl₂ and many other Cp*-containing Re(V) oxo complexes experienced a steady improvement over the last decade. Unfortunately, the best synthetic procedures in terms of yield are the ones that are the least safe. For best yields, Cp*Re(CO)₃ is oxidized by either 100% hydrogen peroxide/MTO system, or by manganese heptaoxide which is highly explosive⁸⁰. The more practical solutions

used in our lab were oxidation with either 30% H₂O₂/benzene mixture⁸¹ or with ozone⁸². Both procedures give about 50% yield. A recent report from Sharpless *et al.* on the use of perrhenic anhydride and *bis*-TMS peroxide as a stoichiometric oxidant to bring about epoxidation of alkenes⁸³ prompted us to test Re₂O₇(cat) / *bis*-TMS peroxide system on the Cp*Re(CO)₃ (Scheme 37). This reaction proceeds smoothly in strictly anhydrous THF and yields of 85% can be obtained. *bis*-TMS peroxide can be readily made from hydrogen peroxide–urea complex and *bis*-TMS-urea in high yield and purity⁸⁴. It is stable in the presence of the transition metals, it is thermally stable up to its boiling point and can be stored almost indefinitely.

Scheme 37.

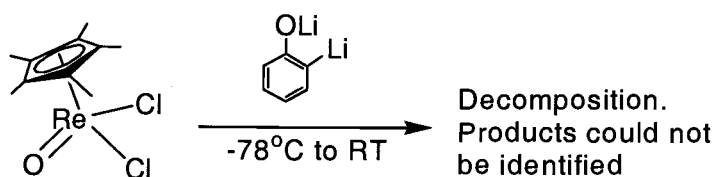


Reaction of Cp*Re(O)Cl₂ with *ortho* - Li, Mg and Zn nucleophiles

When Cp*Re(O)Cl₂ reacts with the lithium *ortho*-lithiophenolate the substitution of the halides takes place as evidenced by the precipitation of lithium chloride (identified by IR). Unfortunately, an extensive decomposition of the organometallic substrate results. We have been unable to identify the products. We suspected the electron transfer from the organolithium compound to the Re(V) center causes reduction of the metal, parallel to what Mayer observed while

attempting to alkylate $\text{TpRe}(\text{O})\text{Cl}_2$ ^{10,76}. In his work, alkyl and aryllithium gave no alkylated products whatsoever, while the treatment of with Et_2Zn resulted only in partial rhenium alkylation. It is conceivable that under the conditions of the experiment there is a competition between the reduction and a halide substitution. It is also likely that the organolithium reagent is highly aggregated in solution because of its high charge and a relatively small size (the related benzylic di-Grignard is polymeric⁸⁵). However, the addition of HMPA to the reaction mixture did not improve the situation. The variation of the solvent (THF, DME, diehtyl ether) and temperature did not prevent the decomposition either. Our next approach was to use a softer nucleophile. Unfortunately, the conversion of dilithium salt into its Mg or Zn derivative through the reaction of the lithium *ortho*-dilithiophenolate with anhydrous MgCl_2 or ZnCl_2 and subsequent addition to the oxo dihalide did not change the course of the reaction. The most puzzling feature was the loss of the Cp^* ligand on Re, resulting in a very complex mixture which we were not able to characterize (Scheme 38).

Scheme 38.



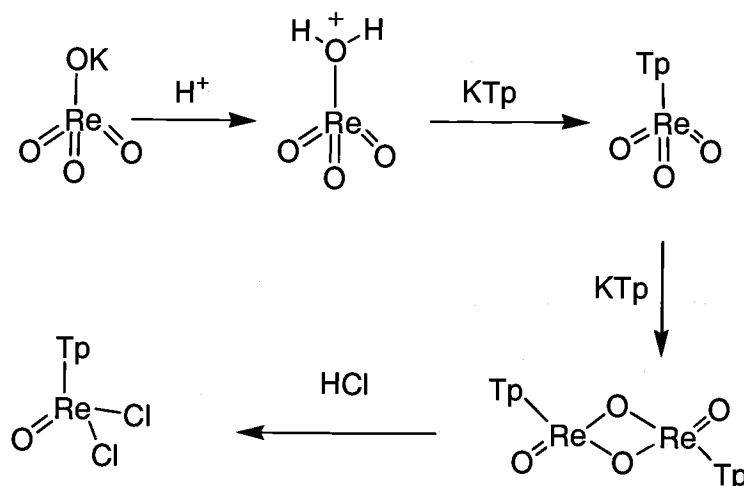
We subsequently turned our attention to more robust, tripodal *tris*(1-pyrazolyl)borate (Tp)- and *tetrakis*(1-pyrazolyl)borate (Tk)- ligands as a means to

increase the overall stability of the organometallic species. We also thought that the nature of the halide might play an important role. If the reason for decomposition was, indeed, an electron transfer, then modifying the leaving group should alter the redox properties and enhance substitution.

Synthesis of some new Tp, Tp', and Tk rhenium(Oxo)dihalides and reaction with organozinc phenolates

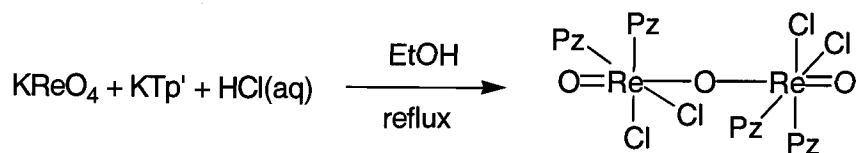
Of the set of compounds of the general formula $L\text{Re}(\text{O})\text{X}_2$ ($L = \text{Tp}, \text{Tp}', \text{Tk}$; $\text{X} = \text{Cl}, \text{Br}, \text{I}$) only a few members of the series have been reported in the literature. The first report on the preparation of $\text{TpRe}(\text{O})\text{Cl}_2$ used the reaction of KTp with KReO_4 in ethanolic HCl (Davison's procedure)⁸⁶. The mechanism of this reaction was not investigated but, most likely, it involves initial hydrolysis to perrhenic acid, formation of TpReO_3 , the reduction of the resulting trioxide to $\text{Re}(\text{V})$ dimer followed by the hydrolytic cleavage by HCl (Scheme 39).

Scheme 39.



An alternative procedure developed by Herrmann's group involves the reduction of Re(VII) trioxide with triphenylphosphine and treatment with TMSCl ⁸⁷. TpRe(O)Br_2 can be prepared with a much lower yield using TMSBr . TpRe(O)I_2 was obtained only as a by-product in reaction of TpRe(O)Ph_2 with iodine¹⁰. No spectroscopic data for diiodo complex was reported. In view of insufficient reducing power of KTk , TkRe(O)Cl_2 can not be prepared by the Davison's procedure but can be synthesized using Herrmann's protocol⁸⁸. The dibromo- and diiodo-complexes were unknown. For the Tp' system, the Davison procedure leads to tetrachloro-(-oxo)-dioxo-tetrakis-(3,5-dimethylpyrazole)dirhenium (V)⁸⁹ (Scheme 40) and Herrmann's methodology gives an inseparable mixture of dichloride and hydroxychloride⁹⁰. Thus, $\text{Tp}'\text{Re(O)Cl}_2$ was never isolated in pure form.

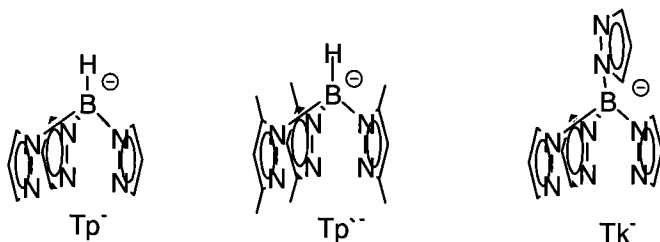
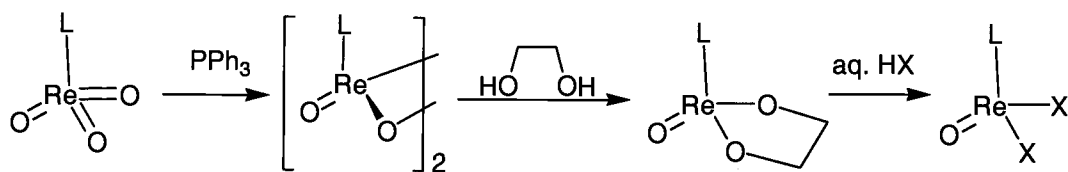
Scheme 40.



An observation made by Santos et al that $\text{TkRe}(\text{O})(\text{OCH}_2\text{CH}_2\text{O})_2$ complex can be easily hydrolyzed with aq. HCl to give $\text{TkRe}(\text{O})\text{Cl}_2$ led us to further extend this methodology on Tp, Tk, and Tp' series. Two routes (A and B) to rhenium oxodihalides were experimentally explored and compared to the two literature procedures (C and D).

Method A involves the synthesis of ethanedioylate followed by the proteolytic fragmentation with an excess of aqueous acid (Scheme 41).

Scheme 41.



Method B is an organometallic variant of a Finkelstein reaction where the rhenium oxodichloride is converted into the rhenium (V) oxodiodide with NaI in

acetone. Methods C and D are procedures published by Herrmann and Davison, respectively (*vide supra*). Table 2 summarizes the yields of rhenium oxohalides obtained by different methods. The advantages of method A are clear. It allows for an easy and straightforward preparation of any $\text{LRe}(\text{O})\text{X}_2$, regardless of the nature of the halide ($\text{X} = \text{Cl}, \text{Br}, \text{I}$) or the nature of the ligand ($\text{L} = \text{Tp}, \text{Tp}', \text{Tk}$).

Table 2. Yields of rhenium oxohalides $\text{LRe}(\text{O})\text{X}_2$ from various methods

Method	Ligand (L)	Halide (X)	Yield, %	Reference
A	Tp	Br	67	This work
A	Tp	I	64	This work
A	Tp'	Cl	23	This work
A	Tk	Cl	70	91
A	Tk	Br	72	This work
A	Tk	I	70	This work
B	Tp	I	43	This work
C	Tp'	Cl	50 ^a	88
C	Tk	Cl	73	86
D	Tp	Cl	85	84
D	Tp	Br	53	This work
D	Tp'	Cl	— ^b	87

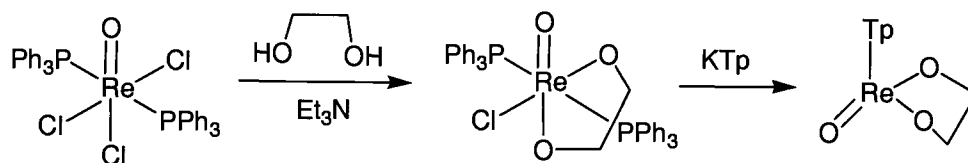
a. inseparable mixture of products

b. Different product

Within the method A we also explored an alternative way of making rhenium (V) oxo diolates. We found that if $\text{Re}(\text{O})\text{Cl}_3\text{PPh}_3$ is reacted with the ethanediol in the presence of a tertiary amine and then treated with KTp the corre-

sponding diolate can be isolated in good yields (Scheme 42). This particular order of reagents is important. It parallels previously made observation that PPh_3 liberated from $\text{Re}(\text{O})\text{Cl}_3\text{PPh}_3$ quickly reduces the $\text{Re}=\text{O}$ bond if an axial alkoxide ligand is absent⁹¹.

Scheme 42.



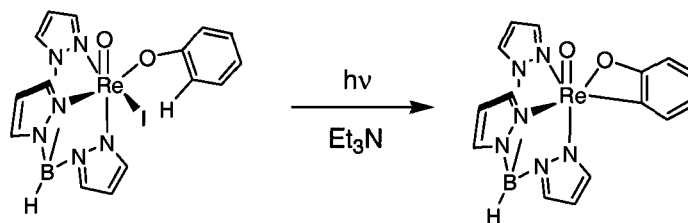
Once again, the reaction with organomagnesium and organozinc nucleophiles gave a mixture of unidentified products. We also found, quite counterintuitively, that the usual in organic chemistry leaving group order is reversed in case of our complexes: chloride can be substituted for bromide or iodide or by phenolates, but dibromo-, and especially diiodo- complexes are unreactive. This trend can be explained by noting that the electrophilicity of the metal center in the $\text{Re}=\text{O}$ fragment is a function of halide present in the molecule. The higher the electronegativity of the halide the more electrophilic Re becomes. The second argument is of stereoelectronic nature. The halide atoms of $\text{Re}-\text{X}$ bond can use their non-bonding electrons to provide for additional bonding. Because of better orbital size match the $\text{Re}=\text{I}^+$ fragment is expected to be more stable than $\text{Re}=\text{Cl}^+$.

Being unable to generate the rhenaoxetane through the halide substitution, we decided to investigate the photochemical means of the ring closure using rhenium iodo phenoxide complex.

The synthesis of TpRe(O)I(OPh) and its photochemistry

Mayer and co-workers¹⁰ reported that irradiation of TpRe(O)I_2 in benzene leads to the formation of TpRe(O)IPh . We believed that due to apparent photochemical lability of the Re-I bond in the diiodo complex the similar chemistry can be done with the iodo- phenoxy substituted compound, but intramolecularly. Ring closure with the extrusion of HI would lead to benzometallaoxetane. (Scheme 43).

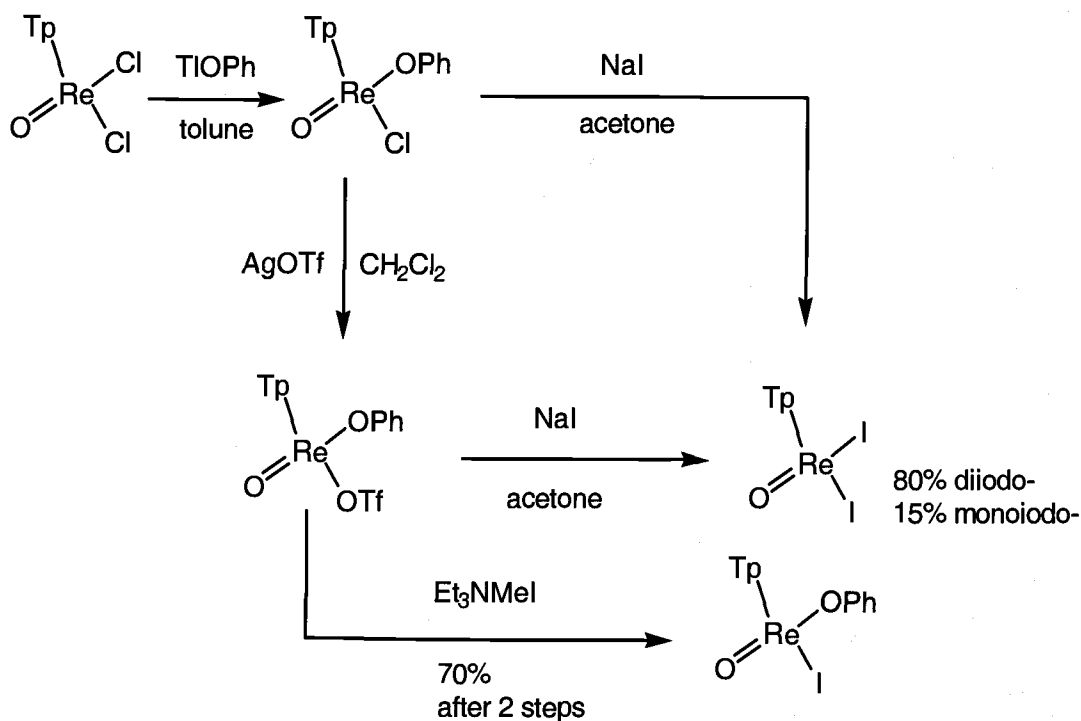
Scheme 43.



TpRe(O)I(OPh) , however, was unknown and its synthesis posed unexpected difficulties. The most straightforward approach would be to react Re(V) oxo diiodide with one equivalent of the phenoxide ion. However, in accord with our previous observations, TpRe(O)I_2 did not react with the phenolate ion, even under forced conditions. TpRe(O)Cl_2 proved to be quite reactive, particularly towards thallium (I) phenoxide. When TpRe(O)Cl_2 is desymmetrized with one equivalent of thallos

phenolate⁷⁶ $\text{TpRe}(\text{O})\text{Cl}(\text{OPh})$ results in good yields. Given our previous success with Cl/I exchange we treated $\text{TpRe}(\text{O})\text{Cl}(\text{OPh})$ with sodium iodide in acetone only to see the exclusive formation of $\text{TpRe}(\text{O})\text{I}_2$. We therefore sought to substitute chloride with a better leaving group. Reaction of $\text{TpRe}(\text{O})\text{Cl}(\text{OPh})$ with AgOTf produced $\text{TpRe}(\text{O})(\text{OPh})\text{OTf}$, which, upon reaction with NaI in acetone gave 15% of the desired $\text{TpRe}(\text{O})\text{I}(\text{OPh})$ and 80% of the diiodo complex. Changing the sodium cation for non-Lewis acidic Et_3NMe^+ suppressed the phenoxide substitution and gave the desired monoiodo phenoxide in a 80% yield (Scheme 44).

Scheme 44.



$\text{TpRe}(\text{O})\text{I}(\text{OPh})$ was then photolyzed in heptane/triethylamine solution at room temperature using uranium glass and/or a pyrex filter (cutoffs: ~450 and 350 nm

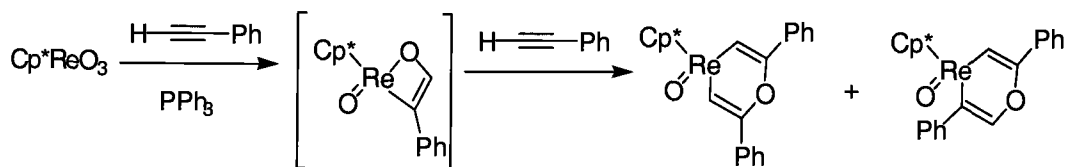
correspondingly). The resulting mixture revealed primarily the formation of TpRe(O)_2 . The absence of triethylammonium salt indicated the inability of $\text{TpRe(O)}\text{I(OPh)}$ to activate aryl C-H bond.

Reaction of the Cp* dimer with cyclooctyne

Our final attempt to construct a metallaoxetane moiety was to directly effect a [2+2] cycloaddition of rhenium oxo bond to the carbon-carbon multiple bond. We envisioned that cyclooctyne would be an appropriate organic substrate for such a transformation. From a thermodynamic point the rhenaoxetane formation with concomitant sp to sp^2 rehybridization of the cyclooctyne carbons would relieve a great deal of strain in the resulting structure. Likewise, the strain in cyclooctyne would prevent the extrusion of the hydrocarbon from the cycloocten-
orhenaoxetane.

The intermediacy of a rhenaoxetene was implicated in the formation of a novel 1-rhena-4-oxacyclohexa-2,5-diene from Cp^*ReO_3 , PPh_3 and an excess of alkyne⁹². The key structural feature of the rhenapyran is the formation of two rhenium-carbon bonds which could be best explained by the initial formation of the rhenaoxetane followed by the insertion of an alkene into the Re-O bond (Scheme 45).

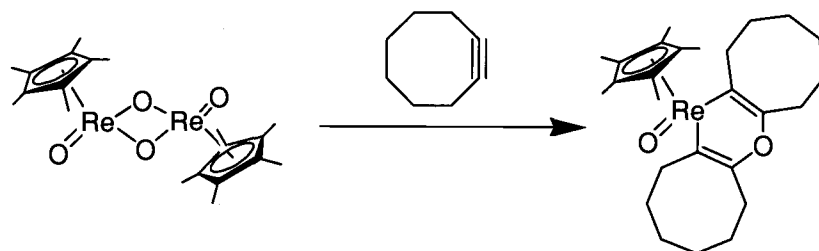
Scheme 45.



The question remained whether it was possible to stop the putative intermediate from reacting with another molecule of alkene.

The cyclooctyne was prepared by the bromination of the cyclooctene followed by the treatment with KtOBu and LDA^{93} . When heated with the $(\text{Cp}^*\text{ReO}_2)_2$, a brown complex was isolated which was assigned a cyclooctene rhenapyran structure on the basis of a spectroscopic analysis (Scheme 46). The key diagnostic features were: the molecular ion (570M^+) and the $\text{Cp}^*/\text{aliphatic}$ proton ratio.

Scheme 46.



CONCLUDING REMARKS

All synthetic approaches to the stable rhenaoxetanes described above failed. The reaction of Re(V) oxo dihalides with *ortho*-metal phenolates consis-

tently resulted in the formation of complex mixtures. This precluded the isolation and identification of the reaction products. In other instances, the alternative reaction pathways resulted in the formation of products other than rhenaoxetane. These results suggest that the rhenaoxetene could, in fact, be an unstable intermediate. Here we would like to discuss a number of mechanistic possibilities. As mentioned in the previous sections, electron transfer to Re(V) from the ortho-metallated phenolate was initially suspected to be the main reason for the extensive decomposition of Re substrate. Although this process is precedented, most notably in the $\text{TpRe}(\text{O})\text{Cl}_2$ case, it was possible to mitigate over-reduction by using milder uni-charged nucleophiles. This approach completely failed in our case where we had to use dianionic nucleophiles. It is reasonable to assume that increased charge density in dianionic nucleophiles compared to monoanions could lead to lowered ionization potential, and consequently, to a better chance to undergo a reduction. It is also possible that the reduction was not the only process responsible for the decomposition of the starting material. In the majority of reactions a sufficient quantities of inorganic salt have been observed suggesting possible halide substitution and the initial formation of the metallaoxetane structure. Although the design of the experiment efficiently blocks the [2+2] retroaddition pathway, the reductive ring expansion as well as a ring contraction are mechanistic possibilities. The structures in Scheme 35 are precedented in the literature. For example, $\text{Cp}^*\text{Re}(\text{O})$ was isolated as a complex with olefins⁹⁴. ^{17}O NMR showed remarkable electron deficiency of the terminal oxo group which

could be easily converted to hydroxo. The complex undergoes easy one-electron oxidation leading to dinuclear Re(IV) species. In another example, $\text{TpRe}(\text{O})$ obtained by photochemical decomposition of $\text{TpRe}(\text{O})$ oxalate in the presence of oxygen undergoes a series of transformations leading to partial decomposition of Tp ligand and to the formation of $[(\text{TpRe}(\text{O}))_2\mu\text{-O},\mu\text{-pz}]^+ \text{ReO}_4^-$. A similar processes can be implicated in the decomposition of a putative rhenaoxetane in our case.

CHAPTER 4. KINETIC ISOTOPE EFFECTS IN CYCLOREVERSION OF RHENIUM (V) DIOLATES

THE CONCEPT OF CONCERTEDNESS

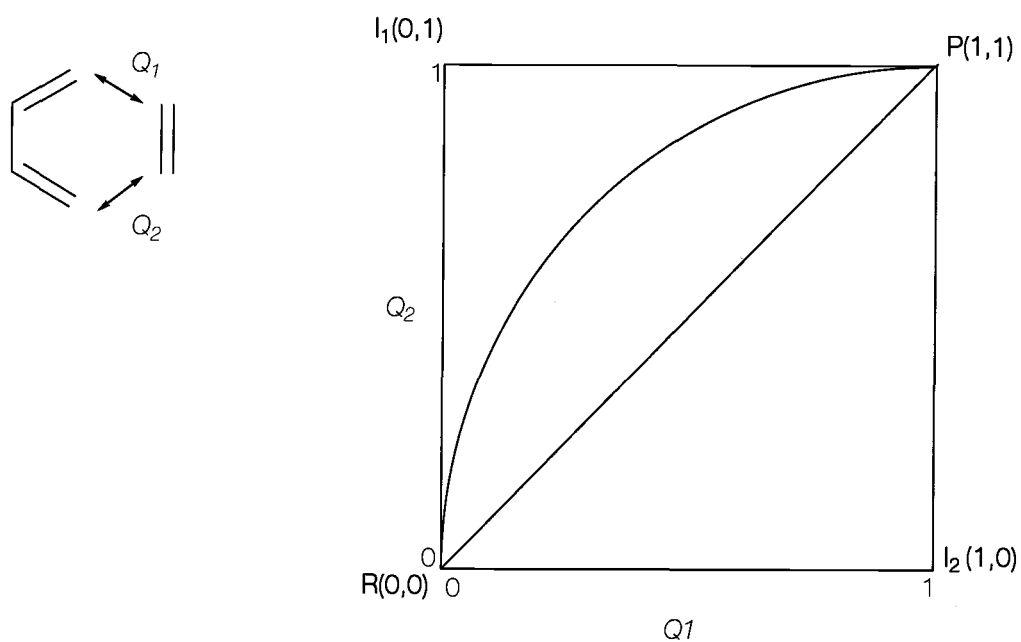
A great number of mechanistic discussions deal with the concept of concertedness. The relative sequence and timing of bond making and bond breaking is of paramount importance to understanding the mechanism of a particular reaction. The most illustrative example is the pericyclic reaction, and in particular, cycloaddition reactions. Since the development of Woodward-Hoffman rules⁹⁵ which emphasized the importance of orbital symmetry in bonding transformations, cycloaddition reactions have been generally believed to proceed in a concerted fashion.

Before going further into the discussion of the concept of the concertedness it is important to define what is actually meant by the term concerted. To be practically useful, the definition has to be tied to the criteria of the concertedness and since those are still in the development⁹⁶ a rigorous definition does not exist. The problem is compounded by the fact that the concept of concertedness has two different aspects: structural and energetic. From the structural point of view, concerted reactions are understood as those where the cleavage and the formation of the chemical bonds are to some degree synchronized. Taking asynchronicity to the limit one arrives at the stepwise process. An important contribution to

the topological description of concertedness is due to the More O'Ferral-Jencks diagrams⁹⁷.

The main idea behind this technique is that the reaction coordinate can be represented by the set of nuclear coordinates, which in a simple case of the Diels Alder reaction can be defined as the lengths of two newly created bonds, Q_1 and Q_2 (Figure 3).

Figure 3. More O'Ferral-Jencks diagram



The degree of individual bond formation is plotted along the X and Y axis. The scale of the axis is relative, ranging from 0 (no bonding) to 1 (full bonding). The ideally concerted process where the degree of the bond formation is absolutely synchronized will then be represented by the diagonal line, connecting the starting material (R) and the product (P). Conversely, in the case of a two-step process

the reaction coordinate vector consecutively follows the axes and passes through the intermediates I1 or I2 located at the upper left and lower right corners of the diagram. Between these idealized extremes there is a continuum of mechanisms which are not fully concerted nor stepwise in terms of More O'Ferral-Jencks criterion. Despite its clearness and simplicity the More O'Ferral-Jencks criterion has one major drawback. The majority of real life situations belong to this asynchronous continuum; and because of the arbitrariness in defining the borderline separating an asynchronous but still concerted process from a stepwise one the More O'Ferral-Jencks criterion has little practical value. Some interesting work has been done to address the problem associated with this ambiguity. The "similarity theory" attempts to dissect More O'Ferral-Jencks diagrams into so-called "catchment regions" which feature the key molecular structures that might be energetically important to the reaction⁹⁸. The theory, however is still early in the development.

A second approach to the issue of concertedness addresses energetic considerations. The apparent energetic advantages of the concerted process is avoidance of a high-energy intermediate and the energy compensation resulting from the synchronous bond making/bond breaking. The disadvantage of the concerted process stems from the larger nuclear motion association with it versus that of a stepwise process and the entropic cost of creating appropriate preorganization.

To test the viability of a possible intermediate in a process it is necessary to examine the potential energy hypersurface (PEH) of the reaction. The existence of an energetically accessible intermediate on the PEH can be used as an argument in favor of a stepwise process. This analysis is usually done with the help of quantum-mechanical computations. However, there are several facts that limit the outcome of computational analysis. First, the computational results are essentially limited by the input. An inability to find a competitive intermediate does not rule out the stepwise process since there might be alternative reaction manifolds that have not been considered. Second, the predictive power of computational chemistry relies on the success of finding critical points on the PEH. Those critical points, particularly the transition state, are relevant to the activation energy of the process. Finding the transition state is not a minor undertaking, especially for large organometallic molecules where a high density of states often results in a flat PEH. Consequently, there is always a possibility for alternative structures. Apart from this practical consideration, there is still some question of how much relevance the critical points bear to the actual structures responsible for the observed chemistry. This is especially true for the transition state since it cannot be experimentally detected. Furthermore, despite its success, classical transition state theory is based on rather crude assumptions⁹⁹ and has been criticized¹. Alternative

1. The classical formalism of TST assumes the activation complex is in quasi-equilibrium with the starting material. The rate constants are derived from the quasi-equilibrium thermodynamic constant. There are two major deficiencies of classical TST as proven by the experiments. (see refs 100): (a) the high temperature overestimations of the rate constants and (b) neglect of quantal effects on the reaction coordinate motion, particularly H-tunneling. The latter is very important for hydrogen transfer in enzymatic catalysis, see refs. 101.

theories are being developed, most notably the Kramer's energy diffusion theory which addresses the nonlinearity of the system arising from the energy dissipation through friction, but these have not seen general application¹⁰².

EXPERIMENTAL TECHNIQUES FOR EXCLUSION OF A CONCERTED MECHANISM

A number of experimental techniques have been developed that allow for ruling out concerted or stepwise mechanisms. The limitations of these techniques will be discussed below.

Stereochemical integrity

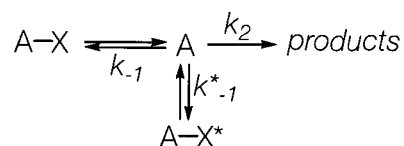
The analysis of stereochemical integrity has been a major tool for ruling out a concerted process. Rearrangements, isomerization, racemization or partial racemization are diagnostic of an intermediate along the reaction path. Racemization is indicative of the processes involving a symmetrical intermediate. The opposite statement is not necessarily true: the retention of configuration can also occur with the participation of an intermediate via double inversion¹⁰³ or it may occur with an intermediate that maintains configurational stability. Likewise, the absence of the rearrangements and isomerization does not rule out the formation of short-lived intermediates.

Analysis of stereochemical integrity usually includes NMR and the measurements of optical rotation.

Isotopic label scrambling

The positional isotopic exchange under reaction conditions can indicate an intermediate. Like the previous case, the absence of the isotopic scrambling does not rule out a stepwise mechanism because, in principle, the product formation step (k_2) might proceed at the higher rate than the formation of an isotopically scrambled intermediate (Scheme 47). In this case the return to A is much slower than the product formation and the intermediate AX^* forms under steady-state conditions.

Scheme 47.



Independent synthesis of a reactive intermediate and its kinetic consistency with the reaction in question

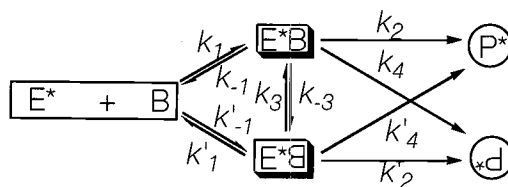
This is, perhaps, the most unambiguous proof of the stepwise process and the most difficult to carry out experimentally. Generally, the reactive intermediates under consideration are highly reactive species. This precludes their isolation or even detection under reaction conditions. One possible way of avoiding this

problem is the independent synthesis of an intermediate under conditions at which it can be isolated and studied, usually under low temperature. One may then hope to obtain the relevant kinetic data at more appropriate conditions. If the needed temperature range is inaccessible due to the secondary processes involving the reactive intermediate, it may be possible to approximate the rate constant using Eyring equation. One possible pitfall of this approach is that the low temperature kinetics may open up alternative pathways such as tunneling. Therefore, the rate constants cannot be directly compared with those approximated by the Eyring plot (see the discussion of the deficiencies of the TST earlier in the chapter).

Isoinversion kinetic relationship

Studying the asymmetric induction in Paterno-Buchi [2+2] cycloaddition Scharf and co-workers found that plotting de vs. reciprocal T consistently produced Λ shaped plots¹⁰⁴. This led to the discovery of an Isoinversion principle which states that "whenever the selectivity is generated on two or more different levels, in any kind of selectivity process, inversion points are expected in the Eyring diagram for temperature-dependent measurement of a selectivity parameter. The isoinversion relationship for any desired selectivity process can be illustrated in a general kinetic scheme. (Scheme 48)

Scheme 48.



The prochiral starting material B reacts with a chiral substrate or chiral catalyst E^* to produce the two diastereomeric intermediates. These can be formed in different proportions and are in equilibrium with each other. Formation of diastereomeric intermediates represents the first level of the stereoselectivity process. The intermediates can either react further, yielding diastereomeric products or return to reactants. The latter step is usually kinetically heavily favored for one of diastereomers. The rate constants k_1 and k'_1 determine the first level of selectivity while the rate constant ratios k_2/k_{-1} and k'_2/k'_{-1} (or k_2/k_3 and k'_2/k'_3) decide the second level of selectivity. Observation of a curved modified Eyring plot ($\log de$ vs. $1/T$) indicates either interconversion or retroformation of the intermediates. On the other hand, truly concerted process should give a linear plot of $\log de$ (ee) vs. $1/T$.

Experimental techniques for exclusion of a stepwise mechanism and other general techniques

Exclusion of a stepwise mechanism presents a bigger challenge. This is due to the fact that a very short lived intermediate can mimic essential features shared by the concerted process, such as preservation of stereochemical integ-

rity and, to a some degree, kinetics. Two primary methods for ruling out a stepwise mechanism include kinetic isotope effect measurements.

Kinetic isotope effects

The observation of a primary kinetic isotope effect at a given position indicates that the bond to this center undergoes scission at the transition state of the rate limiting step¹⁰⁵. This provides a simple means to differentiate the concerted process from the stepwise. The practical complication of the method is that the measurements of KIE have to be made for at least two centers suspected of being active in the transition state. Both primary and secondary deuterium isotope effects can be studied. A kinetic isotope effect of unity means the center is not directly participating in the rate-limiting step. Since the primary analytical method for determining the KIEs used to be a mass spectroscopy, the estimation of the isotope content at multiple positions was a daunting task. In 1995 Singleton proposed a methodology which allows the measurements of ¹³C isotope effects of natural ¹³C abundance materials¹⁰⁶. The method takes advantage of the isotopic fractionation phenomenon. If an isotope resides at the rate-limiting active site, the remaining reactant is enriched in slower reacting component. The proportion of a minor isotopic component in recovered material relative to the starting material (R/R_0) is related to the fractional conversion of reactants ($0 < F < 1$) and the KIE according to the Equation 1.

Equation 1.

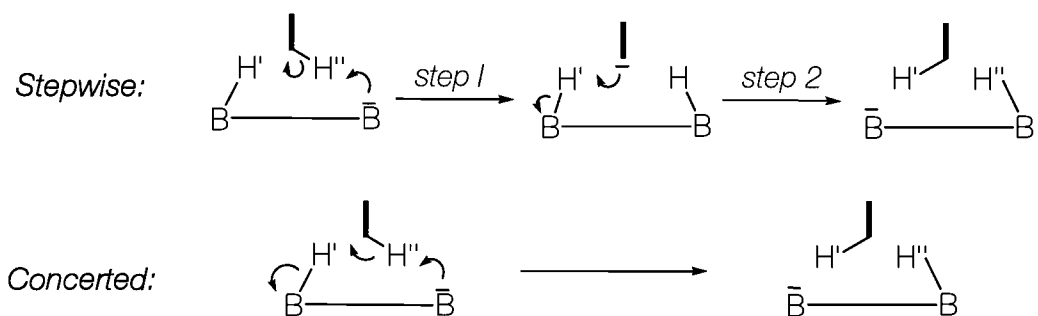
$$KIE = \frac{\ln(1 - F)}{\ln((1 - F)R / R_0)}$$

At high conversions (F tends to unity) the R/R_0 approaches infinity thus greatly magnifying the observed KIE. A center that is not active in the rate limiting step does not undergo isotopic fractionation, and, therefore can be used as an internal standard to which other centers of interest are compared. This methodology uses ^{13}C NMR as an analytical tool which makes it possible to calculate all isotope effects simultaneously. The study of kinetic isotope effects so far provided the most complete and rigorous test for concertedness.

Double isotope fractionation

This sophisticated method was developed by Knowles¹⁰⁷ in 1983. In this experiment, the isotopic fractionation at one site is measured as a function of the isotope at the other. The original experiment studied the racemization of D-proline catalyzed by proline racemase. (Scheme 49)

Scheme 49.



If racemization proceeds via stepwise process the first step is proton (H'') abstraction followed by the solvent-derived proton (H'). If the reaction is run in an H_2O/D_2O mixture there will be a kinetic discrimination against deuterium (step 2 is rate-limiting). As a result, the product will have lower relative deuterium content than the solvent. The product D-content will provide so-called mixed transition state fractionation factor, $\Phi'_{1,2}$. Now, if the same reaction is done with the deuterated substrate, the proton abstraction will be slowed down and the proton delivery from the solvent will be made less rate-limiting. Therefore, the $\Phi'_{1,2}$ will rise. The further kinetic analysis reveals that in case of the concerted process the observed fractionation factor for the solvent-derived site will be the same whether the substrate is deuterated or not.

Computational approach

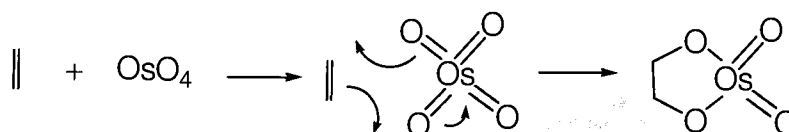
Computational methodologies include the optimization of the ground state structures and the location of the transition states for different reaction pathways. High level *ab initio* methods that incorporate DFT theory have proven to be quite accurate while maintaining significant speed/efficiency versus other correlated methods (MP_n). For better prediction of the energetics the polarization and diffuse functions are added to the basis set. Vibrational analysis can provide a useful set of benchmark parameters, such as thermodynamic properties and vibrational frequencies. The arguments in favor one or the other reaction pathways are con-

structured on the basis of calculated thermodynamic properties and the activation energies which are measured as the difference in the energy levels between ground state and the transition state.

ORGANOMETALLIC SYSTEMS UNDER INVESTIGATIONS: ASYMMETRIC DIHYDROXYLATION

Osmium tetroxide catalyzed dihydroxylation of olefins has captured the attention of many research group around the world. At the first glance, the reaction appears deceptively simple: the T_d symmetrical molecule of OsO_4 reacts with the olefin producing osmium diolate (*syn* addition) which then can be hydrolyzed giving diol and H_2OsO_4 (Scheme 50).

Scheme 50.

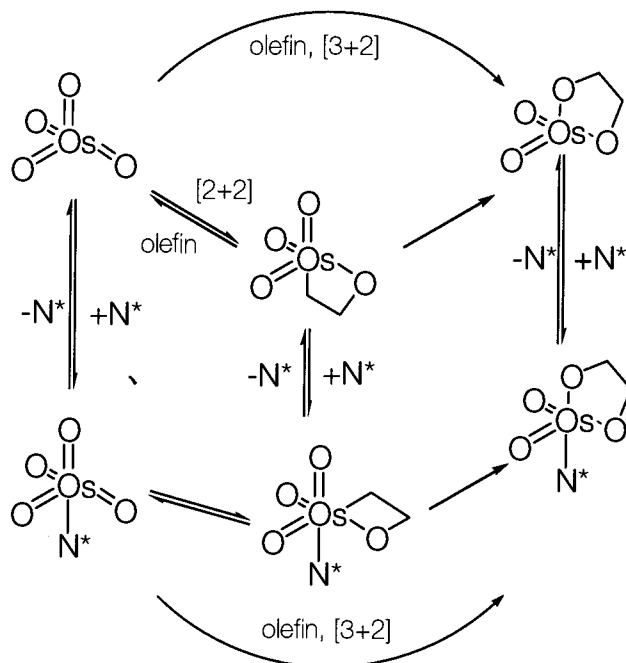


The reaction is stereospecific. Observed stereospecificity argued against the involvement of ionic and radical intermediates and the mechanism of osmylation was initially formulated to proceed via a concerted, [3+2] cycloaddition^{66a,108}. Later, Sharpless et al. suggested a stepwise mechanism involving a [2+2] like addition of the olefin to an Os-O bond which creates a four member osmaoxet-

ane intermediate⁹. This step was later proposed to be reversible. The rate limiting step in this reaction is the ring expansion to the osmium diolate.

The observed acceleration of dihydroxylation by tertiary amines and the ability of H_2OsO_4 to be easily reoxidized introduced a new dimension to the osmylation of olefins leading to the development of asymmetric dihydroxylation (AD). Given the practical importance of the asymmetric catalytic version the subject of further mechanistic investigations shifted towards the AD reaction. Consequently, both concerted and a stepwise mechanisms have been updated to be consistent with the new experimental findings. The generalized scheme for [3+2] and [2+2] pathways is presented below (Scheme 51).

Scheme 51.



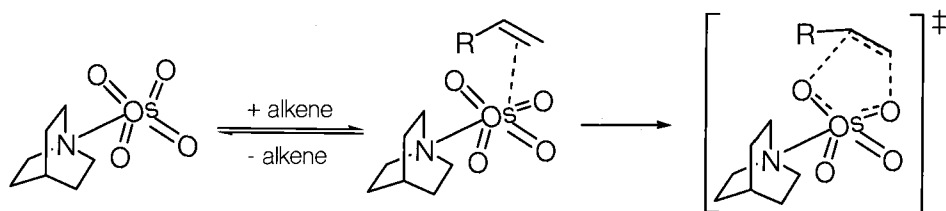
A large variety of experimental techniques were applied to the AD system in an attempt to provide convincing arguments in favor of one of the hypothesis.

Rate studies

Detailed kinetic studies of the stoichiometric reactions of various cinchona alkaloid-OsO₄ complexes with a number olefins have been carried out by Sharpless and co-workers¹⁰⁹. It was found that the electron poor alkenes generally react slower than electron rich alkenes; in the absence of ligand (N*) the rate determining step includes alkene and OsO₄, both in first order. In the presence of the alkaloid ligand (N*) the rate determining step includes OsO₄, alkene and the ligand. The dependence on the ligand is generally first order although in cases of ammonia and pyridine a second order dependence was recorded¹¹⁰. At high amine concentration the rate saturation occurs. The analytical rate laws for each of the proposed mechanism were derived by Norrby and Gable¹¹¹ indicating that both that [3+2] and [2+2] mechanistic schemes might lead to indistinguishable rate expressions. Therefore, it was concluded that the rate expression *alone* cannot differentiate between the two competing mechanistic proposals. An extensive kinetic study of the catalytic AD system was performed by Corey and Noe¹¹². They demonstrated Michaelis-Menten kinetics of the system suggesting enzyme-like reversible formation of a catalyst-substrate complex. This is inconsistent with the [2+2] proposal. To rationalize the data in the framework of the [3+2] hypothe-

sis the latter was adjusted to include the reversible formation of the amine-OsO₄-alkene complex. (Scheme 52)

Scheme 52.



This possibility has been earlier suggested by Norrby and Gable¹¹¹. However, they argued that in order to fit the rate expression the barrier to diolate formation ought to be of the same order of magnitude as the barrier to decomplexation which is unlikely since the ligand dissociation from pyridine-OsO₄ complex is known to be exceptionally rapid [5]. The major problem with this study is the measurements of the *turnover* rates of the catalytic reaction. As it has been shown by Sharpless and the co-worker the turnover-limiting rate in the catalytic AD reaction is not a diolate formation [5] but more likely either reoxidation or phase transfer. The other possibility is the formation of a precomplex by the strong nonbonding interactions between substituents in the ligand and the substrate¹¹³.

Study of electronic effects

The kinetics of stoichiometric osmylation in the presence of the amines has been studied as a function of alkene substituents^{5b} as well as the ligand sub-

stituents. These studies showed that the electronic effects can be directly transmitted from the amine to the metal in the OsO₄-amine complex. As the amine becomes more basic the N-Os bond length decreases and the equilibrium constant for the formation of the amine-OsO₄ complex increases. Surprisingly this has only a minor effect on the rate constant of the osmylation and does not provide any conclusive information about the mechanism. The substrate substituent effects in the amine accelerated AD reaction manifest themselves in a curved Hammett plot while unaccelerated osmylation shows a linear Hammett plot. The location of the minimum in the parabolic Hammett plot depends on the basicity of the amine and on its concentration which suggests two different ligand accelerated pathways. Neither pathways can provide a good explanation for the Hammett data.

Studies on the origin of enantioselectivity in the AD reaction

Great efforts have been put into understanding of the origin of high enantioselectivity in the AD reaction. Since the enantioselectivity is governed by the mechanism of the reaction it is conceivable that different mechanistic models would predict different selectivities which could be used as an argument in favor of one of the proposals. Both Sharpless¹⁰⁹ and Corey¹¹⁴ advanced models rationalizing the stereoselectivity obtained in the AD reaction. In Sharpless' model the stabilization interaction has been attributed to the interaction of the aromatic

ester moiety in the AD ligand with the alkene. According to Corey model the stabilization results from the stacking of the alkene with the quinoline fragment of the ligand. Sharpless' model has also been tested using molecular mechanics and gave the correct stereochemistry. However, the strong parametrization of the Sharpless' model biases the results whereas Corey model is based entirely on the visual inspection of the molecular structure. A more meaningful studies recently appeared from Maseras group¹¹⁵. Using high level DFT calculations they investigated both Sharpless and Corey models using 12 possible approach vectors predicting 99.4% selectivities (experimental 96%). Both models were indeed the lowest energy paths and differed only slightly in energy ($\Delta\Delta E^* = 0.4$ kcal/mol). Another recent study from Norrby and Houk¹¹⁶ used molecular mechanics to estimate the enantioselectivities corresponding to Sharpless and Corey hypothesis. 15 different substrate-ligand combinations have been calculated and compared to experimental results. They found that the major enantiomer is always formed through a TS where the substrate is stabilized by interactions with one of two binding pockets as suggested by Sharpless and Corey. Both models gave good agreement with the experiment, with a slight preference to the Corey model. The main problem of the studies on the origin of enantioselectivity is that they provide only conditional proof. The fact that a model correctly predicts the enantioselectivity does not prove the correctness of the model itself which has to be justified independently. Therefore, the computational approaches presented above lack rigor and provide at most circumstantial evidence.

Nonlinear plot of stereoselectivities vs. $1/T$

Sharpless and co-workers reported that dihydroxylation of several olefins using stoichiometric amount of OsO_4 in the presence of the excess of hydroquinidine ligands produced nonlinear modified Eyring plot over the wide range of temperatures¹¹⁷. Each catalyst/olefin combination showed two linear regions in the Eyring plot with a characteristic inversion point. As been pointed out earlier the existence of the inversion points are indicative of the reaction pathway where at least two enantioselective steps are involved, either the reversible formation or the interconversion of at least two intermediates each going into the unique product. Depending on the temperature, either one or the other reaction manifolds become rate and selectivity determining. The appearance of the inversion point in the modified Eyring plot is consistent with the stepwise [2+2] mechanism and is clearly inconsistent with a simple concerted process. However, if one assumes the formation of the "triple precomplex" (ligand- OsO_4 -alkene) the temperature break in the Eyring plot is indeed expected because of the two levels of stereoselection: (a) reversible, and most likely interconverting OsO_4 -ligand complex formation (1st level), the olefin coordination (2nd level) and the diolate formation (3rd level). Additionally, a system which follows Michaelis-Menten kinetics should also display nonlinear modified Eyring plot. Therefore, in a complex system such as AD reaction, especially in its catalytic version, the existence of the inversion point cannot serve as a definitive test for concertedness.

Computational work

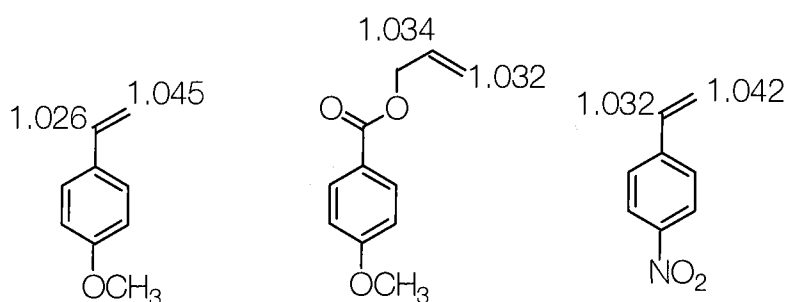
The theoretical analysis of two possible reaction pathways in the dihydroxylation reaction has been done by several groups¹¹⁸. High level DFT *ab initio* calculation with a large basis set and effective core potentials were used. In all cases the activation barriers for the [3+2] pathway were found to be significantly lower than those for the [2+2] cycloaddition, ranging from 1.9 vs. 43 kcal/mol to a more realistic 12 vs. 48 kcal/mol. Acceleration by the amine base was attributed to the distortion of the T_d to C_{2v} symmetry in OsO_4 upon the ligation which leads to the decrease in Os–O overlap, and, consequently to the weakening of the osmium-oxo bond. The computations do provide an unambiguous answer, however the results so far have been limited to simplified versions of the real AD system.

Kinetic isotope effects

Soon after its development, the Singleton ^{13}C KIE methodology was applied to the cinchona alkaloid- OsO_4 catalyzed dihydroxylation of olefins. All three analyzed olefins showed significant primary carbon isotope effects. If the reaction proceeds via concerted [3+2] mechanism, one would expect to observe primary KIE at both alpha and beta positions. The first report on the application of Singleton KIE methodology appeared from Corey group¹¹⁹. A significant asymmetry in KIE for the dihydroxylation of 4-methoxystyrene was experimentally found. The asymmetry was attributed to the increased electron density at the beta

carbon which facilitates the formation of C–O bond. (Scheme 53). Despite the straightforward interpretation of the results for the concerted process and inconsistency of this with the stepwise pathway, the [2+2] mechanism can still be rescued by allowing the formation of two regioisomeric osmaoxetanes. Two processes occurring simultaneously can, in principle, result in the observation of KIEs at both positions.

Scheme 53.



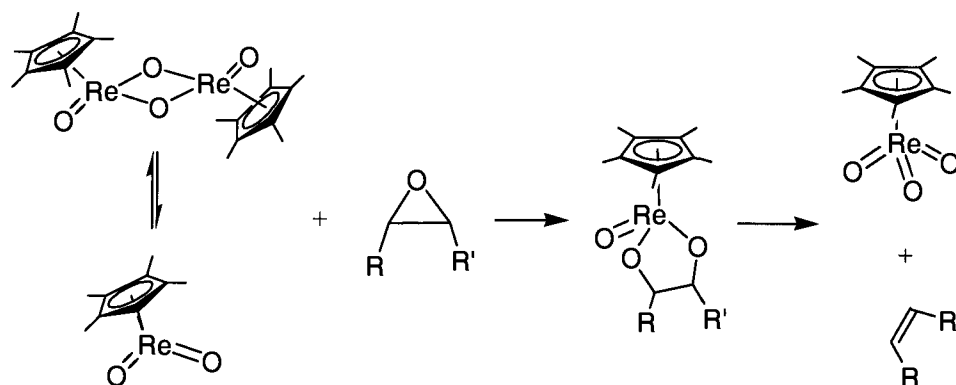
Singleton, Houk and Sharpless followed this report with their own comprehensive studies of catalytic osmylation of *t*-butyl ethylene which attempted to address this argument^{5d}. In this case, the formation of regioisomeric osmaoxetanes is prevented sterically. The primary $^{12}\text{C}/^{13}\text{C}$ and secondary H/D isotope effects were studied both experimentally and theoretically. The calculations used high level DFT theory and predicted primary carbon KIE to be 1.025 for [3+2] pathway versus 0.989 and 1.039 for the [2+2] mechanism. The corresponding secondary D KIEs for the substituted carbon were calculated to be 0.907 for concerted and 0.880 for stepwise case. The experiments gave 1.027 and 1.028 as the primary carbon KIE and 0.906 as the secondary D KIE at the substituted carbon. The agreement

between the predicted and observed kinetic isotope effects is consistent and supports the [3+2] cycloaddition as the rate-limiting step in the OsO_4 -catalyzed dihydroxylation of alkenes.

SELECTED ORGANOMETALLIC SYSTEMS UNDER INVESTIGATIONS: RE(V) DIOLATE CYCLOREVERSION

As we described earlier (see chapters 2 and 3) the cycloreversion of Re(V) diolates represents a convenient model system for olefin osmylation. Gable and co-workers^{16b} showed that the Re(V) system is capable not only of cycloreversion but also of cycloaddition thereby fully justifying the principle of microscopic reversibility employed in the study of this system and bridging the gap between Re(V) and OsO_4 chemistry. Apart from being mechanistically relevant to osmylation rhenium oxo chemistry reveals a direct relationship between epoxidation and hydroxylation. In chapter 2 we described the experimental evidence for the intermediacy of rhenium diolate in deoxygenation of the aliphatic epoxides with LReO_2 dimers ($\text{L} = \text{Cp}^*, \text{Tk}$). (Scheme 54)

Scheme 54.



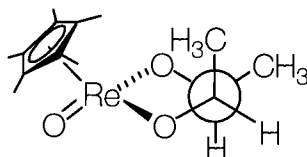
Thus, the Re(V) diolate appears to be the key intermediate linking several O-atom transfer processes. The elucidation of the mechanism of the Re(V) diolate cycloreversion has been primarily and extensively studied by Gable and co-worker. The results taken together strongly suggest that a simple, concerted [3+2] mechanism does not operate.

Conformational studies

The first line of evidence comes from the structure/reactivity studies. As expected for any pericyclic-type reaction, the orbital overlap is one of the major factors governing the energetics of the transition state¹²⁰. In case of Re(V) diolate cycloreversion, the [3+2] mechanism should favor the eclipsed conformation of the diolate ring. In this conformation the two incipient C-C bonds are parallel, and therefore, the overlap is maximized. The [2+2] mechanism favors more a staggered conformation. Using a Karplus relationship Gable and co-workers were able to show that the eclipsed conformation corresponds to a more negative

entropy of activation, and consequently, to a slower rate¹²¹. These results are inconsistent with the concerted mechanism. (Scheme 55)

Scheme 55.



Strain/Kinetic isotope effect studies

The second argument against the concerted pathway comes from the elegant study combining the kinetic isotope effect measurements and the strain effects. Gable and co-worker found that the extrusion of alkenes is virtually independent of strain. This, combined with the substantial secondary kinetic isotope effect (1.25 at 100°C for per-deuterated ethylene¹) indicates that the C-O bond breaks at the transition state, and, at the same time, the transition state does not gain any significant sp^2 hybridization at the extruding carbons^{16b,73}. This argues strongly against the concerted pathway and supports the stepwise mechanism where the hybridization of the diolate carbon does not change. One way to rescue the concerted mechanism would be to propose that the transition state is very reactant-like. However the high activation enthalpies of the diolate cycloreversion argue strongly against that through application of Hammond's postulate.

1. The KIE can be interpreted either as 1.06 per D for the concerted process or 1.13 for a stepwise process.

Computational studies

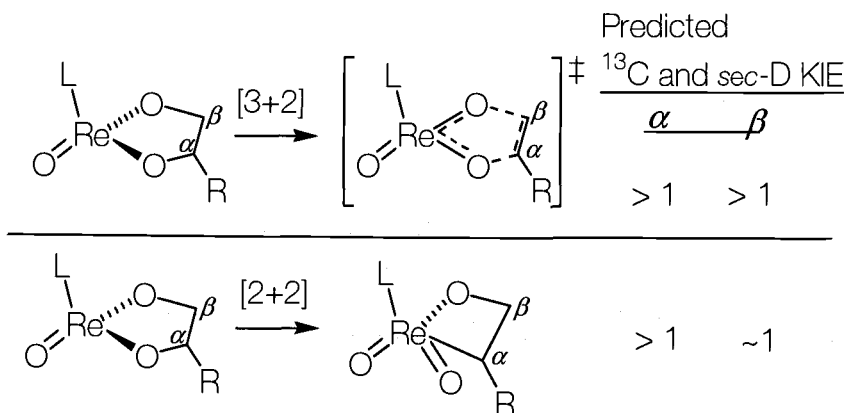
Frenking conducted a detailed theoretical investigation of OsO_4 and a series of rhenium compounds undergoing a cycloaddition to ethylene^{118a}. All ground and transition states were optimized using hybrid DFT theory with the BL3YP functional and a large valence basis set with effective core potential for rhenium. [3+2] and [2+2] pathways were compared. The important outcome of this work was the finding that all LReO_3 compounds ($\text{L} = \text{O}^-$, Cl , Cp) had activation barriers for the [3+2] process (ranging from 13 to 36 kcal/mol) higher than that of OsO_4 (5 kcal/mol) and the activation barriers for [2+2] mechanism lower for ClReO_3 and CpReO_3 than that for OsO_4 (30 and 25 vs. 44 kcal/mol). These results have been found generally applicable to the Cp^*ReO_3 case; however the possibility that 1,2-push pull substituted olefins may yield a rhenaoxetane has also been suggested.

PREDICTED KINETIC ISOTOPE EFFECTS IN CYCLOREVERSION OF Re(V) DIOLATES

Numerous unsuccessful attempts to synthesize a stable rhenaoxetane led us to reconsider the initial experimental approach based on the idea of isolation of a putative intermediate. The alternative way of probing the symmetry of the transition state is the measurements of the primary $^{12}\text{C}/^{13}\text{C}$ and secondary H/D KIE at

the reacting carbons. This methodology proved very successful for establishing the mechanism of osmylation. Each mechanism imposes different constraints on the value of isotope effects at the reacting termini. The concerted [3+2] mechanism implies scission of both carbon-oxygen bonds at the transition state. Consequently, the primary and secondary isotope effects at both carbons are predicted to be higher than unity. In the alternative, [2+2] mechanism, the ring contraction to form a rhenaoxetane leads to the scission of only one carbon oxygen bond. the predicted KIEs for this case would be $KIE > 1$ at one center and near unity at the other (Scheme 56).

Scheme 56.



EXPERIMENTAL DESIGN

General methodology

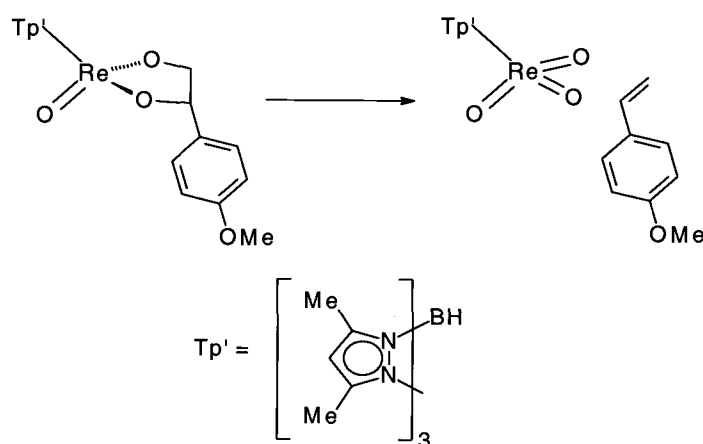
We felt that Singleton's NMR method provides a convenient methodological framework for establishing kinetic isotope effects at both positions of the

diolate simultaneously. The details of the Singleton's procedure and its application to the elucidation of osmylation mechanism were described in previous sections. Several aspects of the original methodology were significantly reworked to make data analysis and data collection more reliable in this particular case. One of the main concerns was over the sensitivity of the NMR analysis. A high signal-to-noise ratio for the NMR data is essential for reliable quantitation. The high cost of rhenium precursors and the lengthy and low-yielding synthesis of Re(V) diolates would lead to significant difficulties in obtaining a sufficient quantities of diolates needed for the experiment at a natural abundance level, as originally described in reference 106. The synthesis of isotopically enriched material was, therefore, desirable. The ^{13}C and D labels must be introduced at both reacting positions of the diolate ring and also at some remote location away from the diolate ring to serve as a marker for the unlabeled material. A typical experiment would include the roughly equimolar mixture of three isotopomers having isotopic labels at the alpha, beta and reference position (R) (Scheme 56). The isotopic composition of the mixture would be determined using NMR. After the thermolysis and recovery of unreacted material the isotopic enrichment is measured again and the KIE are calculated using Equation 1.

The second aspect is the choice of a ligand. A significant amount of earlier studies were done on the Cp* derivatives of Re. For this study we opted for the methylated pyrazolylborate ligand, Tp'. Earlier work from our lab demonstrated general similarity of Cp* and Tp' derivatized organometallics, and, most impor-

tantly, the similar activation energies for the $L\text{Re}(\text{O})$ diolate cycloreversion. ($L = \text{Cp}^*, \text{Tp}'$)^{30b}. The practical advantages of using pyrazolylborate complexes include primarily the air- and moisture stability and the ease of the preparation. The third aspect is the nature of the substituent on the diolate ring. It controls the electronics and influences the steric environment (*syn* and *anti* diastereoisomerism). This substituent was a choice for the introduction of isotopic marker for unlabeled compound. Synthetically, the one of the easiest targets is the CH_3 labeled *p*-methoxyphenyl group. (Scheme 57)

Scheme 57.



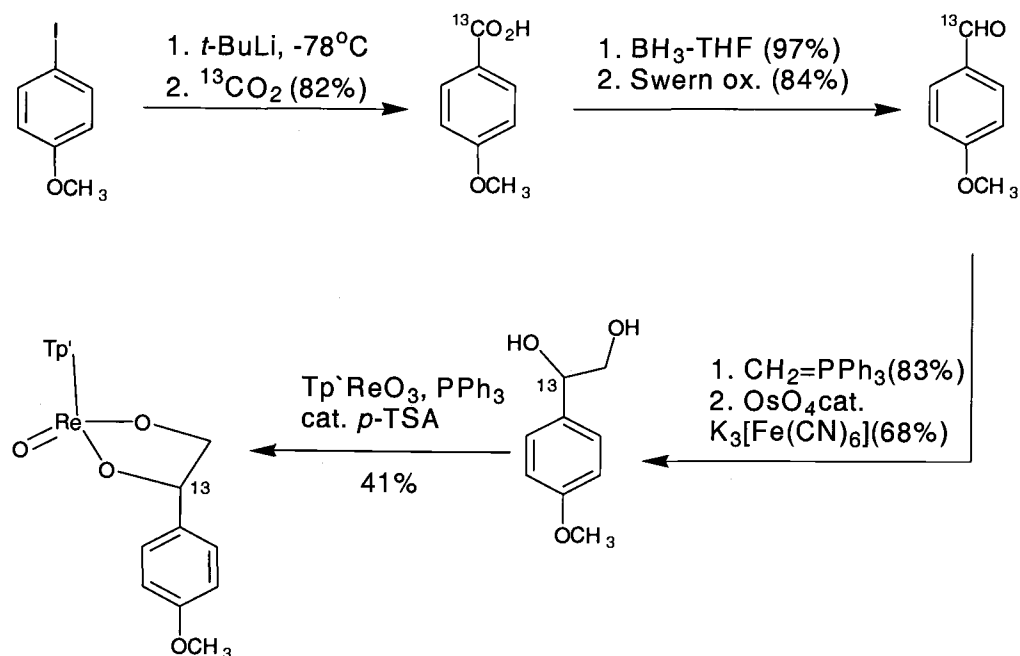
Arguably, an aliphatic group would be an ideal substituent on the diolate ring since the introduction of aromatic substituent might create an electronic bias. On the other hand, a large amount of work has been done on the extrusion of the styrenes from the $\text{Cp}^*\text{Re}(\text{V})$ diolates. A linear Hammett plot demonstrated a consistent change in electronic demand for the cycloreversion throughout a wide range of substituents¹²¹. Furthermore, in a similar osmylation experiment only a small

asymmetry was noted as judged by the magnitudes of primary carbon KIEs.(Scheme 53).

Synthesis of labeled diolates

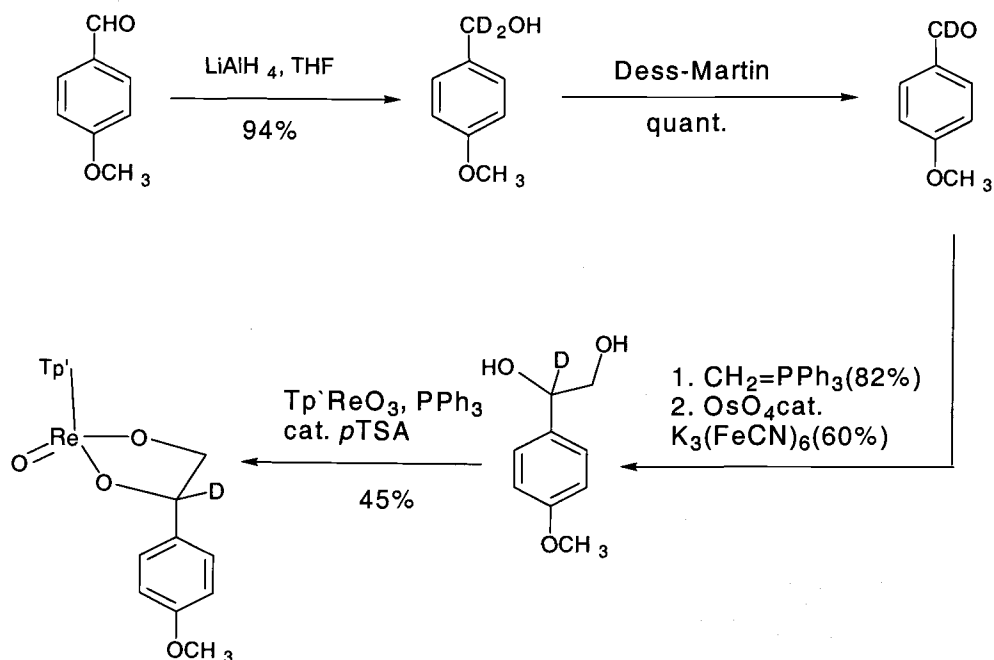
The synthesis of the $\text{Tp'Re(O)(OCH}_2\text{CH(Ph-4-OMe)O)}$ diolate having ^{13}C label at the alpha position is shown on Scheme 58. Para-methoxyphenyl lithium obtained via halogen lithium exchange was quenched with $^{13}\text{CO}_2$ (99% ^{13}C) which represents one of the cheapest sources of ^{13}C . The resulting ^{13}C -anisic acid was quantitatively reduced with BH_3 -THF complex and the resulting benzylic alcohol was subjected to Swern oxidation. The Wittig olefination followed by Yamamoto dihydroxylation gave the required alpha ^{13}C labeled diol (99% ^{13}C) which was converted to the diolate via the reaction with $\text{Tp'ReO}_3/\text{PPh}_3$.

Scheme 58.



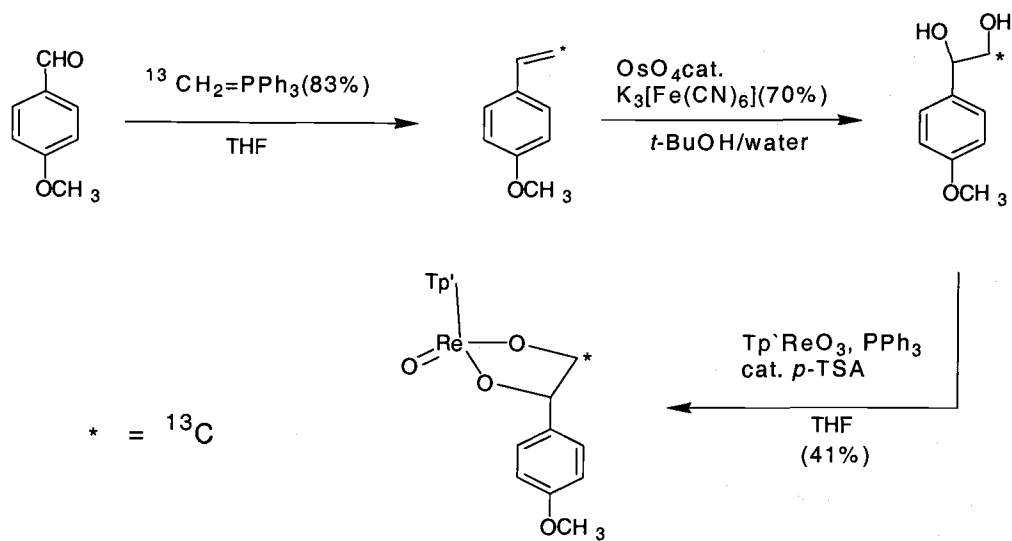
The introduction of deuterium at the alpha position of the diolate was done very similarly. The reduction of anisoyl chloride with LiAlD_4 and subsequent reoxidation of the deuterated benzylic alcohol with the Dess-Martin reagent gave deuterated anisaldehyde. This was transformed into the product using the same reaction sequence as in the previous case. (Scheme 59). The D incorporation, according to NMR, was ~99%.

Scheme 59.



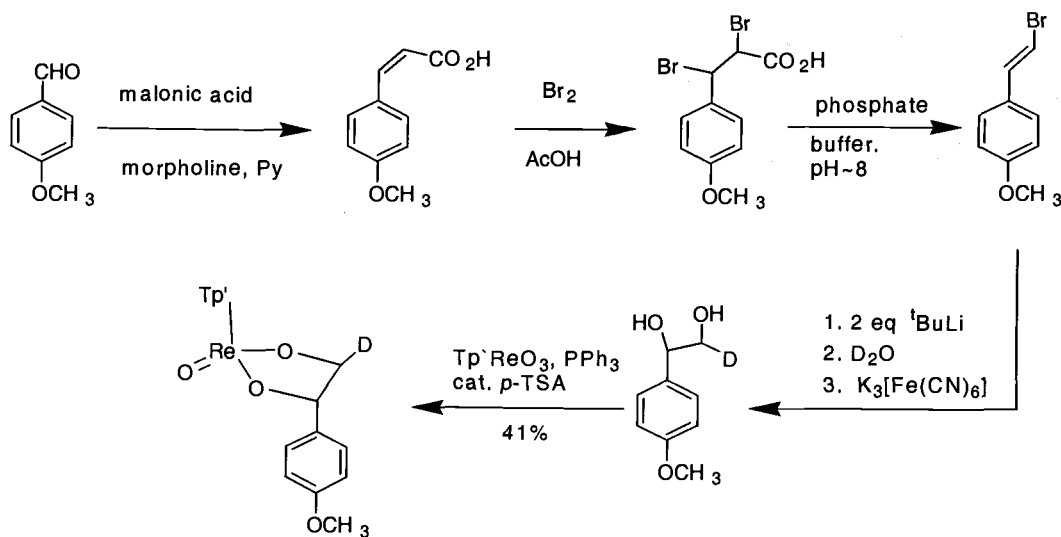
The synthesis of the beta ^{13}C -labeled diolate was carried out using ^{13}C labeled Wittig reagent made from $^{13}\text{CH}_3\text{I}$ (Scheme 60).

Scheme 60.



The introduction of the beta deuterium label was done via Knoevenagel condensation of anisaldehyde with malonic acid. Bromination of the α,β -unsaturated acid furnished dibromide which upon treatment with buffer at pH ~8 underwent elimination and decarboxylation. The resulting *trans*-bromo alkene was treated with BuLi at -100°C which led to a completely stereospecific halogen-lithium exchange as shown by the ^1H NMR spectrum after D_2O quench. The resulting alkene having label at the beta position was dihydroxylated and converted to the diolate (Scheme 61)

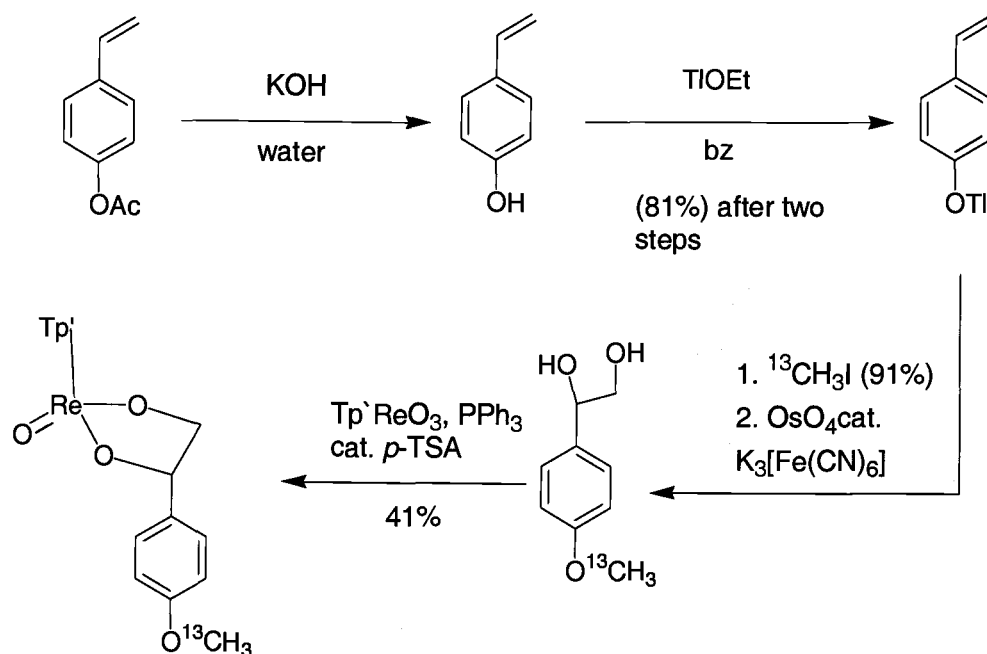
Scheme 61.



The introduction of the reference label in the methoxy group was complicated by the lability of 4-vinylphenol. Mild hydrolysis of 4-acetoxystyrene to the 4-vinylphenol followed by immediate *in-situ* conversion to the thallium (I) salt with the TIOEt in benzene gave a much more tractable species which was extremely easy

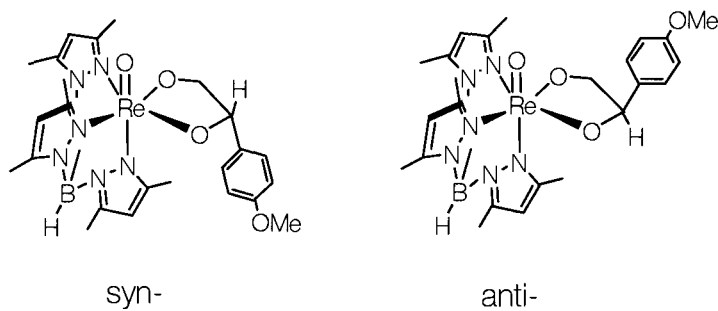
alkylated with labeled $^{13}\text{CH}_3\text{I}$ or CD_3I . Based on ^1H NMR spectra, each diol was >99 atom-% ^{13}C and D. (Scheme 62)

Scheme 62.



The cyclic nature of the diolate gives rise to a possibility to form two diastereomers: the *syn* where the aryl substituent is *syn* to the pyrazol and the *anti* where the aryl substituent is *anti* to the pyrazol (Scheme 63).

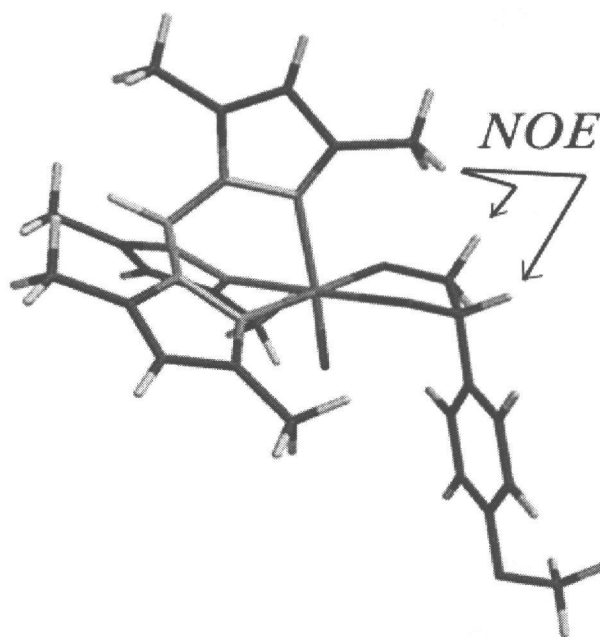
Scheme 63.



In fact, both diastereomers are formed in ~ 10:1 (*anti:syn*) ratio. This was confirmed by the nOe studies. The key spectroscopic handle is the methyl group pointing toward the diolate ring. Its unambiguous assignment provides a way to distinguish the two faces of the diolate ring and complete the assignment of both diastereomers. The following sequence of nOe experiments was performed. First, the irradiation of the vinylic H of the pyrazole *trans* to the oxo ligand¹ produces nOe enhancements of the two neighboring methyl groups. These two were, in turn, irradiated. The one that gave nOe enhancement of the diolate ring protons was used for the further assignment. The major, assigned as *anti* isomer showed nOe between the methyl signal at 2.47 ppm and the diolate signals at 6.23 and 5.65 ppm (Figure 4).

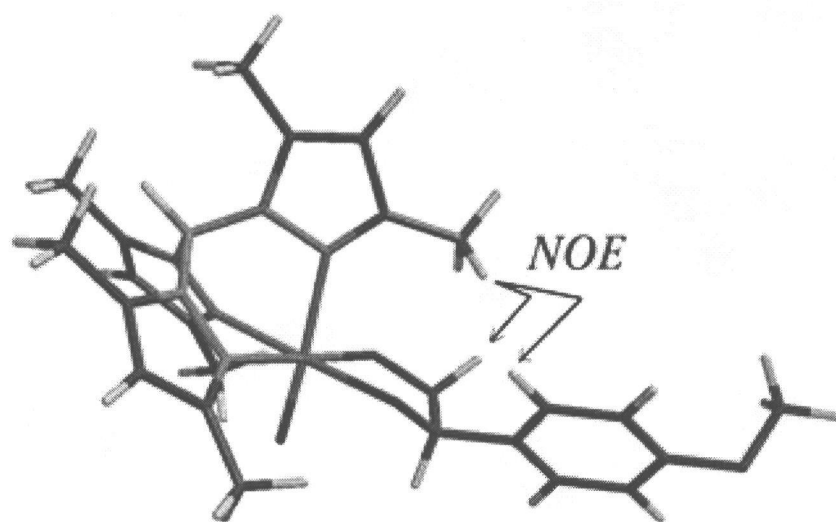
1. The pyrazole *trans*- to the oxo experiences a significant upfield shift of its vinylic H (5.49 ppm). The vinylic Hs of the two other pyrazoles are (5.92 and 5.94 ppm).

Figure 4. The structure of the major, *anti* diastereomer as determined by the NOE



The minor isomer, on the other hand, showed only one nOe between a diolate signal at 5.42 and the pyrazolyl methyl at 2.23 ppm; enhancement was also observed for the *ortho* aromatic protons at 7.63 ppm. DEPT of the major isomer confirmed the identity of α and β carbons at 95.9 and 94.5 ppm, respectively.

Figure 5. The structure of the minor, syn- diastereomer as determined by the NOE



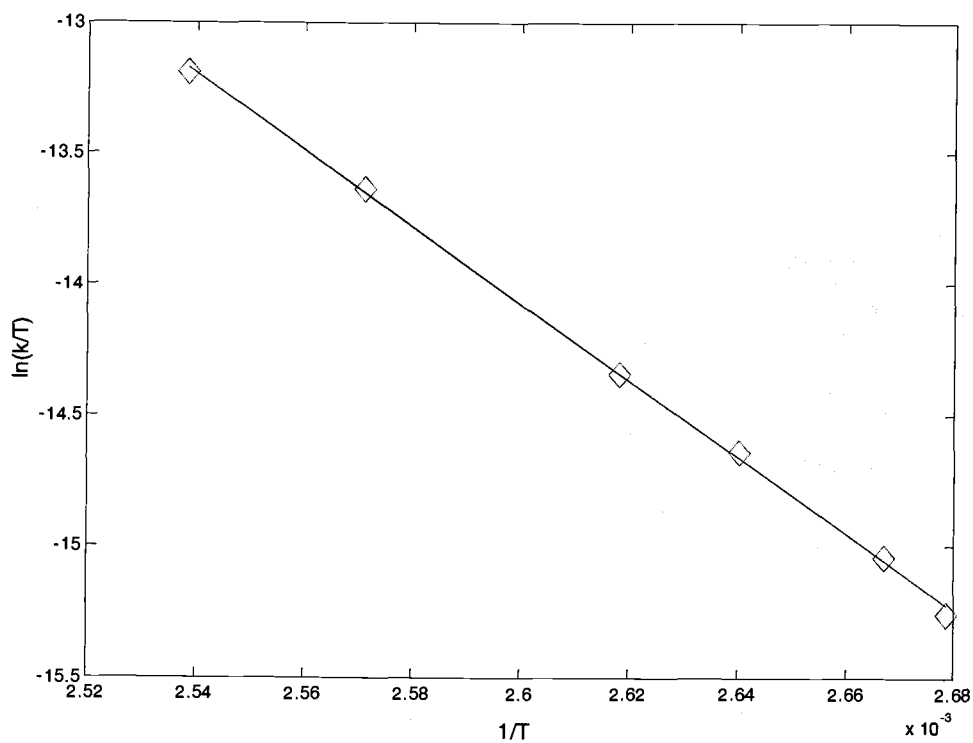
Estimation of conversion

There are two parameters that need to be estimated (see Equation 1): the conversion of the reference diolate (F) and the isotopic enrichment at given position (R/R_0) _{j} .

For any first-order process the conversion of the reacting species is defined as $1-F = \exp(-kt)$, where k is the rate constant and t is time. Timing the reaction provides a convenient way to estimate the conversion if one knows the rate constant to a high degree of precision. The rate constant k is also temperature dependent. By establishing activation parameters it is possible to estimate F at the actual temperature of the experiment. The activation parameters for extrusion of 4-methoxystyrene from the corresponding diolate was studied in toluene-

d_8 at several temperatures. Like the extrusion of styrene, this was found to be cleanly first-order to >4 half lives by ^1H NMR. The Eyring plot is shown in Figure 6.

Figure 6. Eyring plot of Re(V) diolate extrusion



The minor diastereomer was also evaluated kinetically at 120°C ; its rate of cyclor-eversion was only one fourth that of the anti isomer (0.00021 sec^{-1} vs. 0.00080 sec^{-1}).

ESTIMATION OF R/R₀ FROM ¹³C NMR AND D NMR USING INTEGRATION

Theoretical and practical consideration of data acquisition and analysis

The measurements of NMR peak areas is widely used technique for quantitative chemical analysis. It offers several important advantages, including the ease with which multicomponent mixtures can be analyzed, the nondestructive nature of NMR, and the direct proportionality of the integrated resonance intensity (*I*) and concentration (*C*) of nuclei giving the resonance (Equation 2).

Equation 2.

$$I = \alpha C$$

The primary practical complication is that the typical NMR spectrum usually contains multiple signals coming from nuclei in different chemical environments. As a result, the proportionality constant might not be the same for all nuclei. The first major source of this is different spin-lattice relaxation rate for different nuclei. It is therefore advisable that enough time would be given between scans to assure the full relaxation of the slowest-relaxing nucleus because incomplete relaxation may result in underestimation of the integral. Since instrumental noise is also accumulated at long acquisition times and is Fourier -transformed with the signal, use of long acquisition times results in a decrease of signal-to-noise (S/N) ratio. As a practical matter, acquisition times of 5T₁ provide reasonable alternative. At 5

T_1 the intensity of the resonance will be 99.3% of its equilibrium value. Relaxation agents, such as $\text{Cr}(\text{acac})_3$ can also be added.

The second important source of an error in NMR signal intensity is the nOe effect. This is primarily applicable to the experiments which use spin decoupling technique, such as ^{13}C NMR experiment. Typical ^{13}C spectra are measured with broadband ^1H decoupling and the resonance intensities of carbon nuclei are different from the equilibrium intensities due to the nuclear Overhauser effect (nOe). The practical solution to this problem is the inverse gated decoupling pulse sequence. In this experiment composite pulse decoupling is applied only during the short acquisition time and not during the relaxation delay.

There are also four major sources of systematic errors which affect the experimental uncertainties of the quantitative NMR experiment: (1) spectrometer noise, (2) digitization error due to the availability of data at discrete intervals rather than as a continuous function of frequency, (3) truncation error which results from the impossibility of integrating the experimental peak over all spectral frequencies and (4) phase error. The last three errors introduce a bias to the integration, i.e. the measured area is incorrect even when there is no instrumental noise.

Since an NMR signal drops exponentially with time and noise is constant, the S/N ratio can be enhanced by signal averaging. S/N scales as a factor of $N^{1/2}$ by addition of the FIDs from N pulses. An additional way to enhance sensitivity is to use 90° pulses to maximize signal obtained from each sample. However, more

time is required for spin-lattice relaxation. A minimal S/N value of 35 has been suggested¹²².

A number of studies showed that the digitization error is critically dependent on the true position of the peak with respect to the adjacent digital points¹²³. Both positive and negative errors can occur, depending on the number of digital points used to characterize the interval. For example, for a case in which 1024 data points cover a spectral range of 5000 Hz the error in the estimated peak area can reach 380%¹²³. For quantitative NMR work the "golden rule" is to ensure digital resolution of at least 10 points/Hz¹²².

The "truncation error", or the error resulting from overlap of two adjacent signals is a common problem in NMR analysis. There are two main ways of dealing with this problem. If the peak overlap occurs only near the base line, limits of integration for the overlapping bands are chosen in such a way that they do not overlap. In the general case, overlapping signals will have different T_2 values and consequently, different lineshapes. Here it is important to choose the integration range in units of line width. For a typical Lorentzian line, an integration range of 3.08 line width corresponds to 80% of total integral; a 63.6 line-width region gives 99% of the peak area¹²⁴. This method is suitable for well separated peaks but limited in accuracy for strongly overlapping signals since the "wings" of the Lorentzian NMR line extends a considerable distance and will significantly contribute to the integrals of smaller peaks if those happen to lie on the "wings" of a bigger peak. A more accurate approach is to perform a line shape fitting. In this

approach, the line is analytically deconvoluted into several single components. The individual lineshapes are then combined into a composite peak with different coefficients. The coefficients are optimized using least-squares method. The advantage of line shape fitting is the possibility of using non-Lorentzian line shapes, such as Gaussian. The disadvantage is a certain arbitrariness in choosing the percentage of the Gaussian/Lorentzian contributions since different sets can give similar rms values. Lineshape fitting also uses special software which is not always available.

The fourth source of error is the phase error. The spectrum is usually phase-adjusted using zero- and first order phase corrections to obtain a pure absorption spectrum. If phase is not adjusted correctly, integrals will be in error since the left- and right- hand wings of the dispersion will have opposite sign and their partial integrals will cancel each other. Therefore, careful adjustment of the phase is critical. Practically, careful phasing until baseline is "flat" on the both sides of the peak results in a less than one per-cent error in the integral¹²⁵.

Integration of ^{13}C and D NMR spectra

To estimate R/R_0 values the ^{13}C NMR spectra of the ^{13}C labeled isotomeric mixture were collected before and after the thermolysis. The number of scans were chosen to ensure S/N of at least 200 without exponential multiplication to ensure lineshape integrity. A spectral window restricted to the signal of interest was chosen; this provided 12 pts/Hz digital resolution. A narrower spectral window caused foldovers. The T_1 values were measured using inversion recovery method¹²². A relaxation delay of 25 seconds was used. We opted not to add relaxation agents because of the unknown effect the latter may have on the intensity of the observed signals. As recommended¹²⁶ for an analytical ^{13}C NMR experiment the inverse gated decoupling pulse sequence was used. Accurate phasing was made easier by the relatively narrow spectral window; automatic baseline correction was consistently applied for every spectrum.

Despite all these preventive measures, multiple runs gave significant scatter in the R/R_0 values for individual samples. In several cases we actually registered higher R/R_0 at the beta position. Initially, the instrumental noise was suspected to be the primary source of errors in the integration. Application of exponential multiplication to the raw FID increased the apparent S/N ratio but did not improve the consistency of the integration. We also noted unusual line broadening of the alpha and beta carbons. The line broadening of the carbinol carbons in Re diolates have been noted previously, particularly in the case of cyclooctane

diolate^{89a}. It is unlikely that such a broadening is caused by the fluxional behavior of the ring since neither cooling nor heating changes the lineshape. We believe that the nuclear quadrupole of rhenium (for ¹⁸⁵Re, this is 2.18 and for ¹⁸⁷Re, 2.07 barn; compare ²H at 0.00286 barn) is a more likely cause.

The second problem seriously complicating the analysis of the ¹³C NMR was contamination of the sample by the diastereomeric *syn* diolate. In spite of careful purification of the initial sample the *syn* diolate accumulates in the thermolyzed mixture due to its lower rate of cycloreversion. To make the matter worse, the "wings" of para methoxy signals of *syn* and *anti* diolates partially overlap (major: 55.19 ppm, minor: 55.29 ppm). Suspecting the overlap of peak wings is responsible for the integration scatter, Gaussian multiplication was applied to the raw FID. Generally, the application of Gaussian multiplication allows one to increase resolution at the expense of sensitivity. Although after the application of Gaussian multiplication the line separation appeared to be acceptable, the scatter in R/R_0 persisted. Further attempts to perform reliable integration of ¹³C NMR spectra were abandoned.

The preliminary studies of D NMR of the deuterium labeled isotopomeric mixtures (both initial and thermolyzed) revealed that the deuterium peaks, normally wide become extremely wide in the diolate ($\nu_{1/2} = 13.2$ Hz, $\Delta\delta = 36$ Hz). This led to a heavy overlap of deuterons on alpha and beta carbons and to the unacceptable S/N ratio.

ALTERNATIVE METHODS OF NMR DATA ANALYSIS. BAYESIAN ANALYSIS OF TIME DOMAIN DATA

Deficiencies of frequency domain data analysis

The main disadvantage of discrete Fourier Transfer NMR data analysis is the high level of manipulation the raw time-domain data undergoes before it appears in a convenient spectral form. Although fourier transformation results in no data loss (the time domain data can be obtained by the inverse fourier transform) the *posterior* spectral analysis suffers from the three major sources of errors which have been reviewed in the previous section: digitization, truncation and phase errors.

In an attempt to perform numerical integration of the ^{13}C and D spectra of rhenium diolates we found truncation error to be the major source of error. All attempts to mitigate it failed partially because the lineshape manipulations negatively affect both resolution and S/N.

Recently, several alternative methods of NMR data analysis have drawn attention. One of the most interesting and promising is the Bayesian NMR analysis. This is performed using exclusively time domain data. All the necessary information is estimated from the raw FID and no data conversion takes place. In time-domain terminology, the linewidth is equivalent to the decay constant and the integral is equivalent to the amplitude.

Background to the Bayesian approach

Bayesian data analysis is a statistical method which is based on Bayes' Theorem, formulated by the Franciscan monk Thomas Bayes in the 18th century¹²⁷. Bayes' Theorem essentially describes how the probability of a proposition changes as we obtain additional information relevant to the problem. This can be applied quantitatively to NMR data. Much of the methodology has been developed by G. L. Bretthorst who introduced the Bayesian principle to the field of NMR spectral analysis¹²⁸.

The free induction decay (FID, D) consists of N real or complex data points sampled at discrete time intervals ($d(t_i)$). Together with the signal (f_i) the acquired data points also contain the noise (e_i) (Equation 3)

Equation 3.

$$D = \{d(t_i)\} = \{d(t_1), d(t_2), \dots, d(t_N)\}$$

$$d(t_i) = \underset{\text{signal}}{f(t_i)} + \underset{\text{noise}}{e_i}$$

It is the signal that we are interested in. To a high degree of confidence it can be assumed that the FID consists of a sum of M exponentially decaying sinusoids, and the following mathematical model can be used (Equation 4).

Equation 4.

$$f(t_i) = \sum_{k=1}^M \{ [B_k \sin(w_k t_i) + B_{k+M} \cos(w_k t_i)] \exp(-\alpha_k t_i)$$

In this model, amplitudes (B_k) represent the integrals, and the decay constants define the linewidths of individual signals. The Bayesian NMR data analysis

is typically performed with the help of the specialized software. The package that was used in this work (BAYES) is supplied as a part of the XWINNMR suite. The working internals of the program have been briefly communicated by the authors¹²⁹.

The first step of the analysis is the *model selection*. At this stage the following questions should be answered: (1) Can a signal be detected in the data and how well? (2) How many decaying sinusoids are there? The probability of the resulting model is estimated given the data and all prior information. All models are compared and the most probable one is selected for the next stage. The next stage is parameter estimation. Each sinusoid is either allowed its own, individual phase, or the phase can be enforced to characterize coupled multiplets. The decay rates are also nonlinear parameters. The minimal and maximal decay rates may be specified by the user, as well as the most probable ones. The only linear parameter in this model is the amplitude. The model is optimized with respect to the nonlinear parameters; the amplitudes are determined as expectation values at the location of the maximum.

Benchmarking BAYES against simulated data

Before applying the Bayesian NMR analysis methodology to the spectra of isotopomeric mixture of Re diolates we felt it necessary to benchmark it against the simulated data. Furthermore, the simulated data set has to contain not only

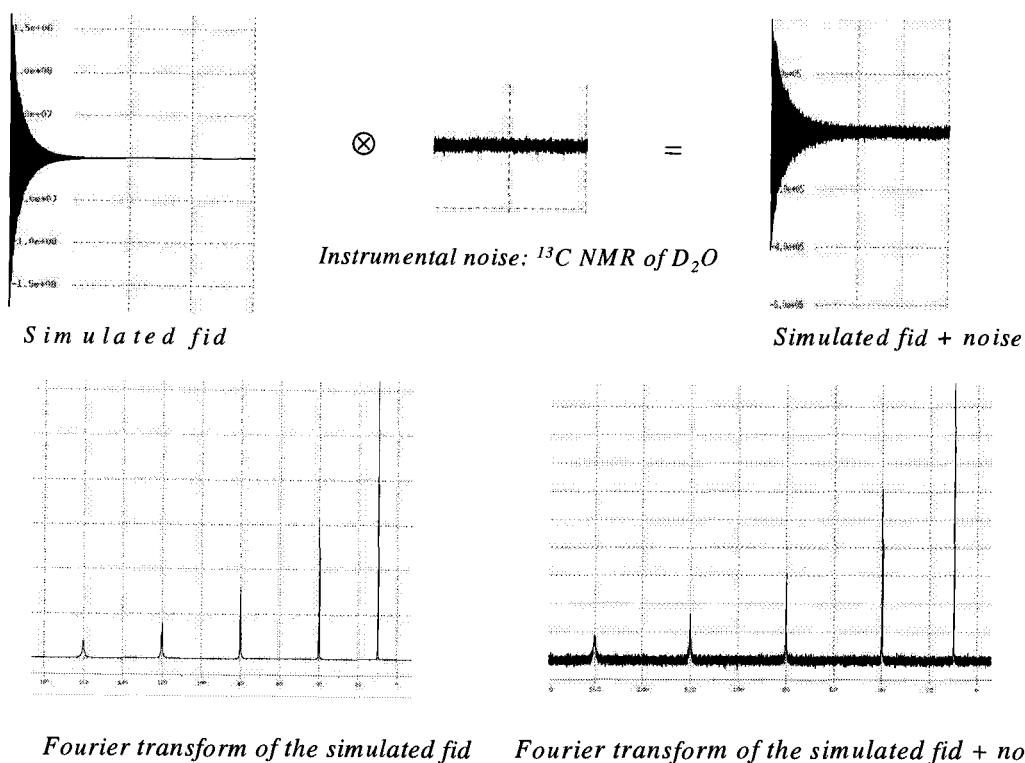
the analytically generated frequencies in the form of the FID, but the signal should also have instrumental noise. This was done in two steps. The analytical FID was constructed using the NMR-SIM program supplied with the XWINNMR suite. All amplitudes, phases and the decay rates have been coded using Bruker scripting language. Then, the sample of noise was collected by acquiring ^{13}C NMR of D_2O . Since two data sets had different intensities of the signal the noise sample was scaled to be approximately 100 times smaller than the biggest signal in simulated data. Finally, using file algebra, the two data sets were added giving the required analytical FID with noise (Figure 7).

The resulting data have been analyzed using BAYES and then compared to the results from performing fourier transform and numerical integration. (Table 3) Clearly, the Bayesian analysis gave superior estimates of integrals based on the smaller relative errors.

Table 3. Bayesian analysis of simulated data vs. numerical integration

Peak no	1	2	3	4	5
δ , ppm	10	40	80	120	160
$\nu_{1/2}$, Hz	1.3	2.5	5	10	20.5
S/N	160	81	41	22	12
Num. Integration rel. error (%)	N/A	0.2	1.5	0.3	2.4
Bayesian rel. error (%)	N/A	0.4	-0.17	0.05	0.3

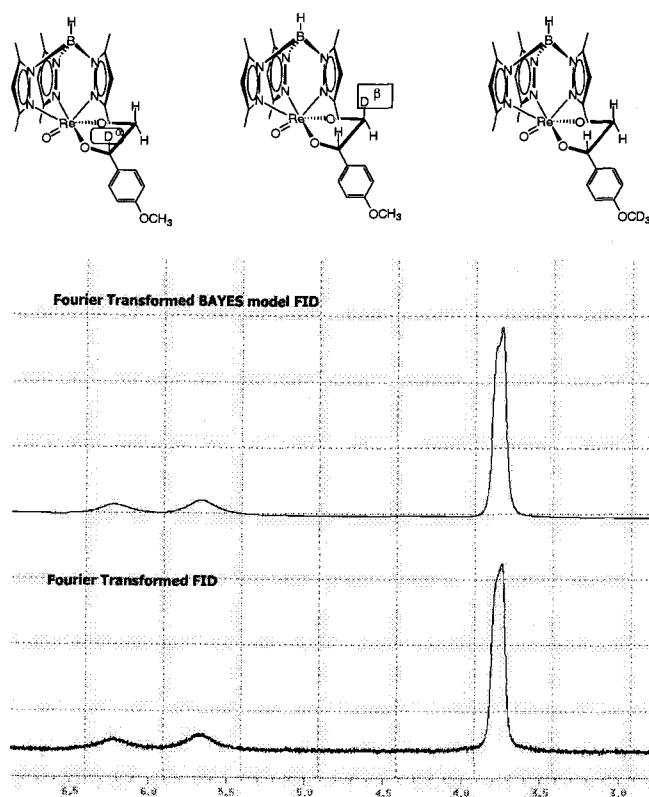
Figure 7. Construction of noise-containing FID



Bayesian analysis of real data

Next, the Bayesian analysis was performed on the FID obtained from the isotopomeric mixture of deuterated Re diolates (Figure 8). R/R_0 values were estimated from the Bayesian amplitudes, the KIEs were calculated and compared to those estimated from ^1H NMR (vide infra). KIE at the alpha position: 1.094 ± 0.023 (BAYES) vs. 1.076 ± 0.008 (^1H FT NMR). KIE at the beta position: 1.020 ± 0.018 (BAYES) vs. 1.017 ± 0.006 (^1H FT NMR).

Figure 8. Bayesian analysis of Re(V) diolate isotopomeric mixture



The tabulated data (Table 4) clearly indicate the superiority of Bayesian approach versus numerical integration of the D NMR. In fact, the latter would give highly erroneous estimate of the KIEs due to large errors in integration of heavily overlapping peaks under low S/N conditions.

Table 4. Relative integral ratios from different methodologies

	$ \alpha/p $	$ \beta/p $
Gravimetrically	0.181	0.238
BAYES	0.183	0.228
FT integration	0.112	0.193

The Bayesian approach is still inferior to the numerical integration of ^1H NMR. However, the results are not directly comparable since data sets of different qualities were used.

Concluding remarks

Bayesian analysis of D NMR time domain data was successfully applied to estimate signal amplitudes and secondary kinetic isotope effects for Re(V) diolate cycloreversion. The Bayesian methodology offers several key advantages over conventional Fourier Transform technique: (1) Fast decaying signals can be estimated with good accuracy; (2) Excellent noise tolerance; (3) Direct error estimates based on a statistical model.

On the other hand, there are several aspects that limit the practicality of the Bayesian NMR analysis. First, for large data sets (>32k) it can be computationally intensive and time consuming. The data set may not necessarily converge. We experienced convergence problems trying to analyze the ^{13}C data. Second, the quality of the Bayesian model depends on the input parameters. The estimation of the latter is not straightforward although some insights might be obtained from the analysis of the corresponding FT spectrum. Third, signal detection may be a concern for data sets with large dynamic range. Finally, the current implementation of BAYES explicitly uses the Lorentzian lineshapes for the decaying sinusoids. If, for example, the acquired signals have some Gaussian character the Bayesian

model will be wrong or may not converge. This could be one reason for convergence problems we experienced with the ^{13}C data.

KIE ESTIMATION FROM THE ^1H NMR

In the proceeding section we reported a high degree of scatter in the numerical integrations of ^{13}C NMR data for isotopomeric diolate mixtures. The reason for that was suspected to be strong quadrupolar interactions of Re and neighboring carbon atoms. Under this circumstance the use of the ^{13}C spectra for direct estimation of R/Ro values was considered to be inadvisable. The D NMR also showed unusual line broadening of carbinolic deuterons. Although the Bayesian analysis of D NMR data provided reasonable estimates of KIEs, we sought ways to substantially improve the quality of the raw data. Fortunately, the ^1H spectra of ^{13}C and D labeled isotopomeric mixture provided a good alternative.

Let us first consider the isotopomeric mixture of ^{13}C labeled Re diolates. Due to ^1H - ^{13}C coupling each individual isotopomer provides a footprint in the spectrum of the mixture. For example, the alpha proton on the alpha ^{13}C labeled compound will be coupled to the ^{13}C atom and will be equidistantly spaced from the signal for protons bound to ^{12}C (central signal). The central signal will then have contributions from the beta and the *para* methoxy labeled diolates only. The

same is true for beta and p-methoxy isotopomers. To calculate the isotopic enrichment at each position it is sufficient to integrate any three different sets of signals. This provides three independent linear equations from which the concentration of three isotopic diolates can be calculated. For example, to estimate the isotopic composition in the starting mixture of the ^{13}C labeled diolates we integrated the central alpha ($^{12}\text{C-H}$), the central reference (O^{12}CH_3) and reference satellite signals (O^{13}CH_3). The system of linear equation relates intensities to relative molarities of the individual components (Equation 5).

Equation 5.

$$\begin{aligned} I_{\alpha} &= n_{\beta} + n_{\rho} \\ I^{\text{sat}}_{\rho} &= 3n_{\rho} \\ I_{\rho} &= 3n_{\alpha} + 3n_{\beta} \end{aligned}$$

where I_{α} , I^{sat}_{ρ} , I_{ρ} are the integrals of central alpha, the central reference and reference satellite signals; n_{α} , n_{β} and n_{ρ} are the corresponding relative molarities of the isotopomers. The coefficients reflect the number of protons in each signal; the value of interest, $R_i = n_i/n_{\rho}$ $i = \text{A, B}$. Since at least three different combinations of signals can be used to obtain the R_i , the ^{13}C satellite method provides an internal check for the consistency of the methodology. Practically, the R_i calculated from different sets will have different accuracies because of widely varying magnitudes of the integrals and the linewidths in each subset. For this reason, we preferred

the integration of the methoxy (central peak and satellites) and either alpha or beta (central peak).

Four experiments have been performed. The last run was taken to a very high conversion (99%). Because of the very small amount of reisolated material the sample was heavily contaminated with the *syn* diastereomer. The S/N of its ^1H NMR was low and the data from this run were discarded as unreliable. Results for the other three runs are presented in Table 5; according to Equation 1 the KIEs are $k_{12\text{C}}/k_{13\text{C}} = 1.036 \pm 0.005$ at the alpha position, and 1.014 ± 0.006 at the beta position.

Table 5. Primary $^{12}\text{C}/^{13}\text{C}$ KIE on extrusion of 4-methoxystyrene

Run	F	R/Ro (α)	R/Ro (β)	KIE (α)	KIE (β)
1	0.905	1.803	1.020	1.035	1.008
2	0.836	1.083	1.023	1.046	1.013
3	0.903	1.100	1.040	1.043	1.017
Average:				1.041	1.013

The analysis of ^1H NMR spectra of D labeled isotopomers was performed in a similar way. Any given signal of interest had the contributions from two isotopomers. The solution of the system of linear equations gave the required isotopomeric composition. Simultaneous solution of linear equations (Equation 6) allowed the isotopomeric composition to be measured. (Correction for the small amount of signal arising from less than 100-atom-per cent labeling showed no discernible

impact.) Results are shown in Table 6; from this data secondary KIEs were $k_H/k_D = 1.076 \pm 0.005$ at the alpha position, and 1.017 ± 0.005 at the beta position.

Equation 6.

$$I_\alpha = n_\beta + n_\rho$$

$$I_\beta = n_\alpha + n_\rho$$

$$I_\rho = 3n_\alpha + 3n_\beta$$

Table 6. Secondary D KIE on extrusion of 4-methoxystyrene

Run	F	R/Ro (α)	R/Ro (β)	KIE (a)	KIE (b)
4	0.888	1.160	1.036	1.073	1.016
5	0.812	1.122	1.012	1.074	1.007
6	0.896	1.178	1.060	1.080	1.027
Average:				1.076	1.017

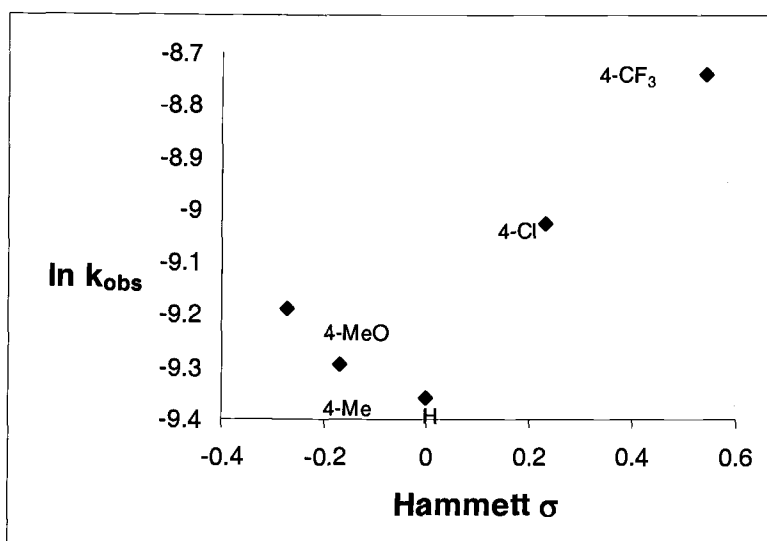
HAMMETT STUDIES

In the previous sections we already discussed the possible mechanistic ramifications of having introduced an aromatic substituent at the alpha carbon. To test the consistency of a mechanism across the substituents with different electronic properties we performed a Hammett study.

All diols were prepared by Os-catalyzed dihydroxylation of the corresponding olefins and converted to rhenium diolates according to prior methodology^{30b}.

The result is shown in Figure 9; two different slopes were observed depending on the electronic nature of the substituent. Electron donors show $\rho = -0.65$, but $\rho = +1.13$ for electron-withdrawing groups. Plotting against σ^+ yields a similar relationship but no better correlation.

Figure 9. Hammett plot for cycloreversion of substituted phenylethanedialates.



COMPUTATIONAL WORK

The cycloreversion of very closely related system, the Tp Re phenylethane diolate was studied theoretically. This omits the methyl groups on the ligand and the methoxy substituent on the phenyl group. The quantum mechanical modeling was intended to provide detailed description of the system, particularly parameters that cannot be observed experimentally such as the geometry of the transition state and the charge distribution. The work involved several stages: (1)

optimization of the reactant and the products; (2) the estimation of the energetics of the overall reaction; (3) location and optimization of transition state; and (4) estimation of activation barrier and comparison to experimental values.

Methodology

The task of estimating the energetics and the study of the transition state required the calculations be performed at the ab initio level of theory. The preference here was given to the DFT theory which enjoys excellent success in the field of transition metal chemistry¹³³. Due to complexity and the large size of the molecule (the system under consideration contains 45 first and second row atoms and one late transition metal atom) the calculations were anticipated to be extremely computationally expensive. From our previous work on related TpRe systems we noted a significant performance advantage of Jaguar software package¹³⁴ over a more standard, Gaussian program. The next critical choice was the choice of a functional. A recent literature review¹³⁵ reports that BP86 and the hybrid B3LYP functionals are by far the best ones for the assessment of the geometries and energetic properties of transition metal complexes. Our previous positive experience with the B3LYP made it a functional of choice. Preliminary geometry optimization of the ground state structures and the location of the transition state was done with LACVP (6-31G for all first- and second-row heavy atoms and hydrogen, relativistic effective core potential for Re) basis set¹³⁶. The final optimization

was performed with the LACVP*+ basis set. This uses d-type polarization functions and diffuse functions for carbon but not hydrogen. The inclusion of diffuse functions was intended to provide a better description of elongated bonds in the transition state.

Optimization of the ground state structures and location of the transition state

The TpReO_3 and the corresponding phenylethanediolate were first optimized at the LACVP level to provide good guess structures. The guess structures were then reoptimized with the higher LACVP*+ basis set. This was found to be the most reliable methodology since the direct analysis of unoptimized geometry at LACVP*+ level resulted in geometry convergence problems on several occasions. We noticed that the reoptimization at LACVP*+ level provided better description of the diolate ring bonding, particularly Re–O and Re=O bonds. A Pulay 6-31G* scaled¹³⁷ vibrational analysis showed that the calculated structures are true minima on the potential energy surface (no imaginary frequencies). The description of the energetics in this system was found to be in a satisfactory agreement with prior experimental results (Table 7).

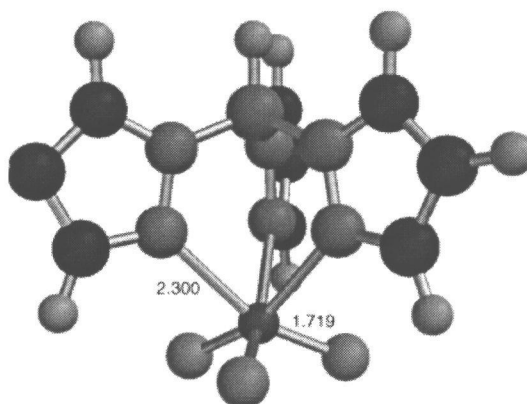
For styrene cycloreversion the zero-point energy corrected enthalpy of the reaction gave +11.8 kcal/mol. The experimental estimate for the ΔH of related systems is between zero and +5 kcal/mol^{16a}.

Table 7. Energies for optimized structures at the B3LYP/LACVP*+ level.

Quantity	Styrene	TpReO ₃	TpRe(O)(OCH PhCH ₂ O)	Transition State
E, Hartree	-309.6605	-1007.2715	-1316.9567	-1316.8998
ZPE, kcal/mol	89.79	149.58	243.05	233.18

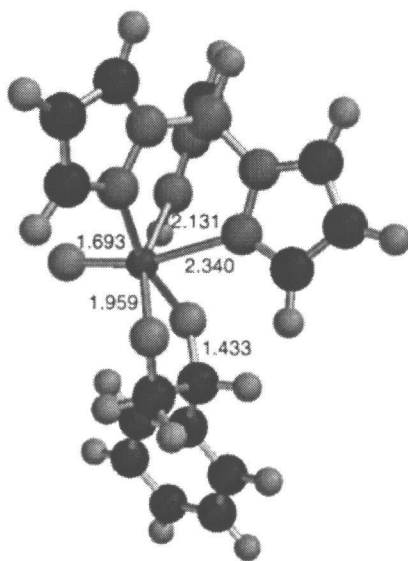
The metrical parameters are also in good agreement with the experiment. For TpReO₃, Re=O bonds were calculated to be 1.719 Å, compared to an experimental value of 1.712 Å¹³⁸.

Figure 10. Optimized structure of TpReO₃ at the B3LYP/LACVP*+ level.



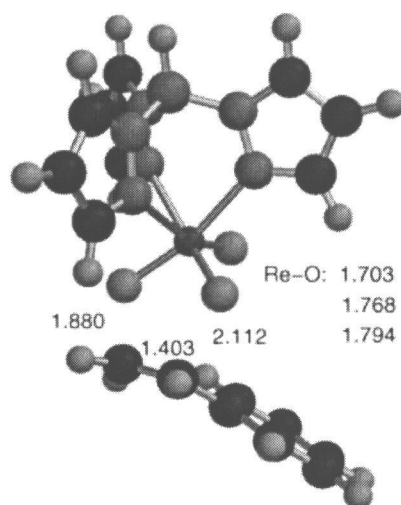
The vibrational frequency of the Re=O stretch was computed to be 909 cm^{-1} , compared to the observed value 911 and 924 cm^{-1} for TpReO_3 and 907 cm^{-1} for $\text{Tp}'\text{ReO}_3$. The phenyethane diolate structure was found to be in agreement with Santos' structure of $\text{TkRe(O)(OCH}_2\text{CH}_2\text{O)}$ (Tk = tetrakis-pyrazolylborate)¹³⁹: the Re=O bond length was 1.693 \AA (vs. 1.677 \AA) Re-N bonds cis to the oxo were shorter (2.173 \AA and 2.131 \AA vs. 2.083 \AA and 2.098 \AA) than that trans to the oxo ligand (2.341 vs. 2.287).

Figure 11. Optimized structure of $\text{TpRe(O)(OCH}_2\text{CHPhO)}$ at the B3LYP/LACVP*+ level



The location of the transition state was performed using QST guided search at the LACVP level. The final optimization was performed with LACVP*+ basis set. Vibrational analysis confirmed a single imaginary frequency. The calculated structure is shown in Figure 12.

Figure 12. Optimized structure of the transition state at the B3LYP/LACVP*+ level



The transition state energy, +35.7 kcal/mol relative to the reactant phenylethanediolate (+25.7 kcal/mol after factoring in ZPE differences), was slightly different but in quite good agreement with the experimentally observed ΔH of 27.6 kcal/mol for the Tp' complex. The structure of the transition state indicates that it is product-like (Figure 12). Most importantly, a substantial asymmetry in the cleavage of the C-O bonds was observed; the difference in bond lengths was almost 0.25 Å. The C-C bond is substantially shortened to 1.403 Å (from 1.537 Å in the phenylethanediolate). Electrostatic potential fitting indicated that the electron flow in the transition state is toward the alkene, and more to the alpha carbon than to the beta.

DISCUSSION

Both primary ^{13}C and secondary D kinetic isotope effects indicate that the cycloreversion of rhenium paramethoxyphenyl diolate proceeds via a highly asymmetric transition state. The cleavage of the C-O bond at the alpha position is substantially greater than at the beta position, although the latter is also significant. Theoretical and experimental results will be considered in the light of two mechanistic hypotheses.

Stepwise migrations: Coordinated epoxide and rhenaoxetane

Although rate-limiting formation of coordinated epoxide has been proposed the mechanism was not elaborated on. It is unlikely to be a classic "nucleophilic" type because of highly unfavorable stereoelectronics. The backside $\text{S}_{\text{N}}2$ attack of one of diolate oxygen on the diolate carbon is prohibitively difficult given the geometry and would lead to the inversion of the configuration which is not seen. The frontside attack is known to be extremely inefficient because of the destructive overlap of nucleophile HOMO and the LUMO of the substrate and low electron density between the atoms¹⁰⁵. If the ring contraction to the coordinated epoxide occurs it would rather include the participation of Re-O HOMO which is oxygen centered and has a substantial π bond character formed by the d orbital on Re and the p orbital on oxygen. In this case the a Re-O HOMO would con-

structively overlap with the C–O antibonding orbital; the electron flow from the carbon atom is accommodated by the incipient Re=O which also has the correct symmetry. According to this mechanism, one carbon-oxygen bond undergoes cleavage at the transition state; therefore, a KIE substantially bigger than unity is expected. The bond order of the second C–O bond is expected to decrease because of the extra bonding experiencing by the oxygen. This effect is expected to be very small and its contribution to the isotope effect negligible. Consequently, the KIE near unity is expected at that site.

In terms of KIE, the formation of rhenaoxetane parallels the situation with coordinated epoxide. Effectively no partial change in bonding of the second C–O bond is expected. The corresponding KIEs are bigger than unity at one site and equal unity at the other can be predicted.

The experimental results are clearly in odds with these two mechanisms. Theoretically, the competitive cleavage at the alpha and the beta position can give the isotope effects at both positions to be bigger than unity. However, the estimation of the KIEs that would be required to satisfy the experimentally observed rate constants makes this situation effectively impossible¹⁴⁰.

Concerted cycloreversion

Computational work suggested that the concerted cycloreversion of TpRe(O) phenyethane diolate proceeds through highly asynchronous product-like

transition state. One can expect that the advanced bond breaking at the alpha position would translate into a significant primary and secondary isotope effects at that position. Conversely, the small degree of bond cleavage at the beta position would manifest itself via small isotope effects. The experimentally observed KIEs fit this description. The values for the secondary deuterium kinetic isotope effects from our experiments are in striking agreement with those obtained from the cycloreversion of Cp*Re diolates if one assumes a concerted process.

The other particularly interesting feature of the system is a highly curved Hammett plot which indicates the rate acceleration by both electron-withdrawing and electron donating substituents. This parallels the observed parabolic Hammett plot of amine accelerated Os dihydroxylation. The electronic effects for electron donors are consistent with a transition state structure that has some positive charge buildup at the benzylic site. However, the rate acceleration by the electron-deficient styrenes would require a transition state with opposite charge distribution. This opens the possibility of two different mechanisms being in competition due to very well balanced stereoelectronics of the system (small charge perturbation changes the mechanism).

In conclusion, we found that both primary ^{13}C and secondary D KIEs for the extrusion of p-OMe styrene from the corresponding rhenium diolate are consistent with the concerted, asynchronous transition state. Computational studies confirm the advanced bond breaking at the alpha carbon. The curved Hammett plot suggests the existence of additional reaction manifold with different electron

demand. The stepwise process was found to be inconsistent with observed KIEs.

CHAPTER 5. CONCLUSION

The experimental investigations into the deoxygenation of epoxides with $\text{Cp}^*\text{Re(V)}$ dimer revealed that:

Inefficient catalysis in Re(V) mediated deoxygenation of epoxides is due to the formation of trinuclear and tetranuclear clusters that remove active rhenium. The clusters are formed by the interaction of $(\text{Cp}^*\text{ReO})_2(\mu\text{-O})_2$ and Cp^*ReO_3 at elevated temperatures. The tetranuclear cluster can be oxidized to a trinuclear cluster with an appropriate O atom donor, such as DMSO, and, presumably, Cp^*ReO_3 . The trinuclear cluster is inactive in epoxide deoxygenation. Faster reduction increase the turnover. Electron deficient epoxides react faster than electron rich ones; aryl substituted epoxides are more reactive than aliphatic epoxides.

Re(V) mediated epoxide deoxygenation of aliphatic diolates can occur through the intermediacy of the corresponding Re(V) diolate. The diolates are formed by the reaction of $(\text{LReO})_2(\mu\text{-O})_2$ ($\text{L} = \text{Cp}^*, \text{Tk}$) and the epoxide at 72-112°C. The resulting diolates are unstable under conditions at which they form; subsequent cycloreversion leads to a formation of LReO_3 and alkene. No cluster formation occurs when $\text{L} = \text{Tk}$. The present study identifies only one pathway of epoxide deoxygenation and does not rule out others that might occur competitively such as concerted fragmentation.

The work on the development of the synthetic approach to a stable rhenaoxetane did not lead to the target structure. Instead, the complex mixtures of organometallic compounds resulted. This precluded the isolation and identification of the reaction products. In other instances, alternative reaction pathways gave products other than rhenaoxetane. Electron transfer to Re(V) from the ortho-metallated phenolate is suspected to be at least partially responsible for the extensive decomposition of the rhenium substrate. Decomposition of rhenaoxetane (V) is also possible.

In the course of this work several general and efficient procedures for the synthesis of a number of Re complexes were developed or improved, including: (a) valuable starting materials Cp^*ReO_3 and $\text{TpRe(O)(OCH}_2\text{CH}_2\text{O)}$; (b) all members of the Re(V) oxo dihalide family, LRe(O)X_2 ($\text{L} = \text{Tp, Tp}', \text{Tk}$; $\text{X} = \text{Cl, Br}$) and dissymmetric derivatives TpRe(O)(OTf)OPh and TpRe(O)OPh .

The mechanism of rhenium diolate cycloreversion was also studied using primary ^{13}C and secondary D kinetic isotope effects (KIE) methodology. Six isotopomers of the parent $\text{Tp}'\text{Re(OCH}_2\text{CH(Ph-4-OMe)O)}$ ($\text{Tp}' = 3,5\text{-dimethyl-hydrido-trispyrazolyl borate}$) having ^{13}C and D labels at the alpha diolate, beta diolato and OMe positions were synthesized. The KIEs were determined via competition experiments; the relative isotopic enrichment at the alpha and beta positions was estimated by ^{13}C and D NMR. However, the large quadrupole of Re led to line broadening and partial overlap with a diastereomeric impurity accumulating in the sample. This caused a significant scatter in the data. An alternative procedure,

using ^1H NMR was developed and allowed for more reliable data analysis. The primary the KIEs were found to be $k_{12\text{C}}/k_{13\text{C}} = 1.041 \pm 0.005$ at the alpha position, and 1.013 ± 0.006 at the beta position. The secondary KIEs were $k_{\text{H}}/k_{\text{D}} = 1.076 \pm 0.005$ at the alpha position, and 1.017 ± 0.005 at the beta position at 103°C .

Alternative methods for treating raw ^{13}C and D data were explored. For the first time, the Bayesian analysis of D NMR time domain data was successfully applied to estimate signal amplitudes and secondary kinetic isotope effects for Re(V) diolate cycloreversion. The Bayesian methodology was found to offer several advantages over the conventional Fourier Transform technique.

^{13}C and D KIEs were found to be consistent with each other in pointing to significantly more bond breaking to the alpha carbon than to the beta carbon and indicating that cycloreversion of 4-methoxystyrene from $\text{Tp}'\text{Re}(\text{O})(\text{OCH}_2\text{CH}(\text{Ph}-4\text{-OMe})\text{O})$ proceeds via a significantly asynchronous but concerted transition state.

Cycloreversion of $\text{Tp}'\text{Re}(\text{O})(\text{OCH}_2\text{CH}(\text{Ph}-4\text{-OMe})\text{O})$ was also investigated theoretically. The ground states of the reactant and the products were optimized using hybrid DFT calculations at LACVP*+ level. A transition state was located. The thermodynamic parameters (ΔH° , ΔH^\ddagger) corrected for ZPE were found to be in good agreement with the experiment. The structure of the transition state revealed distinct asymmetry in bond breaking. The alpha C-O bond was significantly elongated relative to the beta C-O bond; the difference in bond lengths

was almost 0.25 Å. The analysis of the charge distribution showed that the electrons flow toward the alkene, and more to the alpha carbon than to the beta.

A Hammett study on cycloreversion of substituted styrenes from a series of $\text{Tp}^*\text{Re}(\text{O})(\text{diolato})$ complexes showed dichotomous behavior for electron donors and electron withdrawing groups as substituents: $\rho = -0.65$ for electron donors, but $\rho = +1.13$ for electron-withdrawing groups.

Quantitative analysis of the KIEs coupled with the observed impact of aryl substitution on the rate of cycloreversion excludes the possibility of competing single bond-cleaving (stepwise) processes being responsible for the observed KIE values.

The Hammett behavior opens the possibility that depending on a substituent, two different mechanisms might be in competition due to very well balanced stereoelectronics of the system, where charge perturbation changes the mechanism. An alternative explanation is that both types of substituents destabilize the ground state relative to the unsubstituted case. This, however requires that both types of substituents induce similar changes in the transition state.

CHAPTER 6. EXPERIMENTAL

GENERAL PROCEDURES

All reactions were performed using either standard benchtop or inert atmosphere techniques¹⁴¹ in a nitrogen-filled glove-box (Vacuum-Atmospheres Co. HE 493) or on a double-manifold Schlenk line. Solvents were purified by vacuum distillation prior to use; ether and THF were distilled from Na/benzophenone, hexane and benzene from K/Na alloy; dimethyl sulfoxide and toluene were dried with molecular sieves. Molecular sieves (4Å, Fisher) were activated by heating under vacuum (0.01 mbar) at 300°C for at least 4 hours prior to use. Infrared spectra were run on a Nicolet Magna-IR560.

General procedures for kinetic studies has been described elsewhere^{30b}. The tracer method employed in our KIE studies was described^{106,142}.

Triphenylphosphine was recrystallized from ethanol. $^{13}\text{CO}_2$, $^{13}\text{CH}_3\text{I}$ and CD_3I were purchased from Aldrich (>99 atom%). Substituted (4-Cl, 4-CF₃, 4-CH₃, 4-OCH₃) styrenes were used as received from Aldrich.

All diols were obtained from osmylation of the corresponding styrenes¹⁴³ in 40-80% yields.

All LRe(O) diolates (L = Tp, Tp', Tk) were prepared according to the general procedure described in reference 30b.

All intermediates involved in the synthesis of the labeled p-methoxy styrenes were spectroscopically compared to the unlabeled analogs which are commercially available. Relevant spectroscopic information is provided when necessary.

NMR MEASUREMENTS

NMR spectra were obtained on either a Bruker DP300 (operating at 300.133 MHz for proton or 75.469 MHz for ^{13}C) or a Bruker DPX400 (operating at 400.134 MHz for proton or 100.614 MHz for ^{13}C). All chemical shifts are referenced either to residual protons or to carbons in solvent and are expressed in ppm downfield from tetramethylsilane. A T_1 determination was done by the inversion-recovery method¹²². For quantitative NMR work digital resolution of 19 pts/Hz (^1H) and 12 pts/Hz (^{13}C) was used. Relaxation delay of 25 s ($> 5T_1$) was used in both cases. All FIDs and Fourier transformed spectra were baseline corrected. For quantitative ^{13}C NMR work an inversed gated decoupling pulse sequence was used [Braun]. Lineshapes were assumed to be Lorentzian, integrations were determined numerically using a constant integral region set at 3.08 times the peak width at half height (80% total peak area). Uncertainties were determined as previously described¹⁰⁶.

CATALYTIC DEOXYGENATION OF EPOXIDES

Typical procedure: In the glovebox, a sealable NMR tube was loaded with 2.5 mg of Cp*ReO₃, 24 mg of epoxide and 34 mg of PPh₃. The NMR tube was connected to the vacuum line and evacuated. 0.5 ml of toluene-d₈ was vacuum transferred and the tube was sealed. The resulting mixture was thermolyzed, completely submersed under the oil in a thermostated oil bath at a given temperature. The concentration alkenes and epoxides was determined by ¹H NMR relative to 1,4-di-*tert*-butylbenzene. Relaxation delays up to 30 s were used to ensure accurate integration. Sealed NMR tubes were heated in a thermostate bath. Periodically, the tube was removed and the NMR spectrum was measured.

SYNTHETIC PROCEDURES

Cp*Re(CO)₃

This was prepared according to Gladysz¹⁴⁴. A 25 ml round bottom flask was charged with 4.98g (7.63 mmol) of Re₂(CO)₁₀ and 3.52 g (25.8 mmol) of pentamethylcyclopentadiene. This was connected to the oil bubbler equipped with N₂ inlet. The mixture was heated using a heating mantle. At 77°C the evolution of carbon monoxide commenced and the nitrogen flow was turned off. The temperature was slowly raised to 201°C. After 12 hours the evolution of gas

ceased and the heat was turned off. The crystallized content was transferred to a fritted glass funnel and washed with cold hexane. After drying, 4.96g (80%) was obtained. NMR and IR spectra of the product agreed with the literature data.

Cp*ReO₃

This was prepared according to Herrmann. To 0.99 g (2.44 mmol) of Cp*Re(CO)₃ dissolved in 20 ml of benzene 12 ml of H₂O₂ (30%) and four drops of conc. sulfuric acid was added. The mixture was refluxed for 5 hours. The bile-colored benzene layer was separated, the water layer extracted with benzene. Organic layers were combined and washed with water. The solvent was removed and the resulting mixture chromatographed (SiO₂, benzene/CH₂Cl₂, gradient elution) to give 0.40g (44%) of Cp*ReO₃. NMR and IR spectra of the product agreed with the literature data.

bis-TMS peroxide

The synthesis was performed according to the literature procedure¹⁴⁶.
Yield: 75%. Purity by NMR > 99%.

Oxidation of $\text{Cp}^*\text{Re}(\text{CO})_3$ with $\text{BTMSP}/\text{Re}_2\text{O}_7$

50 ml round bottom flask was charged with 100 mg (0.247mmol) of Cp^*ReO_3 and 10 mg Re_2O_7 (0.021 mmol). 15 ml of anhydrous THF was vacuum transferred and the flask was backfilled with Ar. 0.5 ml of BTMSP was added dropwise and the reaction is stirred for additional 15 minutes. Upon completion, 0.3 ml of water was added followed by MnO_2 (25 mg). Solvent was removed *in vacuo* and after chromatography (SiO_2 , CH_2Cl_2), 77mg (85% yield) of Cp^*ReO_3 was obtained as yellow crystals. Spectroscopic data are identical to those of Cp^*ReO_3 obtained by other methods.

Reaction of Cp^*ReO_3 and $(\text{Cp}^*\text{ReO})_2(\mu\text{-O})_2$

A flame-dried flask was charged with 78 mg of Cp^*ReO_3 and 210 mg of polymer-supported PPh_3 . 15 mL was vacuum transferred and the reaction mixture was stirred for two hours producing brown solution. The solution was filtered and the solvent removed *in vacuo*. This was combined with 37 mg of Cp^*ReO_3 ; placed into sealable NMR tube; toluene was vacuum transferred and the tube was sealed under vacuum. The tube was heated at 118°C for 16 hours. The precipitate was filtered, washed with CHCl_3 . The insoluble green crystals were identified as $\{(\text{Cp}^*\text{Re})_3(\mu\text{-O})_6\}^{2+}(\text{ReO}_4^-)_2$ by ^1H NMR and IR. ^1H (CD_3CN): 2.22, s; IR (KBr): 908 (Re=O), 609, 650 cm^{-1} . The purple filtrate was concentrated and

poured into benzene. The purple solid was collected (50.0 mg,) ^1H NMR (CD_2Cl_2): 2.23, s; ^{13}C NMR (CD_2Cl_2): 11.59, 118.41; IR (KBr): 908, (Re=O), 736 cm^{-1} and identified by X ray spectroscopy as $\{(\text{Cp}^*\text{Re})_3(\mu^2\text{-O})_3(\mu^3\text{-O})_3\text{ReO}_3\}^+(\text{ReO}_4^-)$.

Oxidation of $\{(\text{Cp}^*\text{Re})_3(\mu^2\text{-O})_3(\mu^3\text{-O})_3\text{ReO}_3\}^+(\text{ReO}_4^-)$

A round bottom flask was charged with 25 mg (0.019 mmol) of $\{(\text{Cp}^*\text{Re})_3(\mu^2\text{-O})_3(\mu^3\text{-O})_3\text{ReO}_3\}^+(\text{I}^-)$ obtained by pouring acetonitrile solution of $\{(\text{Cp}^*\text{Re})_3(\mu^2\text{-O})_3(\mu^3\text{-O})_3\text{ReO}_3\}^+(\text{ReO}_4^-)$ into aqueous NaI and extracting the resulting iodo cluster with CH_2Cl_2 . 3 ml of benzene and 0.5 ml of Jones' reagent was added and the mixture was stirred for one hour. The benzene layer was separated, washed with water and passed through a short plug of silica eluting with methylene chloride. Yield was 8 mg (0.021 mmol) of Cp^*ReO_3 (37% based on iodo cluster). The product was identical to that obtained by H_2O_2 oxidation of $\text{Cp}^*\text{Re}(\text{CO})_3$.

$\text{Cp}^*\text{Re}(\text{O})\text{Cl}_2$

The synthesis was performed according to the literature procedure¹⁹. Yield: 90%. The product was identified by ^1H , ^{13}C NMR and FT-IR spectroscopy.

***ortho*-lithiophenolate**

A. *ortho*-Lithiation of phenol: The synthesis was performed according to the literature procedure¹⁴⁷. Quenching of the reaction mixture with CO₂ furnished salicylic acid in 30% yield. The product was identified by melting point and IR and compared with the commercial sample of the salicylic acid.

B. From *o*-bromophenol. The synthesis was performed according to the literature procedure¹⁴⁸. Quenching of the reaction mixture with D₂O furnished phenol in 85% yield.

Reaction of *ortho*-Li phenolate with Cp*Re(O)Cl₂

Representative procedure is given here. A 50 mL Round-bottom flask was charged with 0.1g (0.25 mmol) of Cp*Re(O)Cl₂. The flask was evacuated and backfilled with argon. 4mL of tetrahydropyran was added. Resulting green solution was cooled to -41°C and 0.7 ml tetrahydropyran solution of *ortho*-Li phenolate (0.25mmol) was added dropwise. The reaction mixture turned brown. It was stirred for 1 hour at -41°C and then brought to room temperature. Benzene (4 mL) was added and the flask was connected to the double-ended frit. The reaction mixture was filtered from the solids and the brown solution evaporated. ¹H NMR (CCl₄): 1.11 s, 1.21, 1.36, 1.56, 1.89, 2.32, 3.56, 7-18-7.38, all multiplets.

Mg/Li exchange in *ortho*-Li phenolate

A round bottom flask charged with 8.86 g of $\text{MgCl}_2 \cdot 6\text{H}_2\text{O}$ was connected to the vacuum line, evacuated and heated ($\sim 300^\circ\text{C}$). After the content of the flask reached constant weight (5.49 g) it was transferred to the glove box. A 25 mL flask was charged with 0.048 g (0.5 mmol) of anhydrous MgCl_2 . 3 mL of tetrahydropyrene was added and the flask was cooled in an ice bath. To the resulting suspension 2 mL of tetrahydropyrene solution of *ortho* Li phenolate (0.5 mmol) was added. The reaction mixture was stirred 30 min. at 0°C and 30 min. at room temperature. The flask was connected to the double-ended frit and white precipitate of LiCl filtered off. The resulting solution was used without further characterization.

Hydrido-tris-(3,5-dimethylpyrazolyl)boratorhenium (V) (oxo)dichloride

$\text{Tp}^*\text{Re}(\text{O})(\text{OCH}_2\text{CH}_2\text{O})$, prepared as reported in reference 30b (156 mg, 0.27 mmol) was dissolved in 25 mL THF. 5 mL aqueous 10 N HCl was added and stirred for 5 minutes. The green mixture was neutralized with 10 mL triethylamine, filtered, chromatographed on silica gel using dichloromethane. Removal of the solvent gave pure oxodichloride. Yield: 37.5 mg (0.065 mmol, 23%). ^1H NMR (CDCl_3): 2.21 (s, 3H); 2.35 (s, 3H); 2.66 (s, 6H); 2.94 (s, 6H); 5.69 (s, 1H); 6.10 (s, 2H.) ^{13}C NMR: 12.2, 12.3, 14.9, 15.5, 107.9, 109.4, 143.6, 148.1,

155.9, 158.2. IR (KBr): 972 (Re=O). Elemental analysis: Obsd. (Calcd. For $C_{15}H_{22}BCl_2N_6ORe$): C 31.90 (31.59); H 3.72 (3.89); N 14.21 (14.74).

Hydrido-tris-pyrazolyboratorhenium (V) (oxo)dibromide

To a suspension of $Re(O)Cl_3(PPh_3)_2$ (0.833 g, 1.0 mmol) in 5 mL CH_2Cl_2 was added a solution of 0.1 g ethylene glycol (16 mmol) and 0.5 mL triethylamine in 3 mL CH_2Cl_2 . After 2 minutes the yellow rhenium complex had dissolved, and 300 mg KTp (1.2 mmol) was added in small portions. After stirring an additional 10 minutes a lilac purple color had developed. Aqueous extraction, followed by drying the organic layer ($MgSO_4$) and removal of solvent gave the crude product; recrystallization from dichloromethane-heptane gave 320 mg crystalline blue diolate. This was then dissolved in 5 mL THF. 0.1 mL aqueous HBr (48%) was added dropwise and stirred for 3 minutes. Triethylamine (0.5 mL) was added; the solvent was removed in vacuo and the residue subjected to flash chromatography on silica gel with dichloromethane. Removal of the solvent from the turquoise band gave pure product. Yield: 230 mg (0.4 mmol, 40% for two steps). 1H NMR ($CDCl_3$): 5.93 (t, 1H, $J = 2.2$ Hz); 6.56 (t, 2H, $J = 2.7$ Hz); 7.35 (d, 1H, $J = 2.4$ Hz); 7.50 (d, 1H, $J = 2.5$ Hz); 7.89 (d, 2H, $J = 2.6$ Hz); 8.38 (d, 2H, $J = 2.2$ Hz). ^{13}C NMR ($CDCl_3$): 149.2, 148.4, 138.8, 134.5, 108.9, 106.4. Elemental analysis Obsd.(Calcd. $C_9H_{10}BBr_2N_6ORe$: C 19.02 (18.80); H 1.67 (1.75); N 14.55 (14.61). IR: 977 cm^{-1} (Re=O). Application of the previous procedure using aque-

ous HBr in place of aqueous HCl gave 1.58 g of the dibromide (2.7 mmol, 53%) from 1.5 g KReO_4 and 7.0 g KTp.

Hydrido-tris-pyrazolylboratorhenium (V) (oxo)diiodide

TpRe(O)Cl_2 (850 mg, 1.50 mmol) was dissolved with NaI (14 g) in 60 mL acetone and heated to reflux for 48 hr. The mixture was filtered, and the solvent removed. The brown residue was chromatographed on silica (dichloromethane) to give 505 mg (0.61 mmol, 41%) of golden-brown product after removal of solvent. $^1\text{H NMR}$ (CD_2Cl_2): 5.901 (t, 1H, $J = 2.3$ Hz); 6.570 (t, 2H, $J = 2.5$ Hz); 7.415 (d, 1H, $J = 2.3$ Hz); 7.548 (d, 1H, $J = 2.1$ Hz); 7.942 (d, 2H, $J = 2.5$ Hz); 8.611 (d, 2H, $J = 2.4$ Hz). $^{13}\text{C NMR}$ (CDCl_3): 154.0, 151.7, 140.8, 136.5, 110.8, 108.1. IR: 976 cm^{-1} ($\nu\text{Re=O}$). Alternatively, hydrolysis of the ethanediolate with aqueous HI as described above for the bromide gave the same product in 43% yield.

Tetrakis-pyrazolylboratorhenium(V) (oxo)dibromide

The ethanediolate was hydrolyzed with aqueous HBr as described for the Tp complex above. From 63 mg ethanediolate (0.12 mmol), 54 mg dibromide was obtained (0.084 mmol, 72% yield). $^1\text{H NMR}$ (CDCl_3): 5.88 (t, 1H, $J = 2.2$ Hz); 6.46 (t, 2H, $J = 2.3$ Hz); 6.60 (t, 1H, $J = 1.8$ Hz); 7.50 (d, 1H, $J = 2.1$ Hz);

7.70 (d, 2H, J = 2.4 Hz); 7.77 (d, 1H, J = 2.4 Hz); 8.39 (d, 2H, J = 2.0 Hz). ^{13}C NMR (CDCl_3): 106.4, 108.2, 109.1, 128.2, 135.1, 139.0, 142.8, 149.6, 150.2. IR (KBr): 985 cm^{-1} ($\nu_{\text{Re=O}}$).

Tetrakis-pyrazolyboratorhenium(V) (oxo)diiodide

Hydrolysis of the ethanediolate (188 mg, 0.33 mmol) with 0.3 mL aq. HI as described above gave, after neutralization with triethylamine, aqueous extraction and chromatography, 170 mg of the diiodide (0.23 mmol, 70%). ^1H NMR (CD_2Cl_2): 5.95 (t, 1H, J = 2.5 Hz); 6.58 (t, 2H, J = 2.8 Hz); 6.69 (t, 1H, J = 2.2 Hz); 7.67 (d, 2H, J = 2.7 Hz); 7.97 (d, 2H, J = 2.7 Hz); 7.985 (d, 1H, J = 2.5 Hz); 7.99 (d, 1H, J = 2.7 Hz); 8.75 (d, 2H, J = 2.5 Hz). ^{13}C NMR (CDCl_3): 106.5, 108.0, 108.9, 134.5, 135.2, 138.7, 142.7, 151.2, 153.4. IR (KBr): 981 cm^{-1} ($\nu_{\text{Re=O}}$). Elemental analysis: Obsd. (Calcd. For $\text{C}_{12}\text{H}_{12}\text{Bl}_2\text{N}_6\text{ORe}$): C 19.33(19.61); H 1.61 (1.65); 14.85 (15.24).

Photolysis of TpRe(O)IOPh

500 mg of TpRe(O)IOPh dissolved in 450 mL of dry heptane. 2.0 mL of dry pyridine was added. The green solution was degassed by bubbling through dry Ar for 25 minutes and photolyzed for 4.5 hours (Pyrex filter). The brown precipitate

(150 mg) was isolated, centrifuged and washed with heptane. The product was identified as $\text{TpRe}(\text{O})\text{I}_2$ by ^1H NMR and IR.

Tris-pyrazolylboratorhenium(V) (oxo)phenoxiodide.

A round bottom flask is charged with 1.259 g (2.3 mmol) of $\text{TpRe}(\text{O})\text{OPhCl}$ synthesized as described in [Brown, S. N.; Mayer, J. M. *Organometallics*, 1995, 14, 2951-2960.] and 0.74 g (2.9 mmol) of silver triflate. 50 mL of dry methylene chloride is vacuum transferred onto the solids, the flask is wrapped in Al foil and stirred at room temperature for two days. The flask is then connected to a swivel frit, silver chloride is filtered off from the olive-green solution of the triflate complex. The methylene chloride is removed on the line and 15 mL of THF is vacuum transferred into the flask. To this solution 0.62 g (2.55 mmol) of NEt_3MeI was added and the reaction mixture was stirred under vacuum overnight. The flask is opened to the atmosphere, the solvent is removed in vacuo, and the residue is chromatographed (SiO_2 , benzene). Obtained 1.01 g (70%) of $\text{TpRe}(\text{O})\text{OPhI}$. ^1H NMR (benzene- d_6): 5.36 (t, 1H, $J = 2.2$ Hz); 5.63 (t, 1H, $J = 2.9$ Hz); 5.70 (t, 1H, $J = 2.2$ Hz); 6.74 (d, 1H, $J = 2.2$ Hz); 6.84 (t, 1H, $J = 7.4$ Hz); 6.97 (d, 1H, $J = 2.9$ Hz); 7.02 (d, 1H, $J = 2.2$ Hz); 7.08 (d, 1H, $J = 2.2$ Hz); 7.20 (unresolv. s, 1H); 7.47 (t, 2H, $J = 7.4$ Hz); 7.52 (d, 1H, 2.9 Hz); 7.88 (d, 1H, $J = 2.2$ Hz); 8.32 (d, 1H, $J = 2.2$ Hz). $^{13}\text{C}\{^1\text{H}\}$ NMR 105.8, 106.1, 107.8, 107.9, 121.4, 121.9, 133.5, 137.5, 137.9, 145.3, 147.0, 150.2, 179.4. IR

(KBr): 2924, 2853 (s, $\nu_{\text{Car-H}}$), 2520 (m, $\nu_{\text{B-H}}$), 1211 (s, $\nu_{\text{C-O}}$), 968 (s, $\nu_{\text{Re-O}}$). MS: 635.8 (M^+).

Cyclooctyne

The synthesis was performed according to the literature procedure⁹³. From 9.38 g (49.6 mmol) of cyclooctene bromide 1.55 g (29%) of cyclooctyne was obtained. The product was identified by ^1H , ^{13}C NMR and FT-IR spectroscopy.

Pentamethylcyclopentadienyl 1-rhena(oxo)-4-oxacyclohexa-2,5-cyclooctadiene

A Schlenk bomb was charged with 0.374 g (1.01 mmol) of Cp^*ReO_3 , 0.0445 g (0.412 mmol) of cyclooctyne, and 1 g of polymer supported PPh_3 . Dry benzene was vacuum transferred onto the solids and the reaction mixture was stirred at $\sim 40^\circ\text{C}$ overnight. The solvent was removed in vacuo and the residue chromatographed (Al_2O_3 , eluent: CH_2Cl_2 -pentane 1:1). Yield was 0.080 g (34%) of the title compound as red crystals. ^1H NMR (benzene- d_6): 3.12 (t, 1H, $J = 3.6$ Hz); 3.08 (t, 1H, $J = 3.6$ Hz); 2.82 (m, 2H); 2.47 (m, 2H); 1.59 (s, $\sim 15\text{H}$); 1.85-1.31 (m, ~ 18 H). ^{13}C NMR: 11.61, 26.98, 28.47, 28.76, 31.25, 32.72, 42.58, 102.31, 109.48; IR (KBr): 2922, 2848, 1619, 1459, 1166, 1082, 943 ($\text{Re}=\text{O}$); MS 570 (M^+).

Synthesis of unlabeled hydrido-tris-(3,5-dimethylpyrazolyl)boratooxorhenium (V) (4-methoxy-phenyl)-ethane-1,2-diolate

A representative preparation is described here. The syntheses of labeled compounds were all accomplished in the same manner; yields and characterization are below. Yields were not optimized given the need for maximum purity.

A round-bottom flask was charged with TpReO_3 (2.34 g, 4.40 mmol), 1-(4-methoxyphenyl)ethane-1,2-diol (0.620 g, 3.69 mmol), triphenylphosphine (1.90 g, 7.30 mmol), *p*-toluenesulfonic acid (36 mg, 0.2 mmol). THF (50 ml) was vacuum transferred onto the solids and the mixture stirred at room temperature for 24 hours. The blue mixture was filtered and the filtrate reduced to a solid *in vacuo*. The residue was chromatographed on silica using CH_2Cl_2 /acetone (gradient elution). The *syn*-diolate is eluted first followed by the *anti*- diastereomer. Removal of the solvent and recrystallization from chloroform/hexane gave 0.83 g (28%) of the *anti*- and 0.13 g (4.4%) of the *syn*- diolates. *Anti*- diastereomer: ^1H -NMR (CDCl_3 , δ , ppm): 7.37 (d, $J=8.1$ Hz, 2H), 6.88 (d, $J=8.1$ Hz, 2H), 6.23 (dd, $J=6.6, 9.6$ Hz, 1H), 5.97 (s, 1H), 5.96 (s, 1H), 5.65 (dd, $J=6.6, 10.3$ Hz, 1H), 5.53 (s, 1H), 4.59 (t, 9.6Hz, 1H), 3.81 (s, 3H), 2.67 (s, 3H), 2.54 (two unresolved s, 6H), 2.50 (s, 3H), 2.47 (s, 3H), 2.16 (s, 3H). ^{13}C -NMR (CDCl_3 , δ , ppm): 159.2, 157.5, 156.8, 153.7, 147.7, 146.9, 143.0, 138.7, 128.9, 113.6, 108.2, 107.6, 107.5, 95.9, 94.5, 55.4, 14.5, 14.4, 14.0, 12.7, 12.6, 12.5. MS (CI): ($\text{M}^+ + 1$) 667. *Syn*- diastereomer: ^1H -NMR (CDCl_3 , δ , ppm): 7.63 (d, $J=8.2$ Hz, 2H), 6.98

(d, $J=8.2$ Hz, 2H), 6.02 (s, 1H), 5.99 (s, 1H), 5.87 (dd, $J=7.7, 10.6$ Hz, 1H), 5.78 (t, $J=9.53$ Hz, 1H), 5.50 (s, 1H), 5.42 (t, $J=9.88$ Hz, 1H), 3.85 (s, 3H), 2.67 (s, 3H), 2.65 (3H), 2.57 (s, 3H), 2.55 (s, 3H), 2.23 (s, 3H), 2.17 (s, 3H). ^{13}C -NMR (CDCl_3 , δ , ppm): 158.8, 157.5, 157.0, 154.0, 147.7, 147.1, 143.2, 135.0, 127.5, 113.9, 107.9, 107.8, 107.3, 98.0, 89.1, 55.5, 15.5, 14.2, 13.8, 12.7, 12.6, 12.5. MS (CI): ($\text{M}^+ + 1$) 667.

(4-Methoxy-phenyl)-[1- ^2H]ethane-1,2-diol

In 200 ml round bottom flask 22 ml of 1.0 M LiAlD_4 (22 mmol) in THF was diluted with 80 ml of THF and cooled in an ice bath. 5.61g (33 mmol) of anisoyl chloride was added dropwise. The resulting milky suspension was stirred for 30 min in the ice bath, then for 30 min at room temperature and quenched with diluted aq. HCl. The organic layer was washed with water, brine and dried over Na_2SO_4 . Yield was quantitative. The product was taken to the next step without further purification. 3.3 g (23.6 mmol) of resulting α,α -dideutero-4-methoxybenzyl alcohol was treated with 12.35g (29.1 mmol) of Dess-Martin reagent in CH_2Cl_2 . After 30 min at room temperature the reaction mixture was quenched with dilute NaOH. The residue was passed through a short plug of silica (eluent: CH_2Cl_2) to afford 2.7g (84%) of α -deutero-anisaldehyde. This (1.78g, 13 mmol) was treated with 10.5g (26 mmol) of $\text{PPh}_3=\text{CH}_2$ (obtained by alkylation of PPh_3 with CH_3I followed by a treatment with BuLi) in THF at 0°C . After 2 hours in the ice bath and 1

hour at room temperature the reaction mixture was hydrolyzed and extracted with pentane. The organic layer was washed with water, brine and dried over MgSO_4 . The residue was passed through a short plug of silica (eluent: hexane) to afford 1.35g (77%) of the 4-methoxy- α -deuterostyrene. Bishydroxylation of 1.2g of this styrene furnished 0.90g (61%) of the title diol. $^1\text{H-NMR}$ (CDCl_3 , δ , ppm): 7.30 (d, $J=8.8$ Hz, 2H), 6.91 (d, $J=8.8$ Hz, 2H), 3.82 (s, 3H), 3.71 (m, 2H), 2.43 (br. s, $\sim 1\text{H}$), 2.06 (br. s, $\sim 1\text{H}$)

(4-Methoxy-phenyl)-[2- ^2H]ethane-1,2-diol

1.1g (5.16mmol) of *trans-p*-methoxy- β -bromostyrene¹⁵⁰ were treated with 11.36 mmol (2.2 equiv) of *t*BuLi in diethyl ether at -100°C . After stirring at -100°C for 15 min and for 30 min at 0°C the reaction mixture was quenched with 2 ml of D_2O . The organic layer was washed with water, brine and dried over MgSO_4 . The residue was passed through a short plug of silica (eluent: hexane) to afford 0.655g (94%) of the 4-methoxy- β -deuterostyrene. Bishydroxylation furnished 0.49g (60%) of the title diol. $^1\text{H-NMR}$ (CDCl_3 , β , ppm): 7.30 (d, $J=8.8$ Hz, 2H), 6.91 (d, $J=8.8$ Hz, 2H), 4.78 (d, $J=8.2$ Hz, 1H), 3.82 (s, 3H), 3.65 (d, $J=8.2$, 1H), 2.50 (br. s, $\sim 1\text{H}$), 2.16 (br. s, $\sim 1\text{H}$).

(4-[²H₃]methoxy-phenyl)-ethane-1,2-diol

A 100 ml round bottom flask was charged with 3.76g (31 mmol) of 4-hydroxystyrene¹⁵¹, 50 ml of dry benzene and 4.5g (18mmol) of TIOEt. The reaction mixture was stirred at room temperature for 30 min and poured into a large amount of hexane. The resulting thalious phenoxide was collected by filtration, washed with benzene, hexane and dried; yield was 4.8g, (82%). 2.5g of the thalious 4-vinylphenoxide was dissolved in 5 ml of DMSO and the solution of 1g of CD₃I in 1 ml of DMSO was added. After 45 min the yellow crystals of TII were filtered off; the mother liquor was poured into water and extracted with Et₂O. The organic layer was washed with water, brine and dried over MgSO₄. The residue was passed through a short plug of silica (eluent: CH₂Cl₂) to afford 0.84g (89%) of the para- methoxy labeled styrene. Bishydroxylation of 0.7g of this compound furnished 0.3g (34%) of the title diol. ¹H-NMR (CDCl₃, δ, ppm): 7.30 (d, J=8.8 Hz, 2H), 6.91 (d, J=8.8 Hz, 2H), 4.77 (dd, J=3.9, 8.0 Hz, 1H), 3.70 (m, 2H), 2.46(br. s, ~2H).

(4-Methoxy-phenyl)-[1-¹³C]ethane-1,2-diol.

A 250 ml Schlenk bomb connected to Ar manifold was charged with 5.5g (23.5 mmol) of i-iodoanisole, 50 ml Et₂O and cooled to -78°C. To this solution, 24 ml (47 mmol) of tBuLi in pentane (2.1M) was added. The reaction mixture was

stirred for 1h 30 min at -78°C , after which the mixture was frozen with liq. N_2 and the bomb was connected to a vacuum manifold. A lecture bottle containing 2.9g of $^{13}\text{CO}_2$ was connected to the line and $^{13}\text{CO}_2$ was transferred into the bomb. The bomb was stoppered and warmed to -40°C and then left in the bath to reach room temperature overnight. The reaction mixture was opened to the atmosphere and acidified with aq. HCl . The organic layer was washed with water, brine and then dried over MgSO_4 . After solvent removal and recrystallization from THF/heptane 2.96g (82%) of *p*-anisic [α - ^{13}C] acid was obtained. 2.72g (17.8 mmol) of this compound was treated with 26 ml (26 mmol) of BH_3 -THF at 0°C and stirred for 1 hour. The reaction mixture was hydrolyzed with water, extracted with ether, washed with water and brine, and finally dried with MgSO_4 giving 2.4g (97%) of *p*-anisyl [^{13}C] alcohol. This was taken to the next step without further purification.

To a solution of oxalyl chloride in CH_2Cl_2 (17.36 ml, 34.7 mmol) diluted with 50 ml CH_2Cl_2 at -78°C were added a solution of DMSO (3.7 ml, 52 mmol) in 25 ml of CH_2Cl_2 . The mixture was stirred for 10 min at -78°C and a solution of the alcohol (2.41g in 25 ml of CH_2Cl_2) was added. This was stirred at -78°C for 15 min, then 10 ml Et_3N was added and the resulting mixture allowed to reach room temperature. After quenching with water the organic layer was separated, washed with water and brine and dried over MgSO_4 . The residue was passed through a short plug of silica (eluent: CH_2Cl_2) to afford 1.99g (84%) of the *p*-anis-

[^{13}C]aldehyde. Wittig olefination and bishydroxylation performed as described above gave 0.415g of the title diol. $^1\text{H-NMR}$ (CDCl_3 , δ , ppm): 7.30 (dd, $J=3.6$, 8.8 Hz, 2H), 6.91 (d, $J=8.8$ Hz, 2H), 4.78 (ddd, $J=3.7, 8.1$, 144.2 Hz, 1H), 3.82 (s, 3H), 3.70 (m, 2H), 2.47 (br. s, $\sim 1\text{H}$), 2.09 (br. s, $\sim 1\text{H}$).

(4-Methoxy-phenyl)-[2- ^{13}C]ethane-1,2-diol

Wittig olefination of *p*-anisaldehyde with $^{13}\text{CH}_2=\text{PPh}_3$ and bishydroxylation was performed as described in the preparation of the alpha deuterated diol. From 1g of $^{13}\text{CH}_3\text{I}$, 0.15g (13%) of the title diol was obtained. $^1\text{H-NMR}$ (CDCl_3 , δ , ppm): 7.30 (dd, $J=3.6$, 8.8 Hz, 2H), 6.91 (d, $J=8.8$ Hz, 2H), 4.78 (m, 1H), 3.95 (m, $J = 142$ Hz, 1H), 3.82 (s, 3H), 3.47 (m, $J = 140$ Hz, 1H), 2.43 (t, $J=3.7\text{Hz}$ $\sim 1\text{H}$), 2.09 (m $\sim 1\text{H}$).

Synthesis of 1-(4-[^{13}C]methoxy-phenyl)-ethane-1,2-diol

Procedure identical to that described in the preparation of the corresponding deuterated diol. From 1g of $^{13}\text{CH}_3\text{I}$ the yield was 0.68g (57%) of the title diol. $^1\text{H-NMR}$ (CDCl_3 , δ , ppm): 7.30 (d, $J=8.8$ Hz, 2H), 6.91 (d, $J=8.8$ Hz, 2H), 4.77 (dd, $J=3.9$, 8.0 Hz, 1H), 3.82 (d, $J=144$ Hz, 3H) 3.70 (m, 2H).

CYCLOREVERSION OF ^{13}C AND D LABELED HYDRIDO-TRIS-(3,5-DIMETHYLPYRAZOLYL) BORATOORHENIUM (V) (4-METHOXY-PHENYL)-ETHANE-1,2-DIOLATES.

General procedure

Typically, a 12x75 mm glass vessel was charged with ~150 mg of an equimolar mixture of the alpha, beta and *p*-OMe isotopomers (a portion of the mixture was reserved for NMR analysis) 3 ml of toluene was vacuum transferred and the vessel was sealed under vacuum. This was heated in a thermostated bath; temperature was measured with calibrated thermometers to $\pm 0.1^\circ\text{C}$. The percent conversion was estimated by timing the reaction. Upon completion, the vessel was opened and the mixture was chromatographed (SiO_2 , CH_2Cl_2) to reisolate unreacted diolate.

Isotopic molar ratios

The relative molar ratio at each position was obtained from raw integrals after solving the appropriate linear equations (see discussion in Chapter 4).

Table 8. Isotopic molar ratio (H/D) at each position as measured by ^1H NMR

RUN		H/D		
		alpha ($n\beta+n\rho$)/ $n\alpha$	beta($n\alpha+n\rho$) / $n\beta$	reference ($n\alpha+n\beta$)/ $n\rho$
4	initial	3.2921	2.1865	1.2066
	final	2.4260	2.2252	1.3140
5	initial	3.2921	2.1865	1.2066
	final	2.9449	2.2533	1.2772
6	initial	1.2328	3.9009	1.8728
	final	1.0699	4.0467	2.1375

Table 9. Isotopic molar ratio (H/D) at each position as measured by ^1H NMR

RUN		H/D		
		alpha ($n\beta+n\rho$)/ $n\alpha$	beta($n\alpha+n\rho$) / $n\beta$	reference ($n\alpha+n\beta$)/ $n\rho$
4	initial	3.2921	2.1865	1.2066
	final	2.4260	2.2252	1.3140
5	initial	3.2921	2.1865	1.2066
	final	2.9449	2.2533	1.2772
6	initial	1.2328	3.9009	1.8728
	final	1.0699	4.0467	2.1375

EXPERIMENTAL DETAILS FOR THE STRUCTURAL CHARACTERIZATION OF
 $[(\text{Cp}^*\text{Re})_3(\mu^2\text{-O})_3(\mu^3\text{-O})_3\text{ReO}_3][\text{ReO}_4] \cdot \text{NCME}$

The crystals examined were obtained from the microcrystalline sample of $\{(\text{Cp}^*\text{Re})_3(\mu^2\text{-O})_3(\mu^3\text{-O})_3\text{ReO}_3\}^+(\text{ReO}_4^-)$. Prior to crystallization the yellowish solution was decanted off, and the remaining solid was washed with small amounts of THF and CHCl_3 in order to remove a white solid present in the sample tube. The compound was then redissolved in 2 mL MeCN and this solution was layered with ca. 10 mL of Et_2O . Over the course of a few days large plate-like crystals grew from this mixture. From these, a crystal was chosen which was trimmed to yield a sample of approximate dimensions $0.5 \times 0.3 \times 0.2 \text{ mm}^3$, which was then mounted on the end of a Pyrex fiber using a drop of epoxy glue. The crystal was indexed and data was collected using automated procedures described elsewhere¹⁵².

The automated search procedure yielded a list of 10 reflections with $10.5 < 2\theta < 19.4$ from which the crystal was indexed, revealing a monoclinic lattice. Using these parameters, the list was expanded to 70 reflections by centering an additional 34 reflections with $68.4 < 2\theta < 69.8^\circ$, and the lattice parameters refined using this list. All unique data for Laue group $2/m$ were collected for $4 < 2\theta < 115^\circ$. A correction for the effects of absorption anisotropy was done by analytical methods.

The structure was solved by a Patterson search as programmed in SHELXS-

90, which yielded the positions of the four Re atoms. This solution was expanded by alternate cycles of least-squares refinement followed by Fourier synthesis using SHELXL-93¹⁵³. During the final stages of refinement some of the H atoms could be found in the electron density maps. However, to preserve a favorable data-to-parameter ratio all H atoms were placed in idealized positions and all H atoms were given a common thermal displacement parameter.

BIBLIOGRAPHY

1. (a) Feig, A. L.; Lippard, S. J. *Chem. Rev.* **1994**, 759--805 and references cited therein. (b) Riley, D.; Stern, M.; Ebner, J. *The Activation of Dioxygen and Homogeneous Catalytic Oxidation*. Eds. Barton, D.H. R.; Martell, A. E.; Sawyer, D. T. Plenum: New York; pp. 31--44. (c) Collman, J. P.; Hegedus, L. S.; Norton, J. R.; Finke, R. G. *Principles and Applications of Organotransition Metal Chemistry*; University Science Books: Mill Valley, 1987.
2. (a) Stewart, R. *Oxidation in Organic Chemistry* Wiberg, K. B.; Ed., Part A, p.2. Academic Press, New York, 1965. (b) Nugent, W. A.; Mayer, J. M.; *Metal-Ligand Multiple Bonds*; Wiley-Interscience: New York, 1988; (c) Sheldon, R. A.; Kochi, J.K. *Metal Catalysed Oxidations of Organic Compounds*; Academic Press: New York, 1981, (d) *Organic Synthesis by Oxidation with Metal Compounds*, ed. W.J. Mijs, deJonghe, C. R. H. I., Plenum: New York; 1986, (e) Gable, K. P.; *Adv. Organomet. Chem.*, **1997**, 41, 127.
3. Jacobsen, E. N.; Marko, I.; Mungall, W. S.; Schroder, G.; Sharpless, K. B. *J. Am. Chem. Soc.* **1988**, 110, 1968.
4. See, for example: Jacobsen, E. N.; Asymmetric Catalytic Epoxidation of unfunctionalized olefins. In: *Catalytic Asymmetric Synthesis*; Ed. Ojima, I. VCH Publishers: New York, 1993 and references cited therein.
5. For support of osmaoxetane see: (a) Norrby, P. O.; Becker, H.; Sharpless, K. B. *J. Am. Chem. Soc.* **1996**, 118, 35. (b) Nelson, D. W.; Gypser, A.; Ho, P. T.; Kolb, H. C.; Kondo, T.; Kwong, H.-L.; McGrath, D. V.; Rubin, A. E.; Norrby, P.-O.; Gable, K. P.; Sharpless, K. B. *J. Am. Chem. Soc.* **1997**; 119, 1840. For arguments in favor of [3+2] see: (c) Corey, E. J.; Noe, M. C. *J. Am. Chem. Soc.* **1996**, 118, 35. (d) DelMonte, A. J.; Haller, J.; Houk, K. N.; Sharpless, K. B.; Singleton, D. A.; Strassner, T.; Thomas, A. A. *J. Am. Chem. Soc.* **1997**; 119, 9907.
6. *The Activation of Dioxygen and Homogeneous Catalytic Oxidation*; Barton, D. H. R.; Martell, A. E.; Sawyer, D. T., Ed., Plenum Press: New York, 1993, pp. 31-44.
7. *Cytochrome P-450*; Sato, R., Omura, T., Eds; Kodan.
8. (a) Collman, J.P.; Zhang, X.; Lee, V. J.; Uffelman, E. S.; Brauman, J. I. *Science*, **1993**, 261, 1404. (b) Collman, J. P.; Wang, Z.; Straumanis, A.; Quelquejeu, M. *J. Am. Chem. Soc.* **1999**, 121, 460-461.

9. Sharpless, K. B.; Teranishi, A. Y.; Backvall, J-E. *J. Am. Chem. Soc.* **1977**, *99*, 3120-3128.
10. Brown, S. N.; Mayer, J. M. *J. Am. Chem. Soc.* **1996**, *118*, 12119-12133.
11. (a) Conry, R. R.; Mayer, J. M. *Inorg. Chem.* **1990**, *29*, 4862-4867. (b) Pietsch, M. A.; Hall, M. B. *Inorg. Chem.* **1996**, *35*, 1273-1278.
12. (a) Andrews, M. A.; Klaeren, S. A.; *J. Am. Chem. Soc.* **1989**, *111*, 4131-4133. (b) Andrews, M. A.; Klaeren, S. A.; Gould, G. L.; *In Carbohydrates as Organic raw Materials II*; Descotes, G., VCH: New York, 1993; pp 3-25. (c) Cook, G. K.; Andrews, M. A. *J. Am. Chem. Soc.* **1996**, *118*, 9448-9449.
13. Brock, S.L.; Mayer, J. M. *Inorg. Chem.* **1991**, *30*, 2138.
14. Glidwell, C. *Inorg. Chim. Acta*, **1977**, *4*, 149-157.
15. Sanderson, R. T. *Inorg. Chem.*, **1986**, *25*, 3518-3522.
16. (a) Gable, K.P.; Juliette, J.J.J.; Li, C.; Nolan, S.P. *Organometallics*, **1996**, *15*, 5250. (b) Gable, K. P.; Phan, T. N. *J. Am. Chem. Soc.* **1993**, *115*, 3036-3037.
17. Holm, R. H.; Donahue, J. P. *Polyhedron* **1993**, *12*, 571-589.
18. Herrmann, W. A. Roesky, P.; Wng, M.; Scherer, W.; *Organometallics*, **1994**, *13*, 4531.
19. Herrmann, W.A.; Floel, M.; Kulpe, J; Felixberger, J.K.;Herdweck, E. *J. Organomet. Chem.* **1988**, *355*, 297.
20. Gisdakis, P.; Antonczak, S.; Rosch, N. *Organometallics* 1999, *18*, 5044.
21. Seymore, S.B.; Brown, S.N. *Inorg. Chem.* **2000**, *39*, 325.
22. Gable, K. P.; Juliette, J.J.J.; Gartman, M. A. *Organometallics*, **1995**, *14*, 3138.
23. Wittig, G.; Haag, W. *Chem. Ber.* **1955**, *88*, 1654-1666.
24. Ruiz, J.; Vivanco, M.; Floriani, C.; Chiesi-Villa, A. Guastini, C. *J. Chem. Soc. Chem. Commun.* **1991**, 762.
25. Listemann, M. L.; Schrock, R. R.; Dewan, J. C.; Kolodziej, R. M. *Inorg. Chem.* **1988**, *27*, 264.

26. (a) Herrmann, W. A.; Serrano, R.; Ziegler, M. L.; Pfisterer, H.; Nuber, B. *Angew. Chem., Int. Ed. Engl.*, **1985**, *24*, 50. (b) Herrmann, W. A.; Serrano, Kusthardt, U.; Guggolz, E. R.; Nuber, B.; Ziegler, M. L. *J. Organomet. Chem.* **1985**, *287*, 329.
27. Zhu, Z.; Al-Ajlouni, A. M.; Espenson, J. H. *Inorg. Chem.* **1996**, *35*, 1408-1409.
28. Torrent, M.; LiqunDeng, L.; Duran, M.; Sol, M.; and Ziegler, T. *Can. J. Chem.* **1999**, *77*, 1476-1491.
29. Isacacs, N, *Physical Organic chemistry*, Longman: London 1995.
30. (a) Gable, K. P. *Organometallics*, **1994**, *13*, 2486-2488. (b) Gable, K. P.; AbuBaker, A.; Zientara, K.; Wainwright, A. M. *Organometallics*, **1999**, *18*, 173-179.
31. Nelson, D. W.; Gypser, A.; Ho, P. T.; Kolb, H. C.; Kondo, T.; Kwong, H-L.; McGrath, D. V.; Rubin, A. E.; Norrby, P-O.; Gable, K. P.; Sharpless, K. B. *J. Am. Chem. Soc.* **1997**, *119*, 1840-1858.
32. (a) Corey, E. J. Noe, M. C.; *J. Am. Chem. Soc.* **1996**, *118*, 11038-11053. (b) Hamada, T.; Fukuda, T.; Imanishi, H.; Katsuki, T. *Tetrahedron*, **1996**, *52*, 515-530. (c) Wu, Y-D.; Wang, Y.; Houk, K. N. *J. Org. Chem.* **1992**, *57*, 1362-1369.
33. De Pasquale, R., *J. J. Chem. Soc. Chem. Commun.* 1973, 157.
34. Vivanco, M.; Ruiz, J.; Floriani, C.; Chiesi-Villa, A.; Rizzoli, C. *Organometallics*, **1993**, *12*, 1802-1810.
35. (a) Ollis, W. D.; Rey, M.; Sutherland, I. O.; *J. Chem. Soc. Chem. Commun.* **1975**, 573; (b) Dolling, U. H.; Closs, G. L.; Cohen, A. H.; Ollis, W. D. *J. Chem. Soc. Chem. Commun.* **1975**, 545.
36. C. Stara, I. G. Sary, I.; Tichy, M.; Zavada, J.; Hanus, V. *J. Am. Chem. Soc.* **1994**, *116*, 5084-5088.
37. (a) Rappe, A. K.; Goddard, W. A. *J. Am. Chem. Soc.* **1980**, *102*, 5114. (b) Rappe, A. K.; Goddard, W. A. *Nature*, **1980**, *285*, 311.
38. (a) Walba, D. M.; DePuy, C. H.; Grabowski, J. J.; Bierbaum, V. M. *Organometallics* **1984**, *3*, 498. (b) B. Kang, H.; Beauchamp, J. L. *J. Am. Chem. Soc.* **1986**, *108*, 5663.

39. Collman, J. P.; Brauman, J. I.; Meunier, B.; Hayashi, T.; Kodadek, T.; Raybuck, S. A.; *J. Am. Chem. Soc.* **1985**, *107*, 2000.
40. Lee, R. W.; Nakagaki, P. C.; Balasubramanian, P. N.; Bruice, T. C. *Proc. Acad. Sci. U.S.A.* 1988, *85*, 641.
41. Groves, J. T.; Myers, S. J. *J. Am. Chem. Soc.* **1983**, *105*, 5791.
42. Ostovic, D.; Bruice, T. C.; *J. Am. Chem. Soc.* **1988**, *110*, 6906.
43. Traylor, T. G.; Miksztal, A. R.; *J. Am. Chem. Soc.* **1989**, *111*, 7443.
44. Grove, J. T.; Watanabe, Y. *J. Am. Chem. Soc.* **1986**, *108*, 506-507.
45. Ortiz de Montellano, P. R.; Kunze, K. L. *Biochemistry* **1981**, *20*, 7266.
46. Combes, C. R. *Acad. Fr.*, **1889**, *108*, 1252.
47. Samsel, E. G.; Srinivasan, K.; Kochi, J. K. *J. Am. Chem. Soc.* **1985**, *107*, 7606-7617.
48. Finney, N. S.; Pospisil, P. J.; Chang, S.; Palucki, R. G.; Hansen, K. B.; Jacobsen, E. N. *Angew. Chem. Int. Ed. Engl.* **1997**, *36*, 1720-1723.
49. (a) Senanayake, C. H.; Smith, G. B.; Liu, J.; Fredenburgh, L. E.; Ryan, K. M.; Hughes, D. L.; Larsen, R. D.; Verhoeven, T. R. Reider, P. J. *Tetrahedron Lett.* **1995**, *36*, 3993. (b) Senanayake, C. H.; Smith, G. B.; Fredenburgh, L. E.; Liu, J.; Roberts, F.; Hughes, D. L.; Larsen, R. D.; Verhoeven, T. R. Reider, P. J. *Tetrahedron Lett.* **1996**, *37*, 3271.
50. Norrby, P.-O.; Linde, C.; Akermark, B. *J. Am. Chem. Soc.* **1995**, *117*, 11035-11036.
51. Hayashi, Y.; Schwartz, J.; *Inorg. Chem.* **1981**, *20*, 3473.
52. Kafafi, Z. H.; Hauge, R. H.; Billups, W. E.; Margrave, J. L. *J. Am. Chem. Soc.* **1987**, *109*, 4775.
53. (a) Schrock, R. R. *J. Am. Chem. Soc.* **1976**, *98*, 5399. (b) Schrock, R. R.; Fellmann, J. D. *J. Am. Chem. Soc.* **1978**, *100*, 3359.
54. Upton, T. H.; Rappe, A. K. *J. Am. Chem. Soc.* **1985**, *107*, 1206-1218.
55. (a) Schlodder, R.; Ibers, J. A.; Lenarda, M.; Graziani, M. *J. Am. Chem. Soc.*

1974, 96, 6893. (b) Lenarda, M.; Pahor, N. B.; Calligaris, M.; Graziani, M.; Randaccio, L.; *J. Chem. Soc. Dalton Trans.* **1978**, 279.

56. Schiott, B.; Jorgensen, K. A. *J. Chem. Soc. Dalton Trans.* **1989**, 2099.

57. Klein, D. P.; Hayes, J. C.; Bergman, R. G. *J. Am. Chem. Soc.* **1988**, 110, 3704-3706.

58. (a) Bruin, B.; Boerakker, M. J.; Donners, J. J. J. M.; Christiaans, B. E. C.; Schlebos, P. P. J.; Gelder, R.; Smits, J. M. M.; Spek, A. L.; Gal, A. W. *Angew. Chem. Int. Ed. Engl.* **1997**, 36, 2064-2067. (b) Flood, T. C.; Imura, M.; Perotti, J. M.; Rheingold, A. L.; Concolino, T. E. *J. Chem. Soc. Chem. Commun.* **2000**, 1681-1682.

59. (a) Schroder, M. *Chem. Rev.* **1980**, 187-213; (b) Norrby, P.-O.; Becker, H.; Sharpless, K. B. *J. Am. Chem. Soc.* **1996**, 118, 35-42.

60. (a) Hofmann, K. A.; *Chem. Ber.*, **1912**, 45, 3329. (b) Hofmann, K. A.; Ehrhart, O.; Schneider, O. *Chem. Ber.* **1913**, 46, 1657.

61. (a) Milas, N. A.; Sussman, S. *J. Am. Chem. Soc.* **1936**, 58, 1302. (b) Milas, N. A.; Sussman, S. *J. Am. Chem. Soc.* **1937**, 59, 2345.

62. Akashi, K.; Palermo, R. E.; Sharpless, K. B. *J. Org. Chem.* **1978**, 43, 2063.

63. VanRheenen, V.; Kelly, R. C.; Cha, D. Y. *Tetrahedron Lett.* **1976**, 23, 1973-1976.

64. Poli, G. *Tetrahedron Lett.*, **1989**, 30, 7385-7388.

65. Minato, M.; Yamamoto, K.; Tsuji, J. *J. Org. Chem. Soc.* **1990**, 55, 766.

66. (a) Criegee, R.; *Justus Liebigs Ann. Chem.*, **1936**, 522, 75. (b) Criegee, R.; Marchand, B.; Wannowius, R. *Justus Liebigs Ann. Chem.*, **1942**, 550, 99.

67. Norrby, P.-O.; Gable, K. P. *J. Chem. Soc. Perkin Trans. 2*, **1995**, 171-178.

68. Bianchi, G.; DeMicheli, C.; Gandolfi, R. in *The Chemistry of Double Bonded Functional Groups*, Part 1, Supplement A, S. Parai (ed.), John Wiley and Sons, New York 1977, pp. 369-532.

69. (a) Tantillo, D. J.; Hoffmann, R. *J. Am. Chem. Soc.*, **2001**, in press. (b) Mango, F. D. *Coord. Chem. Rev.* **1975**, 15, 109-205.

70. Eisenstein, O.; Hoffmann, R.; Rossi, A. R. *J. Am. Chem. Soc.* **1981**, *103*, 5582.
71. Norrby, P.-O.; Kolb, H. C.; Sharpless, K. B.; *J. Am. Chem. Soc.* **1994**, *116*, 8470-8478.
72. Gable, K. P.; Juliette, J. J. *J. Am. Chem. Soc.* **1995**, *117*, 955-962
73. Gable, K. P.; Phan, T. N. *J. Am. Chem. Soc.* **1994**, *116*, 833-839.
74. Brown, S. N. Ph.D. Thesis, University of Washington, 1994.
75. Herrmann, W. A. *Angew. Chem. Int. Ed. Engl.* **1988**, *27*, 1297-1313.
76. Brown, S. N.; Mayer, J. M.; *Organometallics* **1995**, *14*, 2951.
77. Herrmann, W. A.; Floel, M.; Herdtweck, E. *J. Organomet. Chem.* **1988**, *358*, 321-338.
78. (a) de Boer, E. J. M.; de With, J. *J. Am. Chem. Soc.* **1986**, *108*, 8271-8273.; (b) Herrmann, W. A.; Fischer, R. A.; Amslinger, W.; Herdtweck, E. *J. Organomet. Chem.* **1989**, *362*, 333-343. (c) Herrmann, W. A.; Fischer, R. A.; Herdtweck, E.; *Organometallics*, **1989**, *8*, 2821-2831.
79. Posner, G. H., Canella, K. A. *J. Am. Chem. Soc.* **1985**, *107*, 2571-2573.
80. Herrmann, W. A.; Kiprof, P.; Rypdal, K.; Tremmel, J.; Blom, R.; Alberto, R.; Bejm, J.; Albach, R. W.; Bock, H.; Solouki, B.; Mink, J.; Lichtenberger, D.; Gruhn, N. E. *J. Am. Chem. Soc.*, **1991**, *113*, 6527.
81. Hermann, W. A.; Voss, E.; Floel, M. *J. Organomet. Chem.* **1985**, *297*, C5.
82. Gable, K. P. Phan, T. N. *J. Organomet. Chem.* **1994**, *466*, C5-C6.
83. Yudin, A. K., Sharpless, K. B., *J. Am. Chem. Soc.* **1997**; *119*, 11536-11537.
84. Jackson, W. P. *Synlett* **1990**, 536.
85. Bickelhaupt, F. *Angew. Chem. Int. Ed. Engl.* **1987**, *26*, 990-1005.
86. Abrams, M. J.; Davison, A. *Inorg. Chim. Acta*, **1984**, *82*, 125-128.

87. Degnan, I. A.; Behm, J.; Cook, M. R.; Herrmann, W. *Inorg. Chem.*, **1991**, *30*, 2165-2170.
88. Domingos, A.; Marcalo, J.; Paulo, A.; Pires de Matos, A.; Santos, I. *Inorg. Chem.* **1993**, *32*, 5114-5118.
89. (a) Ness, S. Ph.D. thesis, 2000. (b) Enemarck, J. H.; Backes-Dahmann, G. *Inorg. Chem.* **1987**, *26*, 3960-3962.
90. Coe, B. J. *Polyhedron*, **1992**, *11*, 1085-1091.
91. Botha, J. M.; Umakoshi, K.; Sasaki, Y.; Lamprecht, G. J. *Inorg. Chem.* **1998**, *37*, 1609-1615.
92. de Boer, E. J. M.; de With, J. *J. Am. Chem. Soc.* **1986**, *108*, 8271-8273.
93. Brandsma, L. *Synthesis of Acetylenes, Allenes and Cumulenes*. Verkruijsse, Eds.; Elsevier: Amsterdam: **1981**, pp.119-121.
94. Herrmann, W. A.; Fischer, R. A.; Amslinger, W.; Herdtweck, E. *J. Organomet. Chem.* **1989**, *362*, 333-343.
95. (a) Woodward, R. B. Hoffmann, R. *J. Am. Chem. Soc.* 1965, *87*, 395. (b) Woodward, R. B. and Hoffmann, R. *The Conservation of Orbital Symmetry*, Academic Press, New York, 1970.
96. Ponec, R. *Top. Curr. Chem.*, 1995, *174*, 1-26.
97. (a) More O'Ferrall, R. A. *J. Chem. Soc. (B)*, **1970**, 274.; (b) Jencks, W. P. *Chem. Rev.*, **1972**, *72*, 705.
98. Mezey, P. G. *Theor. Chim. Acta*, **1981**, *58*, 309.
99. For a good overview of classical TST see: Kraut, J. *Science*, **1988**, *242*, 533-540.
100. Garrett, B. C.; Truhlar, D. G.; *J. Phys. Chem.* **1979**, *83*, 1079-10112.
101. Scrutton, N. S.; Barsan, J.; Sutcliffe, M. J. *Eur. J. Biochem.* **1999**, *264*, 666-671.
102. Pollak, E. *J. Chem. Phys.* **1986**, *85*, 865-867.
103. (a) Hayashi, T.; Konishi, M.; Kumada, M. *J. Chem. Soc., Chem. Comm.*

1984, 107. (b) Hayashi, T.; Hagihara, T.; Konishi, M.; Kumada, M. *J. Am. Chem. Soc.* **1983**, *105*, 7767.

104. For review on the isoinversion principle see: Buschman, H. Scharf, H-D.; Hoffmann, N.; Esser, P. *Angew. Chem. Int. Ed. Engl.* **1991**, *30*, 477-515.

105. Carey, F. A.; Sundberg, R. J. *Advanced Organic Chemistry*, Kluwer Academic/Plenum Publisher: New York, 2000, p. 222.

106. Singleton, D. A.; Thomas, A. A. *J. Am. Chem. Soc.* **1995**, *117*, 9357.]

107. Belasco, J. G.; Albery, W. J.; Knowles, J. R. *J. Am. Chem. Soc.* **1983**, *105*, 2475-2477.

108. Dewar, M. J. S. *J. Am. Chem. Soc.* **1952**, *74*, 3341.

109. (a) Andersson, P. G.; Sharpless, K. B.; *J. Am. Chem. Soc.* **1993**, *115*, 7047. (b) Kolb, H. C.; Andersson, P. G.; Bennani, Y. L.; Crispino, G. A.; Jeong, K. S.; Kwong, H. L.; Sharpless, K. B. *J. Am. Chem. Soc.* **1993**, *115*, 12226. (c) Kolb, H. C.; Andersson, P. G.; Sharpless, K. B.; *J. Am. Chem. Soc.* **1994**, *116*, 1278.

110. (a) Burton, K. *Biochem. J.*, **1967**, *104*, 686. (b) Subbaraman, L. R.; Subbaraman, J.; Behrman, E. *J. Bioinorg. Chem.* **1972**, *11*, 2621. (c) Clark, R. L.; Behrman, E. *J. Inorg. Chem.* **1972**, *14*, 1425.

111. Norrby, P-O.; Gable, K. P. *J. Chem. Soc. Perkin Trans. 2*, **1995**, 171-178.

112. Corey, E. J.; Noe, M. C.; *J. Am. Chem. Soc.* **1996**, *118*, 319-329.

113. Ujaque, G.; Maseras, F.; Lledos, A. *J. Org. Chem.* **1997**, *62*, 7892-7894.

114. (a) Corey, E. J.; Noe, M. C.; Sarshar, S. *Tetrahedron Lett.* **1994**, *35*, 2861-2864. (b) Corey, E. J.; Noe, M. C.; Grogan, M. J. *Tetrahedron Lett.* **1994**, *35*, 6427-6430.

115. Ujaque, G.; Maseras, F.; Lledos, A. *J. Am. Chem. Soc.* **1999**, *121*, 1317-1323.

116. Norrby, P -O.; Rasmussen, T; Haller, J; Strassner, T; Houk, K. N. *J. Am. Chem. Soc.* **1999**, *121*, 10186-10192.

117. Gobel, T.; Sharpless, K. B. *Angew. Chem. Int. Ed. Engl.* **1993**, *32*, 1329-1331.

118. (a) Jorgensen, K. A. *Tetrahedron Lett.* **1990**, *31*, 6417-6420. (b) Jorgensen, K. A.; Hoffmann, R. *J. Am. Chem. Soc.* **1986**, *108*, 1867-1876. (c) Torrent, M.; Deng, L.; Duran, M.; Sola, M.; Ziegler, T. *Organometallics* **1997**, *16*, 13-19. (d) Dapprich, S.; Ujaque, G.; Maseras, F.; Lledos, A.; Musaev, D. G.; Morokuma, K. *J. Am. Chem. Soc.* **1996**, *118*, 11660-11661. (e) Deubel, D. V.; Frenking, G. *J. Am. Chem. Soc.* **1999**, *121*, 2021-2031.
119. (b) Corey, E. J.; Noe, M. C.; Grogan, M. J. *Tetrahedron Lett.* **1996**, *37*, 4899-4902.
120. Kahn, S. D.; Pau, C. F.; Hehre, W. J. *J. Am. Chem. Soc.* **1986**, *108*, 7381-7396.
121. Gable, K. P.; Juliette, J. J. *J. Am. Chem. Soc.* **1996**, *118*, 2625-2633.
122. Braun, S. Kalinowski, H., -O.; Berger, S. *150 and More Basic NMR Experiments*. Wiley-VCH: New York, 1999.
123. (a) Weiss, G. H.; Feretti, J. A. *J. Magn. Res.* **1983**, *55*, 397-407. (b) Weiss, G. H.; Kiefer, J. E.; Feretti, J. A. *J. Magn. Reson.* **1992**, *97*, 227-234.
124. Sotak, C. H.; Dumoulin, C. L.; Lewy, G. C. *Anal. Chem.* **1983**, *55*, 782-787.
125. Derome, A. E. *Modern NMR Techniques for Chemical Research*, Pergamon Press, Elmsford, New York, 1987.
126. Rabenstein, D. L.; Keire, D. A.; In *Modern NMR Techniques and Their Application in Chemistry*; Popov, A. I., Hallenga, K., Eds.; Marcel Dekker: New York, 1991, pp. 323-369.
127. Bayes, Rev. T., *Philos. Trans. R. Soc. London*, *53*, 370, 1763, reprinted in *Biometrika* *45*, 293, 1958.
128. Bretthorst, G. L. *Lecture Notes in Statistics: Bayesian Spectrum Analysis and Parameter Estimation* Vol. 48, Springer-Verlag: New York, 1988.
129. Forster, P.; Ziessov, D. *Software Development in Chemistry*, 1993, *7*, 119-133. Koch, W.; Holthausen, M. C.; *A Chemist's Guide to Density Functional Theory*, Wiley-VCH, Weinheim, 1999.
134. Jaguar 4.1, Schrödinger, Inc., Portland, OR, 1991-2000.
135. Frenking, G.; Wagner, T.; *Transition Metal Chemistry in Encyclopedia of Computational Chemistry*, Schleyer, P. v. R. Eds, Wiley, Chichester, 1998.

136. Hay, P. J.; Wadt, W. R. *J. Chem. Phys.* **1985**, *82*, 299.
137. Baker, J. Jarzecki, A. A.; Pulay, P. *J. Phys. Chem. A* **1998**, *102*, 1412.
138. Degnan, I. A.; Herrmann, W. A.; Herdtweck, E. *Chem. Ber.* **1990**, *123*, 1347-1349.
139. Paulo, A.; Domingos, A.; Pires de Matos, A.; Santos, I.; Carvalho, M. F. N. N.; Pombeiro, A. J. L. *Inorg Chem.* **1994**, *33*, 4729-4737.
140. Gable, K. P.; Zhuravlev, F. A. Manuscript in preparation.
141. Shriver, D. F.; Drezdson, M. A. *The Manipulation of Air-Sensitive Compounds*, Wiley: New York, 1986.
142. Melander, L.; Saunders, W. H., Jr. *Reaction Rates of Isotopic Molecules*; Wiley: New York, 1980; pp 95-102.
143. Minato, M.; Yamamoto, K.; Tsuji, J. *J. Org. Chem.* **1990**, *55*, 766.
144. Patton, A. T.; Strouse, C. E.; Knobler, C. B.; Gladysz, J. A. *J. Am. Chem. Soc.* **1983**, *105*, 5804-5811.
145. Hermann, W. A.; Voss, E.; Floel, M. *J. Organomet. Chem.* **1985**, *297*, C5.
146. Yudin, A. K., Sharpless, K. B., *J. Am. Chem. Soc.* **1997**; *119*, 11536-11537.
147. Posner, G. H.; Canella, K. A. *J. Am. Chem. Soc.* **1985**, *107*, 2571-2573.
148. Talley, J. J.; Evans, I. A. *J. Org. Chem.* **1984**, 5267-5269.
149. Dess, D.B.; Martin, J. C. *J. Org. Chem.* **1983**, *48*, 4155-4156.
150. Trumbull, E.R.; Finn, R.T.; Ibne-Rasa, K.M.; Sauers, C.K. *J. Org. Chem.* **1962**, *27*, 2339-2344.
151. Corson, B. B.; Heintzelman, W. J.; Schwarzman, L. H.; Thiefenthal, H. E.; Lokken, R. J.; Nickels, J. E.; Atwood, G. R.; Pavlik, F. J. *J. Am. Chem. Soc.* **1958**, *23*, 544.
152. XSCANS V2.2, Bruker AXS, Inc., 1996.
153. Sheldrick, G. M. *Acta Crystallogr.* **1990**, *A46*, 467.

APPENDIX

Table A1. Crystal data and structure refinement for the cluster

Diffractometer used	Siemens P4	
Wavelength, monochromator	1.54178 Å, graphite	
Empirical formula	$C_{32}H_{48}NO_{13}Re_5$	
Formula weight	1585.71	
Temperature	296(2) K	
Crystal system	Monoclinic	
Space group	$P2_1/c$	
Unit cell dimensions	$a = 11.180(1)\text{Å}$	$a = 90^\circ$.
	$b = 15.631(1)\text{Å}$	$b = 98.614(8)^\circ$.
	$c = 22.612(3)\text{Å}$	$g = 90^\circ$.
Volume	$3906.8(7)\text{Å}^3$	
Z	4	
Density (calculated)	2.696 Mg/m^3	
Absorption coefficient	30.002 mm^{-1}	
F(000)	2904	
Crystal color, shape and size	Brown block, $0.50 \times 0.30 \times 0.20\text{ mm}^3$	
Theta range for data collection	3.95 to 57.36° .	
Index ranges	$-12 \leq h \leq 7$, $-17 \leq k \leq 10$, $-24 \leq l \leq 24$	
Reflections collected	10677	
Independent reflections	5191 [R(int) = 0.0910]	
Absorption correction	Analytical (face indexing)	
Max. and min. transmission	0.0654 and 0.0235	
Refinement method	Full-matrix least-squares on F^2	
Data / restraints / parameters	5191 / 0 / 492	
Goodness-of-fit on F^2	1.115	
Final R indices [$>2\sigma(I)$]	$R1 = 0.0645$, $wR2 = 0.1749$	
R indices (all data)	$R1 = 0.0661$, $wR2 = 0.1768$	
Extinction coefficient	$0.00037(3)$	
Largest diff. peak and hole	3.278 and -1.527 e.Å^{-3}	
Software used	SHELXS-90, SHELXL-93	
Weighting scheme	$w = 1 / [s^2(F_o^2) + (aP)^2 + bP]$, where $P = [2F_c^2 + \text{Max}(F_o^2, 0)] / 3$, $a = 0.1184$, $b =$	
32.8705		
Residuals definitions	$R1 = \sum F_o - F_c / \sum F_o $ $wR2 = \{ \sum [w(F_o^2 - F_c^2)^2] / \sum [w(F_o^2)^2] \}^{1/2}$	

Table A2. Atomic coordinates ($\times 10^4$) and equivalent isotropic displacement parameters for the cluster.

	x	y	z	U(eq)
Re(1)	1052(1)	7369(1)	1352(1)	39(1)
Re(2)	1807(1)	7469(1)	2568(1)	41(1)
Re(3)	3478(1)	7305(1)	1798(1)	40(1)
Re(4)	2242(1)	9236(1)	1820(1)	49(1)
O(1)	1972(12)	9774(8)	2443(6)	70(3)
O(2)	3585(10)	9578(7)	1680(4)	54(3)
O(3)	1266(11)	9672(7)	1261(6)	69(3)
O(11)	677(10)	6753(7)	2052(5)	55(3)
O(12)	905(9)	8296(7)	1962(5)	50(2)
O(21)	3151(9)	6698(7)	2497(5)	54(3)
O(22)	3157(9)	8222(7)	2380(4)	47(2)
O(31)	2348(9)	6607(6)	1252(5)	48(2)
O(32)	2435(9)	8126(6)	1242(4)	46(2)
C(11)	468(15)	7069(14)	386(7)	60(4)
C(12)	16(16)	7878(13)	453(7)	65(5)
C(13)	-827(14)	7818(12)	865(8)	59(4)
C(14)	-923(14)	6990(12)	1011(7)	56(4)
C(15)	-147(15)	6494(11)	732(8)	57(4)
C(16)	1295(16)	6750(2)	-35(7)	94(9)
C(17)	350(3)	8660(2)	121(12)	151(18)
C(18)	-1530(2)	8528(14)	1124(13)	100(9)
C(19)	-1816(19)	6590(2)	1397(9)	112(13)
C(10)	50(2)	5527(13)	789(10)	92(7)
C(21)	2415(16)	7312(13)	3574(7)	61(5)
C(22)	1996(17)	8127(14)	3498(6)	66(5)
C(23)	701(17)	8130(13)	3258(7)	65(5)
C(24)	387(16)	7244(12)	3185(7)	58(4)
C(25)	1391(17)	6715(12)	3372(7)	61(5)
C(26)	3635(18)	7056(17)	3842(8)	78(6)
C(27)	2745(18)	8926(12)	3684(8)	70(5)
C(28)	-124(19)	8846(16)	3106(10)	89(7)
C(29)	-880(18)	6952(15)	3012(9)	85(8)
C(20)	1430(2)	5769(15)	3395(11)	93(7)
C(31)	4939(14)	6374(12)	1733(9)	63(5)
C(32)	4773(14)	6758(12)	1187(8)	63(4)
C(33)	5040(15)	7655(11)	1276(8)	56(4)
C(34)	5463(16)	7778(11)	1907(8)	59(4)
C(35)	5385(14)	6979(12)	2186(8)	58(4)
C(36)	4840(2)	5433(12)	1833(13)	97(8)
C(37)	4421(19)	6316(17)	604(9)	86(7)

C(38)	4983(18)	8349(15)	816(10)	91(8)
C(39)	5932(15)	8551(13)	2225(11)	77(6)
C(30)	5844(19)	6760(2)	2833(10)	98(8)
Re(5)	7156(1)	8498(1)	4455(1)	69(1)
O(51)	6020(2)	8545(14)	3886(10)	143(9)
O(52)	7400(2)	9449(11)	4794(12)	155(10)
O(53)	8438(19)	8140(2)	4249(8)	149(9)
O(54)	6795(17)	7816(11)	4970(8)	104(5)
C(2)	3300(3)	175(15)	111(10)	98(8)
C(1)	3370(4)	847(19)	578(11)	150(15)
N	3200(4)	-290(2)	-222(13)	179(16)

Table A3. Selected bond lengths [\AA] and angles [$^\circ$] for the cluster

Re(1)-O(31)	1.914(9)
Re(1)-O(11)	1.952(11)
Re(1)-O(32)	1.992(10)
Re(1)-O(12)	2.025(11)
Re(1)-C(11)	2.233(15)
Re(1)-C(15)	2.251(14)
Re(1)-C(14)	2.305(15)
Re(1)-C(12)	2.323(14)
Re(1)-C(13)	2.330(15)
Re(1)-Re(3)	2.7499(9)
Re(1)-Re(2)	2.7586(9)
Re(2)-O(11)	1.941(12)
Re(2)-O(21)	1.951(10)
Re(2)-O(22)	2.010(10)
Re(2)-O(12)	2.039(11)
Re(2)-C(25)	2.273(14)
Re(2)-C(21)	2.287(16)
Re(2)-C(24)	2.291(16)
Re(2)-C(22)	2.322(15)
Re(2)-C(23)	2.369(14)
Re(2)-Re(3)	2.7496(9)
Re(3)-O(21)	1.923(11)
Re(3)-O(31)	1.960(10)
Re(3)-O(22)	2.013(10)
Re(3)-O(32)	2.037(9)
Re(3)-C(31)	2.209(16)
Re(3)-C(35)	2.239(15)
Re(3)-C(32)	2.310(17)
Re(3)-C(33)	2.316(17)

Re(3)-C(34)	2.317(18)
Re(4)-O(2)	1.668(10)
Re(4)-O(3)	1.685(13)
Re(4)-O(1)	1.707(12)
Re(4)-O(12)	2.153(10)
Re(4)-O(22)	2.184(10)
Re(4)-O(32)	2.201(10)

O(31)-Re(1)-O(11)	92.7(4)
O(31)-Re(1)-O(32)	74.9(4)
O(11)-Re(1)-O(32)	131.2(5)
O(31)-Re(1)-O(12)	131.7(4)
O(11)-Re(1)-O(12)	75.6(5)
O(32)-Re(1)-O(12)	78.6(4)
O(31)-Re(1)-Re(3)	45.4(3)
O(11)-Re(1)-Re(3)	90.2(3)
O(32)-Re(1)-Re(3)	47.6(3)
O(12)-Re(1)-Re(3)	87.2(3)
O(31)-Re(1)-Re(2)	91.6(3)
O(11)-Re(1)-Re(2)	44.7(3)
O(32)-Re(1)-Re(2)	87.9(3)
O(12)-Re(1)-Re(2)	47.5(3)
Re(3)-Re(1)-Re(2)	59.89(2)
O(11)-Re(2)-O(21)	91.9(5)
O(11)-Re(2)-O(22)	130.7(4)
O(21)-Re(2)-O(22)	74.4(5)
O(11)-Re(2)-O(12)	75.5(5)
O(21)-Re(2)-O(12)	130.2(4)
O(22)-Re(2)-O(12)	78.3(4)
O(11)-Re(2)-Re(3)	90.5(3)
O(21)-Re(2)-Re(3)	44.4(3)
O(22)-Re(2)-Re(3)	46.9(3)
O(12)-Re(2)-Re(3)	87.0(3)
O(11)-Re(2)-Re(1)	45.0(3)
O(21)-Re(2)-Re(1)	90.4(3)
O(22)-Re(2)-Re(1)	87.1(3)
O(12)-Re(2)-Re(1)	47.0(3)
Re(3)-Re(2)-Re(1)	59.90(2)
O(21)-Re(3)-O(31)	93.4(5)
O(21)-Re(3)-O(22)	75.0(5)
O(31)-Re(3)-O(22)	130.3(4)
O(21)-Re(3)-O(32)	131.0(4)
O(31)-Re(3)-O(32)	73.0(5)
O(22)-Re(3)-O(32)	79.2(4)
O(21)-Re(3)-Re(2)	45.2(3)
O(31)-Re(3)-Re(2)	90.9(3)

O(22)-Re(3)-Re(2)	46.8(3)
O(32)-Re(3)-Re(2)	87.2(3)
O(21)-Re(3)-Re(1)	91.2(3)
O(31)-Re(3)-Re(1)	44.1(3)
O(22)-Re(3)-Re(1)	87.2(3)
O(32)-Re(3)-Re(1)	46.3(3)
Re(2)-Re(3)-Re(1)	60.21(2)
O(2)-Re(4)-O(3)	103.2(6)
O(2)-Re(4)-O(1)	105.9(6)
O(3)-Re(4)-O(1)	104.1(6)
O(2)-Re(4)-O(12)	155.7(5)
O(3)-Re(4)-O(12)	90.1(5)
O(1)-Re(4)-O(12)	90.1(5)
O(2)-Re(4)-O(22)	89.2(5)
O(3)-Re(4)-O(22)	157.3(5)
O(1)-Re(4)-O(22)	90.3(5)
O(12)-Re(4)-O(22)	72.2(4)
O(2)-Re(4)-O(32)	88.2(4)
O(3)-Re(4)-O(32)	89.1(5)
O(1)-Re(4)-O(32)	157.5(5)
O(12)-Re(4)-O(32)	71.5(4)
O(22)-Re(4)-O(32)	72.1(4)
Re(2)-O(11)-Re(1)	90.2(5)
Re(1)-O(12)-Re(2)	85.5(4)
Re(1)-O(12)-Re(4)	104.9(4)
Re(2)-O(12)-Re(4)	104.4(4)
Re(3)-O(21)-Re(2)	90.4(5)
Re(2)-O(22)-Re(3)	86.2(4)
Re(2)-O(22)-Re(4)	104.3(4)
Re(3)-O(22)-Re(4)	104.6(4)
Re(1)-O(31)-Re(3)	90.5(4)
Re(1)-O(32)-Re(3)	86.1(4)
Re(1)-O(32)-Re(4)	104.4(4)
Re(3)-O(32)-Re(4)	103.2(4)

Table A4. Bond lengths [Å] and angles [°] for the cluster

Re(1)-O(31)	1.914(9)
Re(1)-O(11)	1.952(11)
Re(1)-O(32)	1.992(10)
Re(1)-O(12)	2.025(11)
Re(1)-C(11)	2.233(15)
Re(1)-C(15)	2.251(14)
Re(1)-C(14)	2.305(15)
Re(1)-C(12)	2.323(14)
Re(1)-C(13)	2.330(15)
Re(1)-Re(3)	2.7499(9)
Re(1)-Re(2)	2.7586(9)
Re(2)-O(11)	1.941(12)
Re(2)-O(21)	1.951(10)
Re(2)-O(22)	2.010(10)
Re(2)-O(12)	2.039(11)
Re(2)-C(25)	2.273(14)
Re(2)-C(21)	2.287(16)
Re(2)-C(24)	2.291(16)
Re(2)-C(22)	2.322(15)
Re(2)-C(23)	2.369(14)
Re(2)-Re(3)	2.7496(9)
Re(3)-O(21)	1.923(11)
Re(3)-O(31)	1.960(10)
Re(3)-O(22)	2.013(10)
Re(3)-O(32)	2.037(9)
Re(3)-C(31)	2.209(16)
Re(3)-C(35)	2.239(15)
Re(3)-C(32)	2.310(17)
Re(3)-C(33)	2.316(17)
Re(3)-C(34)	2.317(18)
Re(4)-O(2)	1.668(10)
Re(4)-O(3)	1.685(13)
Re(4)-O(1)	1.707(12)
Re(4)-O(12)	2.153(10)
Re(4)-O(22)	2.184(10)
Re(4)-O(32)	2.201(10)
C(11)-C(12)	1.38(3)
C(11)-C(15)	1.43(3)
C(11)-C(16)	1.51(2)
C(12)-C(13)	1.42(3)
C(12)-C(17)	1.50(3)
C(13)-C(14)	1.34(3)
C(13)-C(18)	1.52(3)

C(14)-C(15)	1.38(2)
C(14)-C(19)	1.55(2)
C(15)-C(10)	1.53(3)
C(21)-C(22)	1.36(3)
C(21)-C(26)	1.46(3)
C(21)-C(25)	1.49(3)
C(22)-C(23)	1.47(3)
C(22)-C(27)	1.53(3)
C(23)-C(24)	1.43(3)
C(23)-C(28)	1.46(3)
C(24)-C(25)	1.41(3)
C(24)-C(29)	1.48(3)
C(25)-C(20)	1.48(3)
C(31)-C(32)	1.36(3)
C(31)-C(35)	1.43(3)
C(31)-C(36)	1.49(3)
C(32)-C(33)	1.44(3)
C(32)-C(37)	1.49(3)
C(33)-C(34)	1.45(3)
C(33)-C(38)	1.50(2)
C(34)-C(35)	1.41(3)
C(34)-C(39)	1.46(3)
C(35)-C(30)	1.52(3)
Re(5)-O(53)	1.67(2)
Re(5)-O(51)	1.669(18)
Re(5)-O(54)	1.670(16)
Re(5)-O(52)	1.676(19)
C(2)-N	1.04(3)
C(2)-C(1)	1.48(4)
O(31)-Re(1)-O(11)	92.7(4)
O(31)-Re(1)-O(32)	74.9(4)
O(11)-Re(1)-O(32)	131.2(5)
O(31)-Re(1)-O(12)	131.7(4)
O(11)-Re(1)-O(12)	75.6(5)
O(32)-Re(1)-O(12)	78.6(4)
O(31)-Re(1)-C(11)	82.6(6)
O(11)-Re(1)-C(11)	128.6(6)
O(32)-Re(1)-C(11)	97.0(6)
O(12)-Re(1)-C(11)	140.7(6)
O(31)-Re(1)-C(15)	86.6(5)
O(11)-Re(1)-C(15)	91.4(6)
O(32)-Re(1)-C(15)	133.3(6)
O(12)-Re(1)-C(15)	139.2(5)
C(11)-Re(1)-C(15)	37.3(7)
O(31)-Re(1)-C(14)	120.4(6)

O(11)-Re(1)-C(14)	80.4(5)
O(32)-Re(1)-C(14)	146.5(5)
O(12)-Re(1)-C(14)	103.9(5)
C(11)-Re(1)-C(14)	59.6(6)
C(15)-Re(1)-C(14)	35.3(6)
O(31)-Re(1)-C(12)	113.4(6)
O(11)-Re(1)-C(12)	137.6(6)
O(32)-Re(1)-C(12)	89.0(5)
O(12)-Re(1)-C(12)	105.6(6)
C(11)-Re(1)-C(12)	35.1(7)
C(15)-Re(1)-C(12)	59.5(7)
C(14)-Re(1)-C(12)	57.9(6)
O(31)-Re(1)-C(13)	141.0(5)
O(11)-Re(1)-C(13)	104.1(6)
O(32)-Re(1)-C(13)	115.1(6)
O(12)-Re(1)-C(13)	86.9(5)
C(11)-Re(1)-C(13)	59.3(6)
C(15)-Re(1)-C(13)	58.5(6)
C(14)-Re(1)-C(13)	33.7(6)
C(12)-Re(1)-C(13)	35.6(7)
O(31)-Re(1)-Re(3)	45.4(3)
O(11)-Re(1)-Re(3)	90.2(3)
O(32)-Re(1)-Re(3)	47.6(3)
O(12)-Re(1)-Re(3)	87.2(3)
C(11)-Re(1)-Re(3)	118.7(4)
C(15)-Re(1)-Re(3)	132.0(4)
C(14)-Re(1)-Re(3)	163.0(4)
C(12)-Re(1)-Re(3)	132.0(5)
C(13)-Re(1)-Re(3)	162.7(5)
O(31)-Re(1)-Re(2)	91.6(3)
O(11)-Re(1)-Re(2)	44.7(3)
O(32)-Re(1)-Re(2)	87.9(3)
O(12)-Re(1)-Re(2)	47.5(3)
C(11)-Re(1)-Re(2)	171.2(5)
C(15)-Re(1)-Re(2)	136.0(5)
C(14)-Re(1)-Re(2)	118.9(4)
C(12)-Re(1)-Re(2)	152.9(6)
C(13)-Re(1)-Re(2)	125.0(4)
Re(3)-Re(1)-Re(2)	59.89(2)
O(11)-Re(2)-O(21)	91.9(5)
O(11)-Re(2)-O(22)	130.7(4)
O(21)-Re(2)-O(22)	74.4(5)
O(11)-Re(2)-O(12)	75.5(5)
O(21)-Re(2)-O(12)	130.2(4)
O(22)-Re(2)-O(12)	78.3(4)
O(11)-Re(2)-C(25)	89.4(6)

O(21)-Re(2)-C(25)	89.9(6)
O(22)-Re(2)-C(25)	136.4(6)
O(12)-Re(2)-C(25)	136.7(5)
O(11)-Re(2)-C(21)	127.3(5)
O(21)-Re(2)-C(21)	84.2(6)
O(22)-Re(2)-C(21)	98.8(5)
O(12)-Re(2)-C(21)	141.3(6)
C(25)-Re(2)-C(21)	38.3(6)
O(11)-Re(2)-C(24)	80.2(5)
O(21)-Re(2)-C(24)	124.6(6)
O(22)-Re(2)-C(24)	146.1(5)
O(12)-Re(2)-C(24)	100.9(5)
C(25)-Re(2)-C(24)	35.9(6)
C(21)-Re(2)-C(24)	60.6(7)
O(11)-Re(2)-C(22)	139.7(6)
O(21)-Re(2)-C(22)	112.4(6)
O(22)-Re(2)-C(22)	87.9(6)
O(12)-Re(2)-C(22)	107.3(6)
C(25)-Re(2)-C(22)	60.5(7)
C(21)-Re(2)-C(22)	34.3(7)
C(24)-Re(2)-C(22)	59.6(7)
O(11)-Re(2)-C(23)	106.9(6)
O(21)-Re(2)-C(23)	143.9(6)
O(22)-Re(2)-C(23)	111.5(6)
O(12)-Re(2)-C(23)	85.0(5)
C(25)-Re(2)-C(23)	60.6(7)
C(21)-Re(2)-C(23)	59.9(7)
C(24)-Re(2)-C(23)	35.7(7)
C(22)-Re(2)-C(23)	36.5(6)
O(11)-Re(2)-Re(3)	90.5(3)
O(21)-Re(2)-Re(3)	44.4(3)
O(22)-Re(2)-Re(3)	46.9(3)
O(12)-Re(2)-Re(3)	87.0(3)
C(25)-Re(2)-Re(3)	134.3(5)
C(21)-Re(2)-Re(3)	119.4(5)
C(24)-Re(2)-Re(3)	165.8(5)
C(22)-Re(2)-Re(3)	129.5(5)
C(23)-Re(2)-Re(3)	158.3(5)
O(11)-Re(2)-Re(1)	45.0(3)
O(21)-Re(2)-Re(1)	90.4(3)
O(22)-Re(2)-Re(1)	87.1(3)
O(12)-Re(2)-Re(1)	47.0(3)
C(25)-Re(2)-Re(1)	134.4(5)
C(21)-Re(2)-Re(1)	170.6(5)
C(24)-Re(2)-Re(1)	117.5(4)
C(22)-Re(2)-Re(1)	154.3(5)

C(23)-Re(2)-Re(1)	124.8(5)
Re(3)-Re(2)-Re(1)	59.90(2)
O(21)-Re(3)-O(31)	93.4(5)
O(21)-Re(3)-O(22)	75.0(5)
O(31)-Re(3)-O(22)	130.3(4)
O(21)-Re(3)-O(32)	131.0(4)
O(31)-Re(3)-O(32)	73.0(5)
O(22)-Re(3)-O(32)	79.2(4)
O(21)-Re(3)-C(31)	87.9(6)
O(31)-Re(3)-C(31)	90.2(6)
O(22)-Re(3)-C(31)	136.0(6)
O(32)-Re(3)-C(31)	137.3(6)
O(21)-Re(3)-C(35)	81.6(5)
O(31)-Re(3)-C(35)	127.3(6)
O(22)-Re(3)-C(35)	99.1(6)
O(32)-Re(3)-C(35)	143.9(5)
C(31)-Re(3)-C(35)	37.5(7)
O(21)-Re(3)-C(32)	121.5(6)
O(31)-Re(3)-C(32)	79.6(5)
O(22)-Re(3)-C(32)	147.5(5)
O(32)-Re(3)-C(32)	102.5(5)
C(31)-Re(3)-C(32)	34.9(7)
C(35)-Re(3)-C(32)	60.3(6)
O(21)-Re(3)-C(33)	141.8(5)
O(31)-Re(3)-C(33)	105.9(6)
O(22)-Re(3)-C(33)	112.8(5)
O(32)-Re(3)-C(33)	86.7(5)
C(31)-Re(3)-C(33)	60.0(6)
C(35)-Re(3)-C(33)	60.4(6)
C(32)-Re(3)-C(33)	36.3(6)
O(21)-Re(3)-C(34)	111.5(6)
O(31)-Re(3)-C(34)	139.5(5)
O(22)-Re(3)-C(34)	88.0(5)
O(32)-Re(3)-C(34)	108.3(5)
C(31)-Re(3)-C(34)	60.7(6)
C(35)-Re(3)-C(34)	35.9(7)
C(32)-Re(3)-C(34)	60.3(6)
C(33)-Re(3)-C(34)	36.4(7)
O(21)-Re(3)-Re(2)	45.2(3)
O(31)-Re(3)-Re(2)	90.9(3)
O(22)-Re(3)-Re(2)	46.8(3)
O(32)-Re(3)-Re(2)	87.2(3)
C(31)-Re(3)-Re(2)	133.1(5)
C(35)-Re(3)-Re(2)	118.1(4)
C(32)-Re(3)-Re(2)	163.6(5)
C(33)-Re(3)-Re(2)	159.5(5)

C(34)-Re(3)-Re(2)	129.4(4)
O(21)-Re(3)-Re(1)	91.2(3)
O(31)-Re(3)-Re(1)	44.1(3)
O(22)-Re(3)-Re(1)	87.2(3)
O(32)-Re(3)-Re(1)	46.3(3)
C(31)-Re(3)-Re(1)	134.2(5)
C(35)-Re(3)-Re(1)	168.7(5)
C(32)-Re(3)-Re(1)	117.7(4)
C(33)-Re(3)-Re(1)	125.6(4)
C(34)-Re(3)-Re(1)	154.6(5)
Re(2)-Re(3)-Re(1)	60.21(2)
O(2)-Re(4)-O(3)	103.2(6)
O(2)-Re(4)-O(1)	105.9(6)
O(3)-Re(4)-O(1)	104.1(6)
O(2)-Re(4)-O(12)	155.7(5)
O(3)-Re(4)-O(12)	90.1(5)
O(1)-Re(4)-O(12)	90.1(5)
O(2)-Re(4)-O(22)	89.2(5)
O(3)-Re(4)-O(22)	157.3(5)
O(1)-Re(4)-O(22)	90.3(5)
O(12)-Re(4)-O(22)	72.2(4)
O(2)-Re(4)-O(32)	88.2(4)
O(3)-Re(4)-O(32)	89.1(5)
O(1)-Re(4)-O(32)	157.5(5)
O(12)-Re(4)-O(32)	71.5(4)
O(22)-Re(4)-O(32)	72.1(4)
Re(2)-O(11)-Re(1)	90.2(5)
Re(1)-O(12)-Re(2)	85.5(4)
Re(1)-O(12)-Re(4)	104.9(4)
Re(2)-O(12)-Re(4)	104.4(4)
Re(3)-O(21)-Re(2)	90.4(5)
Re(2)-O(22)-Re(3)	86.2(4)
Re(2)-O(22)-Re(4)	104.3(4)
Re(3)-O(22)-Re(4)	104.6(4)
Re(1)-O(31)-Re(3)	90.5(4)
Re(1)-O(32)-Re(3)	86.1(4)
Re(1)-O(32)-Re(4)	104.4(4)
Re(3)-O(32)-Re(4)	103.2(4)
C(12)-C(11)-C(15)	107.5(16)
C(12)-C(11)-C(16)	130(2)
C(15)-C(11)-C(16)	122(2)
C(12)-C(11)-Re(1)	76.0(10)
C(15)-C(11)-Re(1)	72.0(9)
C(16)-C(11)-Re(1)	124.7(11)
C(11)-C(12)-C(13)	107.5(16)
C(11)-C(12)-C(17)	124(2)

C(13)-C(12)-C(17)	128(2)
C(11)-C(12)-Re(1)	68.9(8)
C(13)-C(12)-Re(1)	72.4(9)
C(17)-C(12)-Re(1)	125.7(13)
C(14)-C(13)-C(12)	108.0(17)
C(14)-C(13)-C(18)	122.9(19)
C(12)-C(13)-C(18)	129(2)
C(14)-C(13)-Re(1)	72.1(9)
C(12)-C(13)-Re(1)	71.9(9)
C(18)-C(13)-Re(1)	121.0(12)
C(13)-C(14)-C(15)	110.5(15)
C(13)-C(14)-C(19)	127.3(19)
C(15)-C(14)-C(19)	122.1(18)
C(13)-C(14)-Re(1)	74.2(9)
C(15)-C(14)-Re(1)	70.2(9)
C(19)-C(14)-Re(1)	125.4(12)
C(14)-C(15)-C(11)	106.3(15)
C(14)-C(15)-C(10)	127.4(18)
C(11)-C(15)-C(10)	126.2(18)
C(14)-C(15)-Re(1)	74.5(9)
C(11)-C(15)-Re(1)	70.7(9)
C(10)-C(15)-Re(1)	118.8(12)
C(22)-C(21)-C(26)	126.2(19)
C(22)-C(21)-C(25)	108.3(16)
C(26)-C(21)-C(25)	125.4(19)
C(22)-C(21)-Re(2)	74.3(9)
C(26)-C(21)-Re(2)	124.2(13)
C(25)-C(21)-Re(2)	70.4(8)
C(21)-C(22)-C(23)	110.6(18)
C(21)-C(22)-C(27)	124.6(18)
C(23)-C(22)-C(27)	124.7(19)
C(21)-C(22)-Re(2)	71.4(10)
C(23)-C(22)-Re(2)	73.5(8)
C(27)-C(22)-Re(2)	125.7(11)
C(24)-C(23)-C(28)	125.4(19)
C(24)-C(23)-C(22)	104.5(17)
C(28)-C(23)-C(22)	130(2)
C(24)-C(23)-Re(2)	69.2(8)
C(28)-C(23)-Re(2)	123.6(12)
C(22)-C(23)-Re(2)	70.0(8)
C(25)-C(24)-C(23)	111.2(16)
C(25)-C(24)-C(29)	125.8(19)
C(23)-C(24)-C(29)	122.4(18)
C(25)-C(24)-Re(2)	71.3(9)
C(23)-C(24)-Re(2)	75.1(9)
C(29)-C(24)-Re(2)	127.4(11)

C(24)-C(25)-C(20)	127.9(19)
C(24)-C(25)-C(21)	105.4(17)
C(20)-C(25)-C(21)	126.7(19)
C(24)-C(25)-Re(2)	72.8(9)
C(20)-C(25)-Re(2)	122.5(14)
C(21)-C(25)-Re(2)	71.4(9)
C(32)-C(31)-C(35)	110.1(17)
C(32)-C(31)-C(36)	125(2)
C(35)-C(31)-C(36)	124.7(19)
C(32)-C(31)-Re(3)	76.6(10)
C(35)-C(31)-Re(3)	72.4(9)
C(36)-C(31)-Re(3)	124.4(13)
C(31)-C(32)-C(33)	107.8(16)
C(31)-C(32)-C(37)	125(2)
C(33)-C(32)-C(37)	126.7(19)
C(31)-C(32)-Re(3)	68.5(10)
C(33)-C(32)-Re(3)	72.1(9)
C(37)-C(32)-Re(3)	126.6(12)
C(32)-C(33)-C(34)	107.3(15)
C(32)-C(33)-C(38)	128.4(18)
C(34)-C(33)-C(38)	124.2(18)
C(32)-C(33)-Re(3)	71.6(9)
C(34)-C(33)-Re(3)	71.9(10)
C(38)-C(33)-Re(3)	124.6(11)
C(35)-C(34)-C(33)	106.9(15)
C(35)-C(34)-C(39)	123.6(18)
C(33)-C(34)-C(39)	129.5(18)
C(35)-C(34)-Re(3)	69.0(9)
C(33)-C(34)-Re(3)	71.8(10)
C(39)-C(34)-Re(3)	125.6(12)
C(34)-C(35)-C(31)	107.7(15)
C(34)-C(35)-C(30)	126.7(19)
C(31)-C(35)-C(30)	125.2(19)
C(34)-C(35)-Re(3)	75.1(9)
C(31)-C(35)-Re(3)	70.1(9)
C(30)-C(35)-Re(3)	126.4(12)
O(53)-Re(5)-O(51)	112.6(12)
O(53)-Re(5)-O(54)	106.8(11)
O(51)-Re(5)-O(54)	109.3(11)
O(53)-Re(5)-O(52)	109.6(14)
O(51)-Re(5)-O(52)	111.5(10)
O(54)-Re(5)-O(52)	106.8(11)
N-C(2)-C(1)	177(4)